A REACTIVATOR OF ORGANOPHOSPHORUS NERVE AGENT-INHIBITED HUMAN ACETYLCHOLINESTERASE: CHARACTERIZATION, MECHANISTIC INSIGHTS AND DESIGN

by

C. Linn Cadieux

A dissertation submitted to the Faculty of the University of Delaware in partial fulfillment of the requirements for the degree of Doctor of Philosophy in Chemistry and Biochemistry

Spring 2016

A REACTIVATOR OF ORGANOPHOSPHORUS

NERVE AGENT-INHIBITED HUMAN ACETYLCHOLINESTERASE:

CHARACTERIZATION, MECHANISTIC INSIGHTS AND DESIGN

by

C. Linn Cadieux

Approved: _____

Murray V. Johnston, Ph.D.
Chair of the Department of Chemistry and Biochemistry

Approved: _____

George H. Watson, Ph.D.
Dean of the College of Arts and Sciences

Approved: _____

Ann L. Ardis, Ph.D.
Senior Vice Provost for Graduate and Professional Education

I certify that I have read this dissertation and that in my opinion it meets the academic and professional standard required by the University as a dissertation for the degree of Doctor of Philosophy.

Signed: _____

John T. Koh, Ph.D.
Professor in charge of dissertation

I certify that I have read this dissertation and that in my opinion it meets the academic and professional standard required by the University as a dissertation for the degree of Doctor of Philosophy.

Signed: _____

Sharon Rozovsky, Ph.D.
Member of dissertation committee

I certify that I have read this dissertation and that in my opinion it meets the academic and professional standard required by the University as a dissertation for the degree of Doctor of Philosophy.

Signed: _____

Brian J. Bahnson, Ph.D.
Member of dissertation committee

I certify that I have read this dissertation and that in my opinion it meets the academic and professional standard required by the University as a dissertation for the degree of Doctor of Philosophy.

Signed: _____

Douglas M. Cerasoli, Ph.D.
Member of dissertation committee

DEDICATION

I would like to dedicate this work to my dear grandmother Linda Robinson whose passion for science, both real and imagined, fantasy, and life in general continues to inspire me constantly.

ACKNOWLEDGEMENTS

I would like to thank the following groups and individuals who have not only helped me attain my doctoral degree but made me a better scientist:

The members of my committee for their input and guidance. Dr. John Koh, my mentor at UD, who has always been a great source of organic chemistry knowledge and never failed to point out the holes in my theories and then help me fix them. The entire Koh laboratory at UD, especially Haoyu, Ethan, and Ben for their organic synthesis skills, Wei for his modeling insights, and Gaby for showing me the ropes.

The members, past and present, of the Bioscavenger Group at the USAMRICD, especially Dr. Tony Reeves for convincing me to seek a Ph.D., Dr. Shane Kasten for allowing me to ruin his instruments, Dr. Tamara Otto for her ever-organized presence, and Melanie and Sandy for picking up all the slack I left lying around, especially at the end.

A special thanks to Dr. Douglas Cerasoli for all of his support, scientifically, emotionally, and monetarily, throughout the entire degree-seeking process (not to mention initially convincing me to pursue the degree at all).

My mother and sister, who always reminded me I could do anything I put my mind to. My good friend, partner in crime, “wife”, and fellow grad school traveler, Cay. She knows why.

And, finally, thank you to my other half, John, for being my shoulder to cry on, listening to my science gibberish constantly, and dispensing bear hugs and kicks in the butt as necessary. I couldn’t have done it without you.

DISCLOSURES

This research was supported in part by an appointment to the Postgraduate Research Participation Program at the U.S. Army Medical Research Institute of Chemical Defense administered by the Oak Ridge Institute for Science and Education through an interagency agreement between the U.S. Department of Energy and the U. S. Army Medical Research and Materiel Command.

This research was supported in part by the Defense Threat Reduction Agency - Joint Science Technology Office, Medical Science & Technology Division.

The views expressed in this dissertation are those of the author and do not reflect the official policy of the Department of Army, Department of Defense, or the U.S. Government.

TABLE OF CONTENTS

LIST OF TABLES

LIST OF FIGURES

LIST OF ABBREVIATIONS

1. ADOC - 4-amino-2-((diethylamino)methyl)phenol
2. OP – organophosphorus
3. GA – tabun
4. GB – sarin
5. GD – soman
6. GF – cyclosarin
7. AChE – acetylcholinesterase
8. PB – pyridostigmine bromide
9. BuChE – butyrylcholinesterase
10. 2PAM – pralidoxime
11. AtCh – acetylthiocholine
12. BtCh – butyrylthiocholine
13. DTNB – dithionitrobenzoic acid
14. HuAChE – recombinant human acetylcholinesterase
15. SAR – structure-activity relationship
16. HuBuChE – human butyrylcholinesterase, recombinant or human plasma-derived
17. QM – quinone methide
18. QI – quinone imine
19. sQI – semiquinone imine

20. ITC – isothermal titration calorimetry

21. LC/QQQ – liquid chromatography coupled with triple quadrapole mass spectrometry

22. CMP – cyclohexylmethyl phosphonic acid

ABSTRACT

Organophosphorus nerve agents are highly toxic compounds which pose a threat worldwide. These compounds induce toxicity by covalently binding to the active site serine of acetylcholinesterase, which results in inhibition of the enzyme. Without functional acetylcholinesterase, the levels of the neurotransmitter acetylcholine in neuromuscular junctions rise quickly causing overstimulation of the nervous system, which will culminate in death if not treated. Current treatments rely on small molecules to interact with inhibited enzyme to disrupt the covalently bound phosphorus moiety at the active site. The most effective molecules incorporate a pyridinium oxime which acts via direct nucleophilic attack on the phosphorus to achieve reactivation of the enzyme. These compounds have limited effectiveness as the charged portion of the molecule does not allow them to cross into the central nervous system where acetylcholinesterase inhibition is most harmful. This study characterizes a small molecule reactivator that does not incorporate an oxime but is capable of reactivating nerve agent-inhibited enzyme as well as or better than current treatments *in vitro*. Through the use of a structure-activity relationship study and several biochemical techniques, the phenol moiety of 4-amino-2-((diethylamino)methyl)phenol (ADOC) was determined to be essential for the reactivation characteristics of this molecule, likely through an indirect water-activation mechanism. This information was then used in the design of a second-generation molecule that showed increased reactivation potential.

Chapter 1

INTRODUCTION

1.1 History

Chemicals have been used in warfare for thousands of years in forms ranging from primitive weapons such as poison-dipped arrows and boiling tar to the advanced weaponry of today which includes the focus of the countermeasures in this study: organophosphorus (OP) nerve agents. The age of modern chemical warfare is generally considered to have begun during World War I in April, 1915, when the German military launched the first large scale chemical attack using chlorine gas, which causes asphyxiation [1, 2]. Several other chemicals were used in WWI, the most notable being phosgene, which causes pulmonary edema, and the vesicating agent mustard gas [1-3]. During the course of the war, an estimated 91,000 deaths were caused by the use of weaponized chemicals.

1.1.1 Nerve Agents

The first OP nerve agent, tabun, was discovered in 1937 by the German scientist Dr. Gerhard Schrader during his search for improved pesticides [1, 4]. Sarin was discovered shortly thereafter and both agents were immediately classified top secret by the German government; research into the weaponization of these compounds commenced. Soman and cyclosarin, two additional OP nerve agents, were discovered after the outbreak of World War II. Although Germany successfully produced weapons incorporating both tabun and sarin during WWII, these weapons

were never deployed. The Allies discovered the existence of OP nerve agents when the advancing Russian army captured a factory and storage facility in Dühernfurt, Germany, with intact stocks of both tabun and sarin weapons [5, 6]. After the end of the war, a sulfur-containing OP pesticide with potency greater than that of sarin and soman was discovered by Ghosh and Newman [7]; the compound was quickly recognized as a potential chemical weapon by the British government. This agent was later dubbed VX and, along with the Russian-developed structural isomer VR, comprises the final class of commonly studied OP nerve agent compounds.

Although OP nerve agents were never deployed as a weapon during WWII, they have been used several times by both military forces and terrorists. The most recent of these events occurred in 2013 when sarin was released in the suburbs of Damascus, Syria, killing approximately 1,400 civilians [8]. Events such as this underscore the need for improved treatments of nerve agent intoxication such as those explored in this study.

1.2 Organophosphorus Nerve Agents

1.2.1 Chemical Structure

OP nerve agents consist of two main classes, known in the U.S. as the G and V agents after the classifications assigned by the U.S. Army (Figure 1-1) [1]. The G agents, so named because of their initial development by the Germans, consist of tabun (GA), sarin (GB), soman (GD) and cyclosarin (GF). These agents all incorporate a central phosphorus atom with an oxygen, an ester, a methyl group, and a fluorine with the exception of GA which has an amide in place of the methyl group and a cyanide in place of the fluorine leaving group. The V agents, consisting of VX and

Russian VX (VR), incorporate a sulfur-containing group in place of the fluorine of the G agents. The ester of all compounds differs in size and branching.

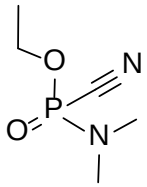

Ethyl dimethyl-phosphoramidocyanidate (Tabun or GA)

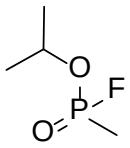

O-Isopropyl methylphosphonofluoridate (Sarin or GB)

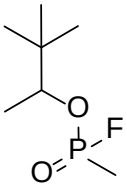

Pinacolyl methylphosphonofluoridate (Soman or GD)

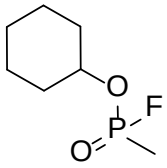

Cyclohexyl methylphosphonofluoridate (Cyclosarin or GF)

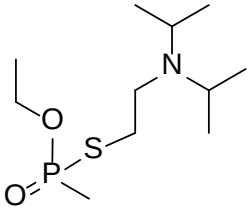

O-ethyl S-[2-(diisopropylamino) ethyl]methyl-phosphonothioate (VX)

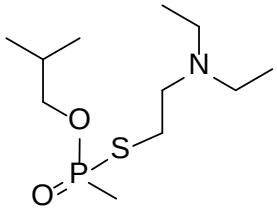

N,N-diethyl-2-(methyl-(2-methylpropoxy) phosphoryl) sulfanylethanamine (VR)

Figure 1-1. Chemical structures of G- and V-class OP nerve agents.

1.2.2 Mode of Action

All nerve agents cause toxicity via the same mechanism. At a molecular level, OP nerve agent acts as a covalent inhibitor of the enzyme acetylcholinesterase (AChE), thereby rendering it incapable of hydrolyzing the neurotransmitter acetylcholine (Figure 1-2) [9]. The continued presence of excess neurotransmitter causes overstimulation of the neuron, leading to many physiological symptoms including seizures, respiratory failure and, without intervening treatment, death.

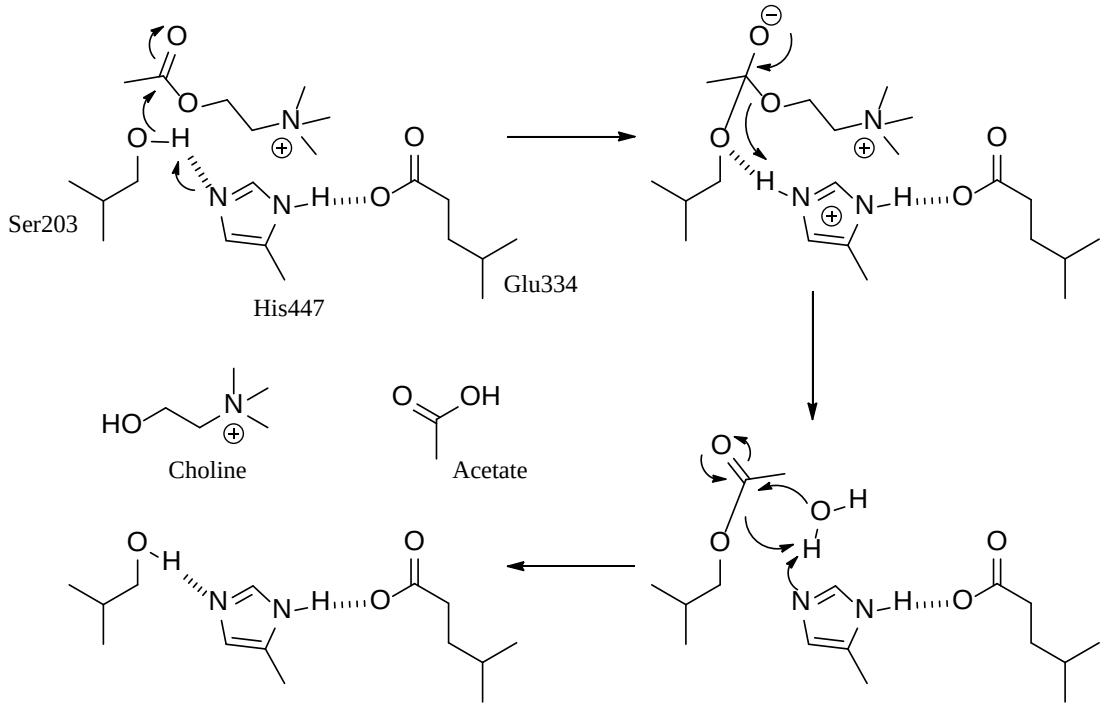

Figure 1-2. Acetylcholinesterase mechanism of acetylcholine hydrolysis.

The inhibition of AChE occurs when the nerve agent forms a covalent bond with the active site serine (203) of the enzyme. Upon bond formation, fluorine (GB, GD, and GF), cyanide (GA), or a sulfur-containing group (VX and VR), commonly

referred to as the leaving group, is released by the OP (Figure 1-3). All nerve agents have at least one stereocenter (GD has two) and therefore at least two stereoisomers. In all cases, AChE is known to preferentially bind one of these stereoisomers: the stereoisomer with the phosphorus in the S (P^S) or minus (P(-)) configuration [10-13]. This detail was used for experimental design purposes in Chapter 3.

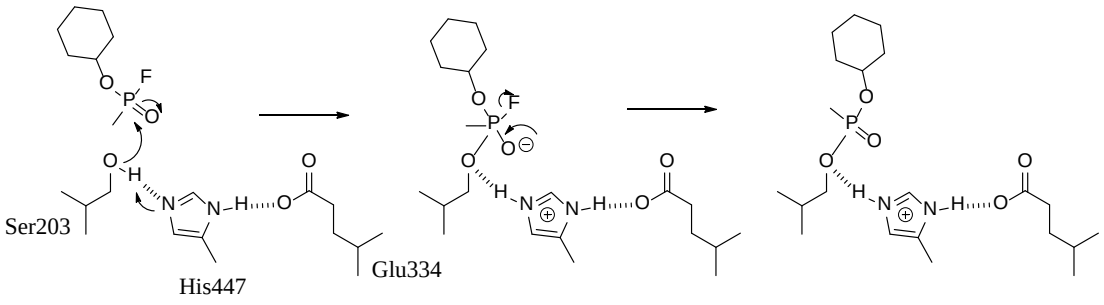

Figure 1-3. Mechanism of OP nerve agent (GF) inhibition of AChE.

Once AChE is inhibited by an OP nerve agent, a secondary dealkylation of the ester, known as “aging,” occurs at rates dependent upon the identity of the OP nerve agent and environmental factors (Figure 1-4) [14, 15]. This dealkylation event leads to a negatively charged adduct on the active site serine of AChE [14, 16] which is unable to be removed by current means, an important detail for the work discussed in Chapters 2 and 3.

Organophosphorus compounds that have structures similar to nerve agents but are not nearly as toxic have been used as pesticides worldwide [17]. This reduced toxicity, coupled with strict government regulations on the use of nerve agents, have led to the use of these pesticides as an alternative to OP nerve agents for study in many

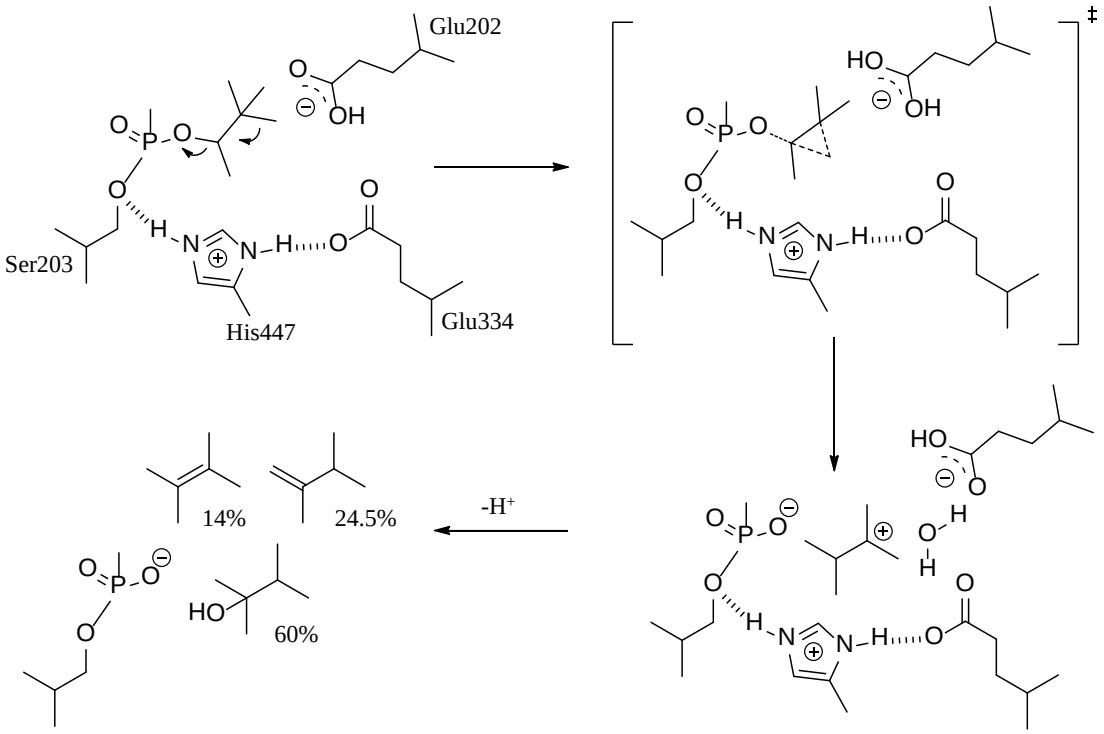

Figure 1-4. Mechanism of dealkylation event known as “aging” in GD-inhibited AChE [15]. Transition state is indicated in brackets. Products are indicated at the levels detected as a percentage of the total.

research laboratories. Unfortunately, treatments developed using OP pesticides are often not effective to the same degree against OP nerve agents. Despite the structural and reactivity differences between pesticides and nerve agents [18], some pesticide studies, such as the high through-put screening study referenced in Chapter 2, have led to breakthroughs in nerve agent research.

1.3 Prophylactics and Treatments of OP Nerve Agent Intoxication

The symptoms of intoxication progress rapidly from miosis to death when the subject is exposed to lethal doses of OP nerve agents [19-21]. In efforts to save the lives of victims of nerve agent exposure, two major areas of research have emerged: 1)

prophylactics, or pre-treatments, which can be administered to a subject before the exposure event to provide protection from intoxication and 2) treatments, meant to be administered after exposure, for both the alleviation of the cause of intoxication (AChE inhibition) and mitigation of secondary symptoms (respiratory depression, overstimulation of acetylcholine receptors, secondary activation of convulsions) [1]. While the following work focuses on the development of treatments for AChE inhibition, which is the cause of intoxication, general knowledge of other avenues of research is useful for later discussion and comparisons.

1.3.1 Prophylactics and Pretreatments

Prophylactics and pretreatments for nerve agent intoxication are most useful for the military community, which may have knowledge of possible exposure prior to the event such as in the case of entering a battlefield, or first responders, who would be responding to an exposure event to treat victims. To these ends, compound-based pretreatments and enzyme-based bioscavenger prophylactics have been explored.

Pyridostigmine bromide (PB), a carbamate pretreatment for nerve agent exposure currently used by the U.S. military, is a reversible covalent inhibitor of AChE [22-26]. When this compound is present at a sufficient level before exposure to an OP nerve agent, the covalent interaction with the active site serine of AChE sequesters this enzyme from any interaction with the nerve agent [22]. As nerve agent rapidly clears from the body, these sequestered AChE molecules are able to regain acetylcholine hydrolysis activity as they become disassociated from PB. The protection provided by PB hinges on the balance between maintaining a level of the drug that will sequester enough AChE to be effective in the event of a nerve agent exposure while not causing any undesirable side effects resulting in stringent

procedures for use [27]. Given the safety concerns for this sort of pre-treatment, especially in the event of misuse, the search for safer and more effective prophylactics has moved to the study of bioscavengers.

Bioscavengers are comprised of molecules, where to date only proteins have been successful candidates, which can interact with nerve agent before it can reach the nerve junction areas where AChE activity is critical for survival [1, 28]. To this end, two separate types of bioscavenger proteins have been studied: 1) stoichiometric bioscavengers, generally enzymes such as cholinesterases that irreversibly bind nerve agent molecules, and 2) catalytic bioscavengers, which not only bind to nerve agents but catalyze hydrolysis into less toxic products.

Currently, human butyrylcholinesterase (BuChE) is one of the most studied stoichiometric bioscavengers. This enzyme, thought to be a result of a duplication event of the gene encoding AChE [29], is present in human blood plasma and, while it hydrolyzes acetylcholine, does not have any known physiological function in humans [30, 31]. Studies comparing AChE with BuChE have uncovered the major differences between these enzymes, including structural alterations and variances in expression. In humans, BuChE is typically found as a soluble tetramer in blood plasma [32] whereas the major form of AChE is a “tailed” form which associates with anchoring proteins such as ColQ, primary as a dimer or tetramer, at cholinergic synapses [33]. Structurally, BuChE differs from AChE in three main regions: the peripheral binding site [34], the gorge leading to the active site, and the acyl binding pocket within the active site [35]. In all three locations, large aromatic residues found in AChE have been replaced by smaller, hydrophobic residues in BuChE, allowing the enzyme to more easily accommodate the larger substrate butyrylcholinesterase[36]. Additionally,

these amino acid substitutions account for the selective inhibition of BuCHE by bisquaternary inhibitors as compared to AChE [34]. Finally, as a result of the structural differences noted above, while BuChE is inhibited by nerve agents in a manner identical to AChE, the enzyme undergoes aging at differing rates [37] , an important factor in Chapter 3.

By binding nerve agent in the blood before it can enter the central nervous system, BuChE acts as a nerve agent "sink," sequestering one molecule of agent per molecule of BuChE away from AChE and increasing the level of nerve agent required to induce intoxication. Both human plasma-derived and recombinant forms of BuChE have been shown to successfully provide protection against nerve agent intoxication in animal models [38-40]. Recently, some work has been done to show that with certain nerve agents administered via specific routes, BuChE may be useful as a post-exposure treatment as well as a prophylactic [41-43].

While attempts have been made to design catalytic functionality into the stoichiometric bioscavenger BuChE [44, 45], these efforts generated enzymes that displayed limited hydrolytic activity and provided no protection *in vivo*. In contrast, several other candidate catalytic bioscavengers that show much greater protective efficacy against a variety of nerve agents have been engineered; the two front-runners are evolved variants of human paraoxonase 1 [46-51] and organophosphorus hydrolase originally discovered in *Brevundimonas diminuta* [52-55]. These enzymes have several advantages over stoichiometric bioscavengers, including the fact that each molecule of enzyme can bind and hydrolyze multiple molecules of nerve agent, allowing one dose of a catalytic bioscavenger to possibly protect against several exposure events, depending upon the stability of the enzyme in circulation [56, 57].

While all prophylactics offer some protection against nerve agent intoxication, they need to be administered prior to exposure in order to be most effective. This is unlikely to happen in the event that nerve agents are used in terrorist attacks or other scenarios where the agents are released amongst the civilian population. Once an exposure event has occurred, treatments are the only viable course of action to increase survival.

1.3.2 Treatments

Current treatments for nerve agent intoxication can be grouped into two major categories: indirect and direct treatments. Compounds such as atropine and diazepam indirectly treat intoxication by moderating the symptoms. Atropine achieves this by inhibiting the receptor of acetylcholine to minimize signal induction by excess acetylcholine, while diazepam acts as an anticonvulsant by binding to gamma-aminobutyric acid (GABA) receptors [58]. While these treatments modulate the effects of OP intoxication, the cause of the symptoms (inhibition of AChE) is not affected by these drugs.

The only direct treatment of OP intoxication currently fielded is a class of compounds commonly referred to as oxime-based AChE reactivators (Figure 1-5). These compounds act directly on OP-inhibited AChE, and BuChE, to return the enzyme to an active conformation by removing the bound phosphonyl moiety via a direct nucleophilic attack mechanism (Figure 1-6). This mechanism is known to occur both in the enzyme active site (reactivation [59, 60]) and in a direct manner in solution (known as oximolysis [61]), an important point in Chapter 3.

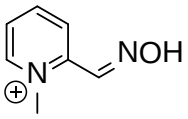

2-[(hydroxyimino) methyl]-1-methyl pyridinium (2PAM, Pralidoxime)

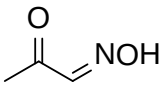

Monoisonitrosoacetone (MINA)

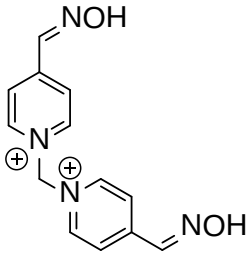

1,1'-Methylenebis[4-[hydroxyimino) Methyl]-pyridinium (MMB4)

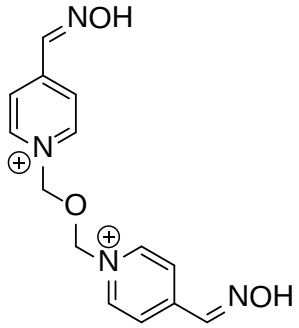

1,1'-[oxybis(methylene)]bis-4-(hydroxyimino)methyl] pyridinium (LuH-6, Obidoxime)

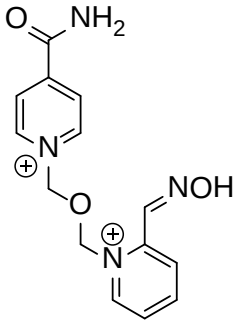

1-(((4-(aminocarbonyl)pyridinio) methoxy)methyl)-2-((hydroxyimino)methyl) pyridinium (HI-6, Asoxime)

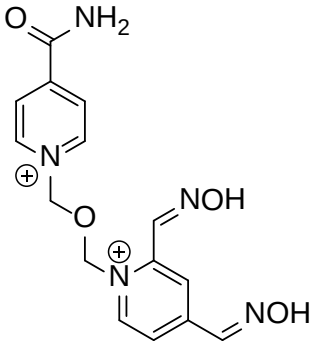

1-(((4-(aminocarbonyl)pyridinio) methoxy)methyl)-2,4-bis((hydroxyimino)methyl) pyridinium (Hlo-7)

Figure 1-5. Structures of common oxime-based reactivators.

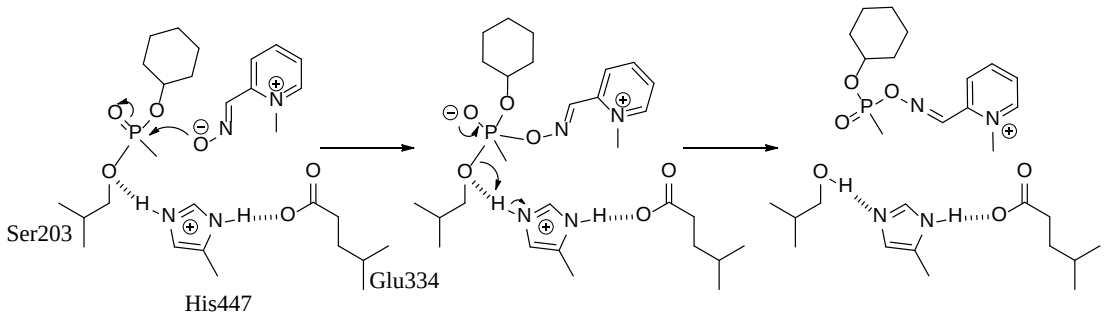

Figure 1-6. Oxime-based nucleophilic reactivation mechanism [63].

While currently recognized as the best treatment for OP nerve agent intoxication, oxime-based reactivators have several drawbacks. First, as seen in Figure 1-5, all currently fielded reactivators, with the exception of MINA, which is currently not fielded by any army, incorporate a permanent positive charge in the chemical structure. This charge has two major effects: 1) it acts to lower the pK_a of the oxime moiety, thereby making it more likely to act as a nucleophile at a physiologically relevant pH [62], and 2) by imparting a permanent charge to the molecule, it greatly reduces/eliminates the passage of the compound across the blood brain barrier [64]. MINA demonstrates that this lack of brain penetrance by charged pyridinium oxime reactivators is important because this molecule increases protection against nerve agent intoxication despite greatly decreased reactivation potential *in vitro* [65, 66]. The importance of reactivation in the brain has been established and is a driving force behind the search for novel reactivators that can cross into the central nervous system.

1.4 Reactivation Techniques and Theories

The *in vitro* characterization of reactivators is a common starting point for evaluating suitability for *in vivo* testing of efficacy against nerve agents provided by

these compounds. As with all assays developed to measure interactions at the active site of an enzyme, several compromises are made to create a system that mirrors *in vivo* conditions while simultaneously simplifying the parameters of the experiment. In order to discuss these variables for reactivation, a general discussion of enzyme kinetics is required.

1.4.1 Enzyme Kinetics

Generally, the kinetic parameters of an enzyme, especially those of a model enzyme like AChE, are described using the Michaelis-Menten model of kinetics [67]. In short, the initial rate of hydrolysis of a substrate at varying concentrations is measured using a fixed amount of enzyme, and these rates are then plotted against the concentrations of substrate. The resulting data are curve fit using an equation that incorporates the variables maximum rate of hydrolysis (V_{max}) and apparent binding affinity of the substrate (K_M; Figure 1-7). Several assumptions are made in order to use this simple system for modeling enzyme activity: 1) the concentration of the substrate does not change during the initial rate measurement (free ligand approximation), 2) the amount of enzyme-substrate complex does not change (steady state approximation), and 3) the rate of product formation is much slower than the rate of substrate binding and dissociation (rapid equilibrium approximation).

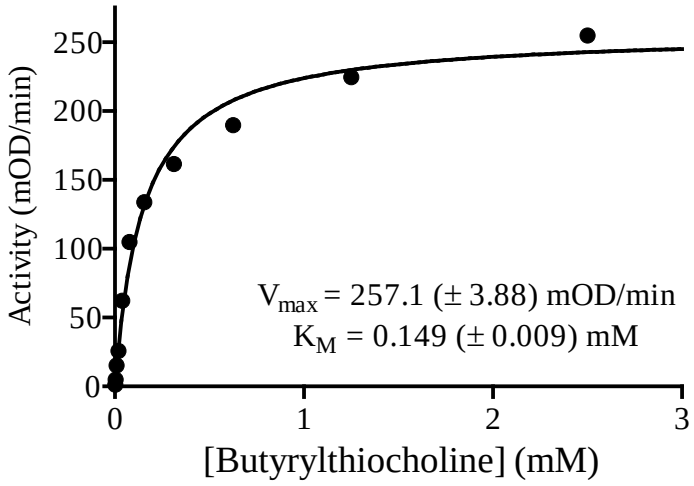

Figure 1-7. Example of Michaelis-Menten kinetic parameter determination using a colorimetric assay to measure the rate of substrate (butyrylthiocholine) hydrolysis by a recombinant form of butyrylcholinesterase.

The commonly used *in vitro* substrate system for AChE is acetylthiocholine (AtCh), which is hydrolyzed by the enzyme to acetyl and thiocholine. The thiocholine then interacts with dithionitrobenzoic acid (DTNB, Ellman's Reagent [68]) to form the easily detectable product 2-nitro-5-thiobenzoate (TNB). The formation of TNB is faster than that of thiocholine, so this system is an excellent reporter even for AChE, which is known to work at diffusion-limited rates except in the presence of AtCh concentrations that cause substrate inhibition [69]. This substrate inhibition behavior must be considered when designing experiments to determine parameters for reactivators such as enzyme inhibition and reactivation.

1.4.2 Reactivation Theory

Reactivation kinetic parameters are typically determined using a pseudo-Michaelis-Menten model (Figure 1-8) in which the inhibited phosphonylated enzyme and reactivator associate to form an intermediate complex which can then dissociate to the starting materials or undergo reactivation in which the phosphonyl group is removed from the enzyme active site [18, 70-73].

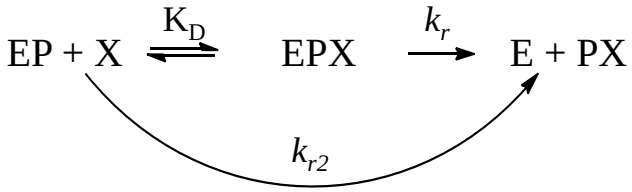

Figure 1-8. Reactivation scheme depicting pseudo-Michaelis-Menten kinetics [18].

Using this model, the dissociation constant (K_D), which is inversely proportional to the affinity of the reactivator for the phosphonylated enzyme, and the reactivation rate constant (k_r) for the removal of the phosphyl residue from the enzyme of a particular reactivator against a specific nerve agent can be determined. These parameters are determined by measuring the reactivation of inhibited enzyme over time at varying concentrations of reactivator. Using linear or non-linear regression analysis, the observed rate of reactivation (k_{obs}) is calculated by plotting the percent reactivation versus time for each concentration of reactivator. These values can then be replotted against the reactivator concentrations ([R]) tested, similar to a Michaelis-Menten substrate vs. velocity comparison, and fit using Equation 1. An overall reactivation rate constant (k_{r2}), calculated from the ratio of k_r and K_D, can be used to

compare the efficiency of reactivators. Alternatively, the half-time of reactivation ($t_{1/2}$, the time required to reach 50% reactivation in the presence of a specific reactivator concentration) can be used for comparison purposes if materials are available in limited quantities, similar to experimental methods described in Chapter 2.

$$k_{obs} = \frac{k_r \times [\mathrm{R}]}{K_D + [\mathrm{R}]} \quad (1)$$

As with Michaelis-Menten kinetics, some assumptions are made to validate this model: 1) reactivation will continue to completion (all enzyme will be dephosphonylated by the reactivator) and 2) the reactivator concentration is in excess of the initial concentration of inhibited enzyme (similar to the assumption that substrate is in excess of enzyme in the Michaelis-Menten system). While the second assumption is easy to confirm, the first can pose a problem given the aging phenomenon mentioned earlier in this chapter. Since the amount of aged enzyme increases over time, the dealkylation event is generally avoided as much as possible by measuring reactivation over a relatively short period of time (< 1 hour) and performing data analysis with the assumption intact.

1.4.3 Reactivation Techniques

As an important note to the discussion above, no laboratory method directly measures the reactivation event. The technique currently used to measure reactivation relies on the fact that the main product of reactivation is uninhibited enzyme which can hydrolyze substrate. To this end, reactivation assays are a discontinuous measurement of the amount of active enzyme in aliquots of a sample of inhibited enzyme that has been exposed to reactivator. This activity is compared to the activity

of a time-matched control to calculate the percent reactivation. These percentages at discreet time points are used to calculate the observed rate of reactivation.

While this method is effective, minute changes to details in experimental design can greatly change the assay. For instance, the source of enzyme (common sources include red blood cell ghosts and purified recombinant protein expressed in mammalian or insect systems), the method of inhibition (titration versus exposure to molar excess of agent followed by removal of unbound agent), along with standard enzyme assay concerns such as buffer, pH, and temperature, can greatly affect measurements of reactivation. Additionally, reactivator interaction with the AtCh/DTNB reporter system used to measure activity and direct inhibition of AChE by the reactivator can become concerns for some reactivators such as the one discussed in Chapter 2. Finally, the amount of sample handling by the operator and data manipulation required during analysis can introduce a large amount of error into the values generated using this method. However, at this time, no viable alternative to the indirect reactivation assay exists, a subject further discussed in Chapter 4.

1.5 Dissertation Overview

Novel reactivators are needed that can both eliminate the need for the pyridinium oxime moiety and thereby eliminate the need for the permanent positive charge which impedes passage into the brain. The work presented here characterizes a novel reactivator of nerve agent-inhibited AChE that does not rely on an activated oxime to mediate reactivation.

Chapter 2

A NOVEL REACTIVATOR: INITIAL CHARACTERIZATION AND STRUCTURE-ACTIVITY RELATIONSHIP

(Contents of chapter drawn from manuscript submitted for publication [74].)

2.1 Initial Discovery and Characterization of ADOC

In a study using high through-put screening to search for novel reactivators of AChE inhibited by the OP pesticide diisopropyl fluorophosphate (DFP), Katz *et al.* identified 4-amino-2-((diethylamino)methyl)phenol (**1**; ADOC; Figure 2-1) as a small molecule of interest [75]. In collaboration with these scientists, the United States Army Medical Research Institute of Chemical Defense (USAMRICD) tested ADOC *in vitro* for reactivation potential with recombinant human acetylcholinesterase (HuAChE) inhibited by sarin (GB) or VX. While reactivation was noted in both cases, complete reactivation to uninhibited HuAChE activity levels was not observed at the highest concentrations of reactivator tested (Figure 2-2).

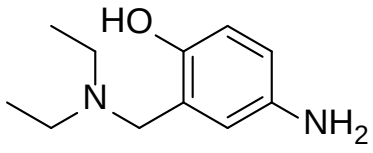

4-amino-2-((diethylamino) methyl)phenol (ADOC)

Figure 2-1. Chemical structure of ADOC.

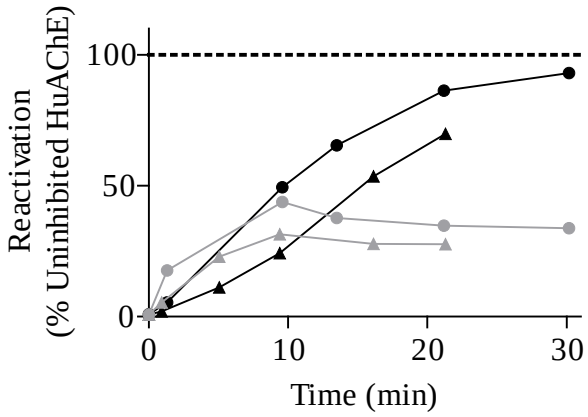

Figure 2-2. Initial reactivation by ADOC of HuAChE inhibited by GB (▲) or VX (●). ADOC present at 1 mM (grey) or 0.1 mM (black). Each time-point was measured in triplicate. Errors bars are smaller than data point symbols.

To determine if the lack of complete reactivation in the presence of 1 mM ADOC was due to direct inhibition of the apo enzyme by the reactivator, IC_{50} values (the concentration of compound at which enzyme activity is one half that of uninhibited enzyme) for ADOC (17.8 µM) and 2PAM (456 µM) were determined at a fixed concentration of HuAChE (Figure 2-3, Section 6.2.1). In a clinical setting, 2PAM is administered at a dose of 145 µmol/kg [76], translating to a maximum theoretical concentration of ~2 mM in human blood plasma. This estimate assumes that a 70 kg adult has 5 L of blood and the full dose of administered drug reaches the blood stream. A study showed that in fact only a maximum 2.5% to 3% of 2PAM can be detected in the plasma after intramuscular injection [77], equating to a plasma concentration of approximately 60 µM after administration of the current recommended emergency treatment (Mark I Nerve Agent Antidote Kit) of three autoinjector doses per patient displaying symptoms of nerve agent exposure [76]. The

IC_{50} determined in this study (456 µM) suggests that 2PAM at the above concentration would not cause toxic effects via acetylcholinesterase inhibition. However, ADOC (IC_{50} = 17.8 µM) administered at a similar dose could result in toxic effects from the direct inhibition of acetylcholinesterase, assuming that the molecule has a pharmacokinetic profile similar to that of 2PAM.

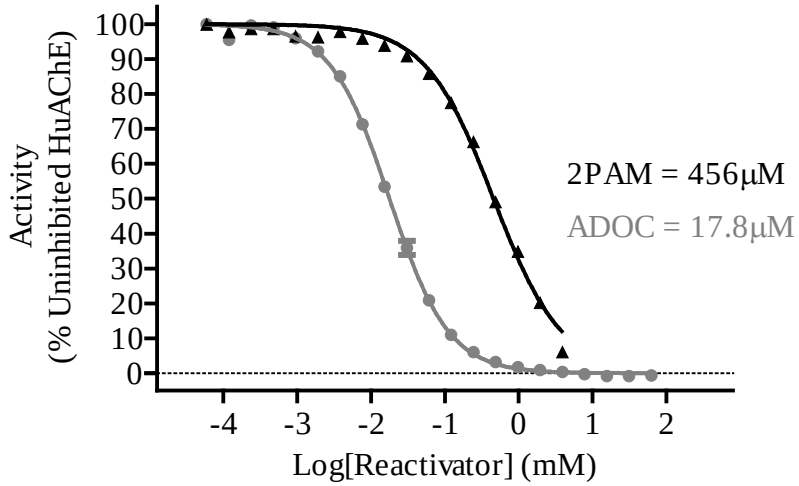

Figure 2-3. IC_{50} of ADOC(●) and 2PAM (▲) measured with HuAChE.

Reactivation of OP-inhibited HuAChE is generally measured using an established discontinuous, indirect method. In short, the activity of an enzyme sample that has been inhibited by an OP is monitored and compared to a buffer-matched uninhibited control at several time points after the addition of a reactivator, typically at a variety of concentrations (Section 6.2.3). Because the high level of inhibition displayed by ADOC against apo HuAChE could interfere with *in vitro* reactivation testing, a traditional inhibition assay was conducted to determine the type of inhibition

caused by ADOC (Figure 2-4, Section 6.2.2). The referenced figure displaying the linear regressions of the inverse velocity of the enzyme versus the inverse substrate concentration at increasing concentrations of ADOC intersecting at a positive y-value and a negative x-value (not directly on either axis) is a classic example of a mixture of competitive (K_i = 6.3±0.9 µM) and noncompetitive (K_i' = 37.4±2.1 µM) reversible inhibition. Mixed inhibition suggests the possibility of two binding sites for ADOC, a finding in agreement with Katz *et al*. [75], who proposed this idea after observing that reactivation rates of pesticide-inhibited HuAChE plotted versus ADOC concentration appeared sigmoidal in nature, generally indicating cooperativity, a phenomenon discussed later.

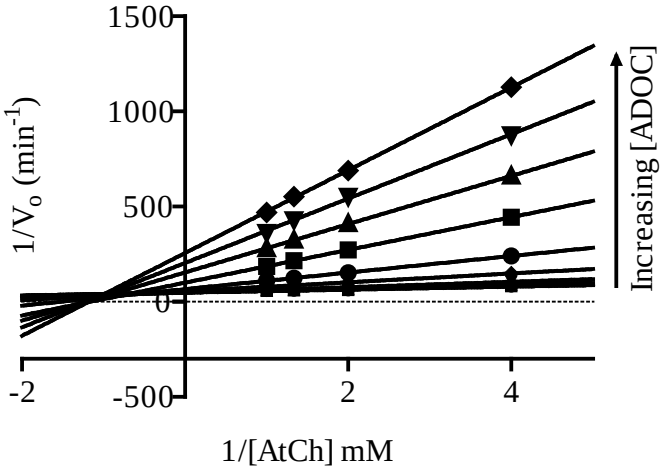

Figure 2-4. Inhibition assay for ADOC as the inhibitor using AtCh as the competitive substrate in HuAChE.

Given these results, the extent of inhibition of HuAChE by reactivator molecules (ADOC or 2PAM) needed to be controlled for in all subsequent experiments. To accomplish this, the activity of the enzyme in the presence of each concentration of reactivator (absent any OP) was used as the baseline activity level (100%) for the corresponding OP-inhibited sample. This was crucial to allow for the determination of appropriate experimental parameters used to test the reactivation potential of ADOC against nerve agent-inhibited HuAChE.

As an additional note, cooperative behavior, the condition in which more than one molecule must bind to an enzyme to achieve maximum activity (substrate activation is a well-known example of this), was previously described during ADOC-mediated reactivation of HuAChE after inhibition with OP pesticides [75]. No evidence of this was observed in the following experiments under the conditions described, and no attempts were made to analyze the data using a cooperativity model. Upon closer inspection of the article that describes this cooperativity phenomena, the behavior noted could have been due to the experimental conditions used by the author, which included an extended incubation of enzyme and reactivator (3 hours) prior to measuring reactivation and a substrate concentration that can cause substrate inhibition [78] especially at the enzyme/substrate concentration ratios used.

2.2 Reactivation Potential of ADOC

Under experimental conditions controlling for reactivator inhibition, the kinetic parameters of reactivation by ADOC and 2PAM of HuAChE inhibited by various OP nerve agents were measured using established reactivation methods (Figure 2-5, Section 6.2.3) [18, 70, 71, 79, 80]. In the cases of GB, GF, VX, and VR the rate of reactivation (k_r, Figure 1-8) by ADOC (0.34±0.14 min^{-1}, 0.13±0.03 min^{-1}, 0.50±0.20

min^{-1}, 4.01±2.37 min^{-1}, respectively) was 3- to 67-fold greater than that mediated by 2PAM (0.06±0.02 min^{-1}, 0.04±0.02 min^{-1}, 0.06±0.01 min^{-1}, 0.06±0.04 min^{-1}, respectively). This increase was only statistically significant in the case of GB, VX, or VR-inhibited HuAChE but overall was an indication that ADOC is better able than 2PAM to perform the removal of the nerve agent adduct from the active site of HuAChE. However, the dissociation constant (K_D) of ADOC (7.61±4.07 mM, 4.45±3.37 mM, 2.08±0.94 mM, 5.46±2.02 mM respectively) relative to 2PAM (0.71±0.13 mM, 2.43±0.65 mM, 0.54±0.15 mM, 1.34±0.79 mM respectively) was similarly elevated, again with statistical significance in the case of GB, VX, and VR. This trend indicates that 2PAM displays better affinity for the active site of inhibited HuAChE than does ADOC.

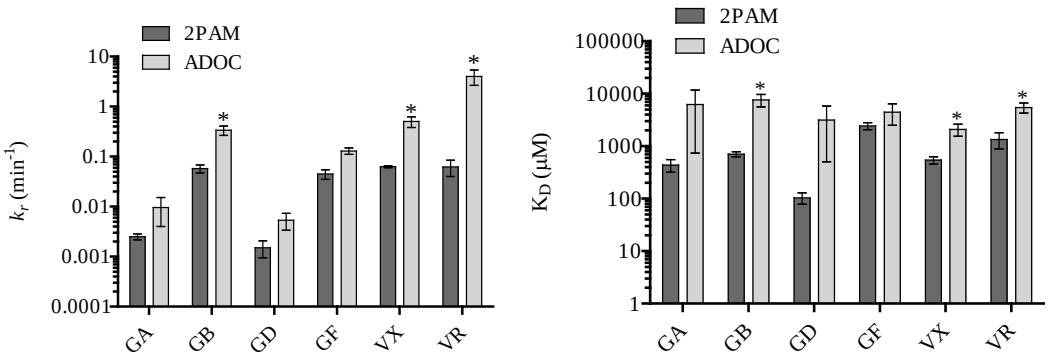

Figure 2-5. Reactivation rate constants (k_r, min^{-1}) and dissociation constants (K_D, μM) for the reactivation of inhibited HuAChE by 2PAM (dark grey) and ADOC (light grey). Significant differences between 2PAM and ADOC values are indicated by *(t-test, $p<0.05$).

The increase in both the reactivation rate constants and the dissociation constants of ADOC as compared to 2PAM results in only one significant increase in

reactivation efficiency (overall rate constant of reactivation ($k_r/K_D = k_{r2}$)) by ADOC relative to 2PAM: that for the reactivation of HuAChE inhibited by VR (Table 2-1).

Table 2-1. Overall reactivation rate efficiency (k_{r2}) for 2PAM and ADOC with several agents.

Reactivator	k_{r2} (M^{-1} min^{-1})					
	GA	GB	GD	GF	VX	VR
2PAM	7.0 ±4.4	81.0 ±16	17.6 ±16	18.4 ±4.2	121 ±29	46 ±1.2
ADOC	4.5 ±3.3	45.4 ±7.2	5.6 ±4.1	40.5 ±29	266 ±109	719* ±386
Standard deviation of three independent experiments is indicated below value. Statistically significant increase of reactivation rate by ADOC as compared to 2PAM is indicated by *(t-test, $p<0.05$).						

While this result is slightly disappointing, the opportunity does exist to design novel reactivators using ADOC as a scaffold if the molecular components responsible for the mechanism of reactivation and those important for binding can be identified. With this in mind, a structure-activity relationship (SAR) study was undertaken.

2.3 Structure-Activity Relationship Study of ADOC

2.3.1 Determining the Importance of the Ring Substituents of ADOC

An initial structure-activity relationship study was conducted using several ADOC structural analogs. As a general explanation of the assay conducted, the reactivation potential of analogs was determined using nerve agent-inhibited HuAChE. Each selected analog, along with ADOC and 2PAM as internal standards, was added (final concentration of 1 mM) to aliquots of a single batch of inhibited

enzyme and a buffer-matched apo control. Reactivation was measured at several time-points by removing a small aliquot of each reaction and measuring the activity against AtCh as described earlier. The reactivation levels over time were fit using a non-linear regression analysis to calculate the half-time of reactivation ($t_{1/2}$) for each analog. These experiments were conducted three times for each agent/analog combination. Every experiment contained an inhibited enzyme sample which only received buffer to act as a control for spontaneous reactivation. The reactivation potential of a given analog was compared to the reactivation of the spontaneous reactivation control by determining if there was a statistically significant decrease in the half-time of reactivation in the presence of the compound. To more easily compare these values, the fold increase in reactivation was calculated by determining the ratio of $t_{1/2spontaneous}$ to $t_{1/2compound}$ such that a larger ratio indicates a more effective reactivator. These values are reported in the following tables. As a visual reference, any analog that did not reactivate inhibited enzyme significantly faster than spontaneous levels has been colored grey.

First, the importance of each substituent of the benzyl ring for reactivation of OP nerve agent-inhibited enzyme was explored (Table 2-2). The removal of the aniline group, as in compound **2,** or the benzyl amine group, as in compound **3,** caused a decrease in the magnitude of reactivation as compared to ADOC but also substantially decreased the inhibitory effects on apo HuAChE. These combined results could indicate that these substituents play a role in binding rather than reactivation chemistry, especially in light of the fact that removal of the phenol substituent, as in compound **4,** abolishes all reactivation activity. Similarly, blocking the phenol, as an ether in compound **5,** causes the loss of reactivation potential against enzyme inhibited

Table 2-2. Initial exploration of active moieties of ADOC. Ratio (spontaneous/compound) of half-times ($t_{1/2}$) of reactivation for compounds (1 mM) with HuAChE after inhibition by the indicated agent.

		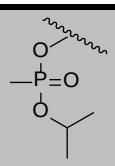 GB	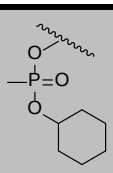 GF	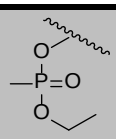 VX	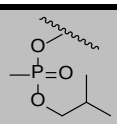 VR	Inhibition of HuAChE[Ŧ]
Spontaneous Reactivation ($t_{1/2}$ in days)		2.01 (±0.07)	1.25 (±0.14)	1.18 (±0.21)	0.35 (±0.07)	
1	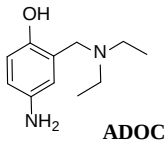 **ADOC**	361* (158-824)	164* (97.3-277)	1,069* (393.6-2911)	14,723* (6.46-33,573,761)	60% (±1)
2	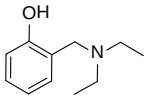	1.51* (1.12-2.03)	1.54* (1.34-1.78)	1.87* (1.24-2.84)	3.65* (3.14-4.24)	0% (±6)
3	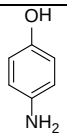	2.24* (1.98-2.53)	1.48* (1.15-1.91)	2.24* (1.16-4.32)	14.3* (8.86-23.0)	0% (±6)
4	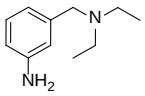	0.98 (0.81-1.20)	0.93 (0.89-0.97)	0.97 (0.66-1.43)	0.96 (0.61-1.51)	0% (±6)
5	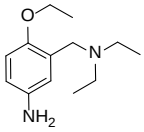	1.54* (1.28-1.84)	0.89 (0.77-1.03)	1.11 (0.53-2.34)	1.25 (0.90-1.73)	5% (±4)

* - indicates that $t_{1/2}$ in presence of compound is significantly less than spontaneous using a ratio t-test with $p<0.05$. Grey boxes are not significantly greater than spontaneous reactivation.
Standard deviation of at least three independent experiments is indicated for spontaneous reactivation half-times in days. Ninety-five percent confidence intervals of ratios are indicated below each value.
[Ŧ]All half-times were determined using HuAChE in the presence of 1 mM compound as the positive control. The far right column indicates the level of inhibition of HuAChE caused directly by the compound at the concentration in the reaction well (~24.4 μM) when compared to a buffer only control of HuAChE. Standard deviation of this value determined using controls from all independent experiments is indicated.

by three of the agents, with GB-inhibited HuAChE displaying greatly decreased reactivation as compared to ADOC. Taken together, these results strongly suggest that the phenol substituent is essential for reactivation.

2.3.2 The Role of the Benzyl Amine in ADOC

Given that **3**, in which the benzylic amine had been removed, was somewhat more reactive than **2**, in which the aniline was removed, additional analogs of ADOC were used to probe the importance of this substituent (Table 2-3). In **6**, altering the relative position of the benzylic diethylamine on the ring reduced the reactivation potential of the molecule but also nearly eliminated the inhibitory potential of **6** against apo HuAChE. Interestingly, reducing the bulk of the benzylic diethylamine in the form of the dimethylamine of **7** greatly increased the inhibitory potential of the molecule against apo HuAChE; however, this affect could be negated by again altering the relative position of this smaller dimethylbenzyl amine to a position *meta* to the phenol, as in **8**, similar to **6**. In the hope of counteracting the inhibitory effects of **7**, analog **9** incorporated diisopropylbenzyl amine at the position *ortho* to the phenol, effectively increasing the steric bulk at that site. Surprisingly, **9** also displayed increased inhibitory potential against apo HuAChE. Further increasing the bulk in **10** to a dicyclohexylbenzyl amine resulted in loss of both inhibitory potential and reactivation potential, most likely from sterically driven decreased binding of the small molecule to the HuAChE active site. Given all of these results and the relatively high pK_a (between 8.14 [81] and 8.66 [82]) of the diethylbenzyl amine, which would cause it to be mostly in a protonated state at physiological pH, it seems likely that this portion of the molecule contributes mainly to the binding strength, orientation and selectivity of ADOC rather than to playing a direct role in the reactivation functionality of the molecule. The possibility remains that this substituent could play an indirect role in reactivation, an idea that will be further explored in Chapter 3.

Table 2-3. Exploring the role of the benzylamine group of ADOC. Ratio (spontaneous/compound) of half-times ($t_{1/2}$) of reactivation for compounds (1 mM) with HuAChE after inhibition by the indicated agent.

		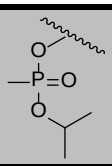 GB	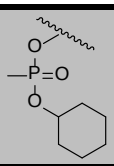 GF	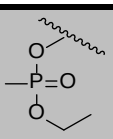 VX	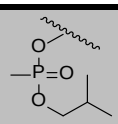 VR	Inhibition of HuAChE[Ŧ]
1	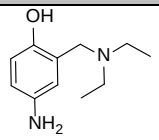 **ADOC**	361[*] (158-824)	164[*] (97.3-277)	1,069[*] (393.6-2911)	14,723[*] (6.46-33,573,761)	60% (±1)
6	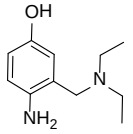	1.97[*] (1.54-2.52)	1.80[*] (1.46-2.22)	2.76[*] (1.95-3.93)	4.06[*] (3.01-5.49)	1% (±4)
7	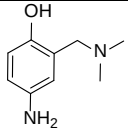	---	---	---	---	95% (±1)
8	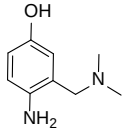	2.13[*] (1.63-2.78)	1.96[*] (1.92-2.01)	2.72[*] (2.12-3.48)	5.65[*] (1.20-26.5)	18% (±6)
9	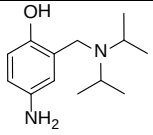	---	---	---	---	94% (±1)
10	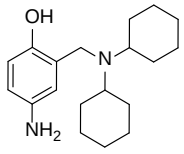	0.88 (0.65-1.20)	0.74 (0.60-0.90)	1.09 (0.60-1.98)	0.93 (0.76-1.14)	9% (±4)

---Reactivation could not be determined due to high level of inhibition by compound.
* - indicates that $t_{1/2}$ in presence of compound is significantly less than spontaneous using a ratio t-test with $p<0.05$. Grey boxes are not significantly greater than spontaneous reactivation.
Standard deviation of at least three independent experiments is indicated for spontaneous reactivation half-times in days. Ninety-five percent confidence intervals of ratios are indicated below each value.
[Ŧ]All half-times were determined using HuAChE in the presence of 1 mM compound as the positive control. The far right column indicates the level of inhibition of HuAChE caused directly by the compound at the concentration in the reaction well (~24.4 μM) when compared to a buffer only control of HuAChE. Standard deviation of this value determined using controls from all independent experiments is indicated.

2.3.3 The Role of the Aniline in ADOC

Additional studies were conducted to analyze the contribution of the aniline substituent to the reactivity of ADOC (Table 2-4). The role of the electron-donating potential of the aniline group was explored by both increasing the electron-donating potential, as in the dimethylaniline group of **11**, and decreasing that potential, as in the acetamide **12,** as compared to ADOC based on the reported Hammett values (σ_p) for these substituents [83]. While both of these modifications displayed significantly increased reactivation compared to spontaneous levels for all agents, reactivation was markedly decreased compared to that of ADOC. Additionally, the alteration of the aniline in both cases abolished all inhibition of HuAChE, raising the question of whether the decreased reactivation activity of these molecules was a result of decreased binding (increased K_D) or decreased reactivation rate (lower k_r). Measurement of these values (K_D: **11** = 0.39±0.23mM; **12** = 0.92±0.12mM; k_r: **11** = 0.07±0.02min^{-1}; **12** = 0.03±0.01min^{-1}) for each compound supports the conclusion that the loss of reactivation potential is due to a lower rate of reactivation rather than to a decrease in binding, a concept addressed again in Section 3.4.

Given these data, compounds **13** and **14**, which can still take advantage of the electron-donating affect (via the *meta* relationship of the aniline and the phenol) but were more sterically congested about the phenol, were tested for reactivation potential. While both of these compounds retained reactivation potential above that of spontaneous rates for some agents, reactivation rates were decreased by 100- to 10,000-fold compared to ADOC. Taken together, the results suggest that while the *para* relationship of the aniline to the phenol is important, this relationship may have more to do with positioning the phenol upon binding to the inhibited HuAChE enzyme than to any electronic effects of the substituent.

Table 2-4. Exploring the role of the aniline group of ADOC. Ratio (spontaneous/compound) of half-times ($t_{1/2}$) of reactivation for compounds (1 mM) with HuAChE after inhibition by the indicated agent.

		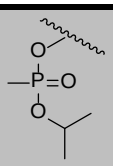 GB	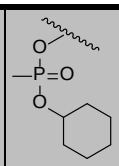 GF	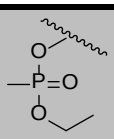 VX	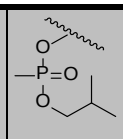 VR	Inhibition of HuAChE ₸	Hammett Values (σ_p) [83]
1	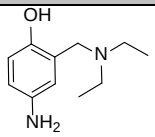 **ADOC**	361* (158-824)	164* (97.3-277)	1,069* (393.6-2911)	14,723* (6.46-33,573,761)	60% (± 1)	-0.66
11	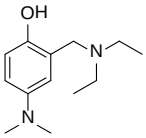	6.15* (4.98-7.60)	3.07* (2.92-3.23)	16.5* (13.0-20.8)	32.7* (24.1-44.4)	0% (± 6)	-0.83
12	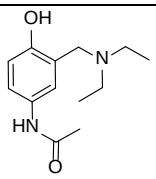	3.85* (3.22-4.61)	1.72* (1.67-1.77)	6.95* (5.03-9.59)	19.0* (15.2-23.7)	0% (± 5)	0.00
13	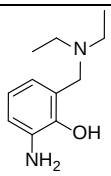	1.43* (1.37-1.50)	1.09 (0.80-1.49)	1.24 (0.99-1.56)	1.65* (1.54-1.78)	35% (± 4)	N/A
14	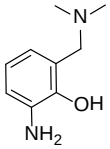	1.70* (1.40-2.06)	1.30 (0.90-1.89)	1.61* (1.17-2.21)	1.59* (1.35-1.87)	43% (± 11)	N/A

* - indicates that $t_{1/2}$ in presence of compound is significantly less than spontaneous using a ratio t-test with $p<0.05$. Grey boxes are not significantly greater than spontaneous reactivation.
Standard deviation of at least three independent experiments is indicated for spontaneous reactivation half-times in days. Ninety-five percent confidence intervals of ratios are indicated below each value.
₸All half-times were determined using HuAChE in the presence of 1 mM compound as the positive control. The far right column indicates the level of inhibition of HuAChE caused directly by the compound at the concentration in the reaction well (~24.4 µM) when compared to a buffer only control of HuAChE. Standard deviation of this value determined using controls from all independent experiments is indicated.

Recently, an article discussing the reactivation potential of the antimalarial drug amodiaquine (Figure 2-6) against nerve agent-inhibited HuAChE was published [84]. This molecule displayed modest reactivation potential against VX with reactivation occurring at a slower rate than that observed for ADOC (amodiaquine reactivated approximately 20% of VX-inhibited HuAChE in 30 minutes whereas ADOC at the same concentration reactivated >95%; see Figure 2-2). If amodiaquine is considered to be an ADOC analog with a large moiety attached to the aniline nitrogen, then this finding falls in line with compounds **11** and **12** discussed here and supports the hypothesis that the aniline, and any substituents attached at that site, are responsible for positioning the phenol in the active site. This idea may be further supported by the data of Bierwisch *et al*. [84] showing that amodiaquine-mediated reactivation of OP nerve agent-inhibited butyrylcholinesterase, which has a larger active site than HuAChE, occurs much faster.

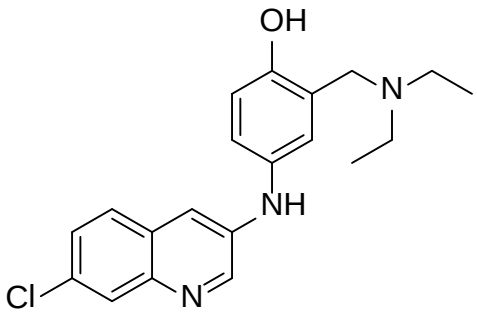

Figure 2-6. Structure of amodiaquine.

2.4 Summary

In summary, structural analogs were used to probe the mechanism of ADOC by systematically exploring the importance of each substituent of the benzyl ring. Both

the diethylbenzylic amine and the aniline appear to contribute to the binding, orientation, and specificity of ADOC. The possibility remains that these substituents may play indirect roles in the reactivation mechanism. Currently, only the phenol group appears to be essential for reactivation with functionality abolished when this substituent is removed or blocked.

Chapter 3

A NOVEL REACTIVATOR: MECHANISM OF REACTIVATION

Having identified the phenol substituent of ADOC as essential for the reactivation of OP nerve agent-inhibited HuAChE, the next goal was to determine the mechanism(s) by which reactivation occurs. Two potential mechanism categories were initially postulated: 1) the direct or indirect nucleophilic action of the phenol substituent or 2) the formation of a reactive quinone or semiquinone intermediate. Both of these possibilities are explored here.

3.1 General Properties of ADOC

An initial discussion of the chemical properties of ADOC seems appropriate before exploring the postulated mechanism of reactivation. ADOC incorporates several substituents around a benzyl ring allowing the molecule to take advantage of the delocalized nature of the π system of the aromatic ring [85]. This means that both the nature and position of the substituents are important, as discussed in Chapter 2 Section 2.3. As mentioned earlier, the aniline group, which is positioned *para*- to the phenol and *meta*- to the diethylbenzylic amine, displays electron-donating properties in similar molecules (σ_p = -0.66 [83]). Of interest is the fact that the phenol group also displays electron donating properties (σ_p = -0.37 [83]) though not as strongly as the aniline. The benzylic amine group would be neutral or slightly electron withdrawing depending upon the protonation state of the amine.

The protonation state of the benzylic amine is dependent upon the pK_a ($-\log_{10}$ of acid dissociation constant) of that group and the pH of the environment; if the pH is higher (more basic) than the pK_a, the group is less likely to be protonated, while if the pH is lower (more acidic) than the pK_a the reverse is true. The reported pK_a of diethylbenzyl amine is 9.48 [86]. However, studies of amodiaquine (Figure 2-6) have measured the pK_a of the benzylic amine to be 8.14 [81] and 8.66 [82], respectively, reducing the amount of this group that would be protonated from >99% (calculated using the Henderson-Hasselback equation [85]) to 93.3% to 97.9% at the pH used in this study (7.0). Hawley *et al*. [81] attribute this reduction in the pK_a of the benzylic amine to hydrogen bonding between the amine and the hydrogen of the phenol group. The phenol group, pK_a = 10.3 [87], is likely (>99%) to retain a hydrogen at physiological pH (7.4) which would be well positioned to interact with the lone pair electrons of the benzylic amine. Conversely, the aniline group, with a pK_a of 5.50 [88], is likely (96.9%) to be present in basic form. Taken together, the predominant form of ADOC in solution at the pH used in the experiments described here (7.0) is likely to resemble Figure 3-1, before any activation to an intermediate state.

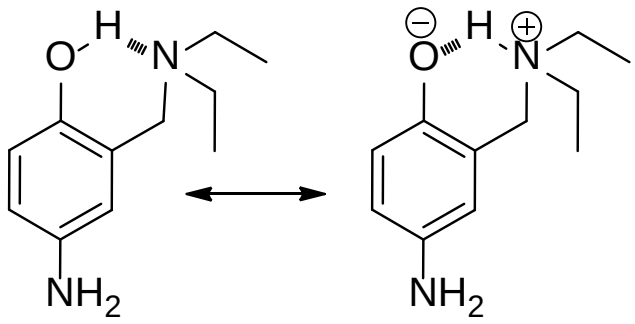

Figure 3-1. Predicted forms of ADOC in solution at pH 7.0.

3.2 Exploring Possible Mechanisms of ADOC-Mediated Reactivation

3.2.1 Direct and Indirect Nucleophilic Attack

The proposed initial form of ADOC (Figure 3-1), along with the structure – activity relationship study of Chapter 2, suggests the possibility that the phenol, with the hydrogen participating in a hydrogen bond with the benzylic amine nitrogen, could act as a nucleophile (Figure 3-2). This nucleophilic interaction could result in bonds forming with either the phosphorus atom of the OP adducted to HuAChE or with the hydrogen atom of a water molecule [75]. Precedents for both of these reactions exist. Oxime-mediated reactivation proceeds via direct nucleophilic attack of the phosphorus by the oxygen of the oxime group and leads to the production of a phosphonylated oxime product, which can be characterized using liquid chromatography and mass spectrometry [59, 60].

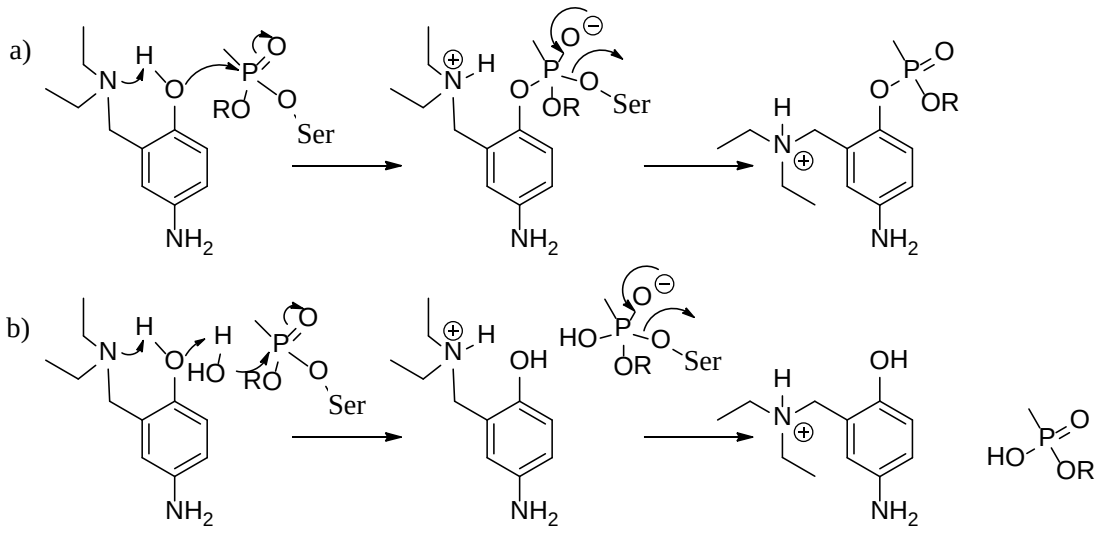

Figure 3-2. ADOC nucleophilic reactivation mechanisms. a) depicts the direct nucleophilic reactivation mechanism mediated by the phenol group. b) depicts the indirect nucleophilic reactivation mechanism mediated by the phenol group.

As an example of an indirect nucleophilic mechanism, a variant of human butyrylcholinesterase , the stoichiometric bioscavenger discussed in Section 1.3.1, in which a glycine as residue 117 has been mutated to a histidine (G117H BuChE) gained the capacity to hydrolyze OP nerve agents [89]. This hydrolytic activity has been postulated to be mediated by H117 acting as a general base which activates a water molecule that attacks the phosphorus center [90-92]. The phenol of ADOC acting similarly as a general base to create an activated water molecule may be a viable possibility as a reactivation mechanism.

The first interaction, a direct nucleophilic attack, would lead to the production of a phosphonylated ADOC product. Alternatively, the second interaction, an indirect nucleophilic attack, would generate a hydroxide ion which could then attack the OP adducted phosphorus, leading to the generation of a phosphonic acid product. While the phenol moiety of ADOC would be the most likely candidate for these reactions, the possibility remains that the aniline nitrogen could also participate in the same manner.

3.2.2 Interaction of ADOC with OP Nerve Agent in Solution

In an effort to determine if a direct interaction between ADOC and OP-nerve agent is possible, experiments monitoring the interaction of OP nerve agent and ADOC in a buffered solution were conducted. These experiments were meant to discover if ADOC can interact with nerve agent in a manner similar to oximolysis [61] and to other phenols [93]. If ADOC directly interacted with the OP in solution, then a product would form, and the structure of that product would likely be dependent upon the group (phenol or aniline) involved in a direct nucleophilic interaction. While these experiments were indicative of whether a product of direct interaction could form,

formation of any similar product during the reactivation of OP-inhibited enzyme is explored in later sections of this chapter.

3.2.2.1 Absorbance Shifts of ADOC and Products of Solution Reaction

Earlier work has shown that the products formed during oximolysis can be measured by tracking the shift of absorbance spectrums over time [61]. Given the aromatic nature of the chemical structure of ADOC, a similar approach was explored as a possible detection method for product formation in solution. The maximum absorbance of ADOC (λ_{max}) in a buffered solution at pH 7.0 was measured at 303 nm (Figure 3-3).

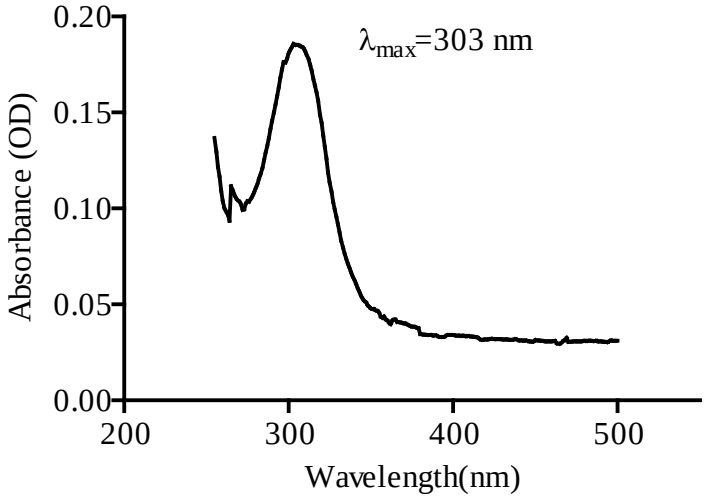

Figure 3-3. Absorbance spectrum of ADOC (λ_{max} = 303 nm).

With this initial value determined, agent was added to a final concentration at 100-fold molar excess of ADOC, and the absorbance spectrum of the solution was

measured at several time points (Figure 3-4). Over the course of a three-hour incubation, the maximum absorbance of the spectra of the solution of ADOC and either GF or GD shifted from 303 nm to 297 nm. Meanwhile, an ADOC-only negative control under the same conditions showed no shift over the same time frame. These results indicate that there is a direct reaction of agent and ADOC in solution which results in formation of a product with altered absorbance properties.

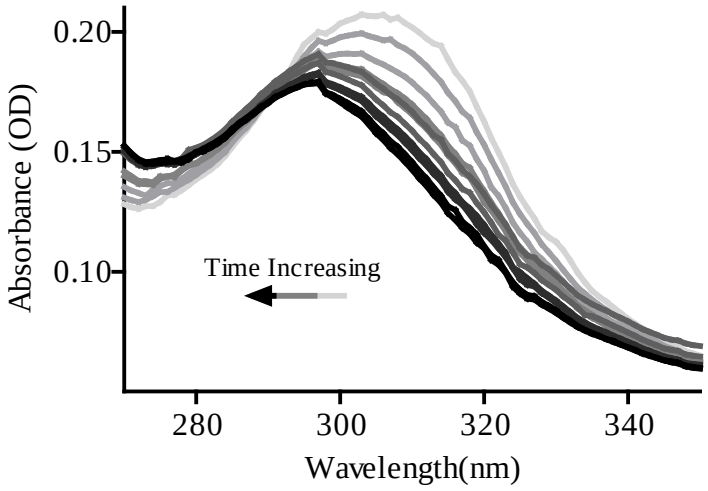

Figure 3-4. Absorbance spectra of the 180-minute time course of ADOC in the presence of 100-fold molar excess GF (λ_{max} shifts from 303 nm to 297 nm).

3.2.2.2 Liquid Chromatography/Mass Spectrometry Analyses

To further characterize the product formed during the experiment described above, the reactions were repeated and monitored by LC-mass spectrometry. Signal of the predicted mass/size ratio for products of both GF and GD direct nucleophilic attack interactions with ADOC (Figure 3-5) were detected (Figure A.1). Signal

strength of these ions increased as a function of time during the reaction, while the signal strength of the ion associated with $ADOC^{+1}$ decreased compared to a negative control (Figure A.2 and A.3). Notably, all of the predicted products of the direct interaction of ADOC via a nucleophilic substituent (either phenol or aniline) with GF or GD would have the same mass/size ratio, respectively, and cannot be differentiated using this technique.

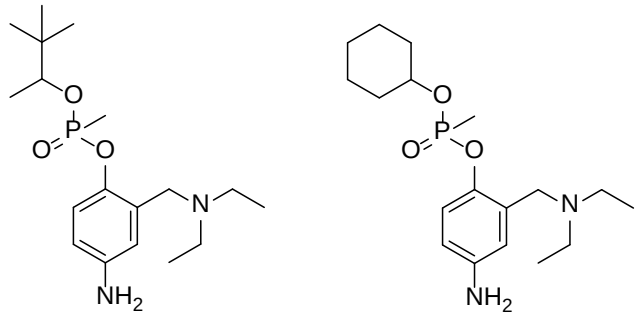

m/z: 356.22 (100%), 357.23 (20.0%), 358.23 (2.5%)

m/z: 354.21 (100%), 355.21 (19.9%), 356.21 (2.6%)

Figure 3-5. Predicted products of direct interaction of ADOC with GD (left) or GF (right). Calculated mass/size ratio (m/z) for each product is displayed at the bottom. Note: Products with adducts attached at the aniline nitrogen would result in the same mass/size ratios.

Previously, phosphylated oximes have been purified using chromatographic methods [59, 60], so this approach was explored as a way to purify the product of the direct reaction of ADOC with GF in the hopes of determining the structure of the molecule. Because ADOC is not highly soluble in organic solvents, a reverse-phase chromatography system was utilized. After exploring several different conditions, a simple water/methanol gradient mobile phase was utilized with a C-18 functionalized

column to purify the product of the direct interaction of GF and ADOC in solution (Figure A.4 and A.5). Initially, two distinct products with different retention times and conditions were detected; these were later determined to be the protonated and non-protonated forms of the same product (Figure A.6).

3.2.2.3 ADOC/Agent Reaction Product Structure

3.2.2.3.1 High Resolution Mass Spectrometry and NMR

The purified product of ADOC and GF in solution was analyzed using high resolution mass spectrometry to determine exact mass (355.2156 m/z) and elemental composition, which corresponded to the predicted products in Figure 3-5 (Figure A.7 and A.8). Nuclear magnetic resonance (NMR) experiments were performed in an effort to determine the absolute structure of the molecule. A carbon (^{13}C) NMR spectrum verified the presence of all expected carbons in the molecule (Figure A.9). A proton (^{1}H) NMR spectrum was able to verify the presence of three protons attached to the aromatic ring (Figure 3-6). These signals were later clarified using heteronuclear multiple-quantum correlation (HMQC) NMR to verify the bonding of these protons to aromatic carbons (Figure A.10). This information will be referenced again later in this chapter while discussing other possible mechanisms of reactivation. While this information confirmed that the purified product was indeed a result of the direct interaction of GF and ADOC, NMR could not differentiate between the attachment of the phosphorus moiety at the phenolic oxygen or the aniline nitrogen.

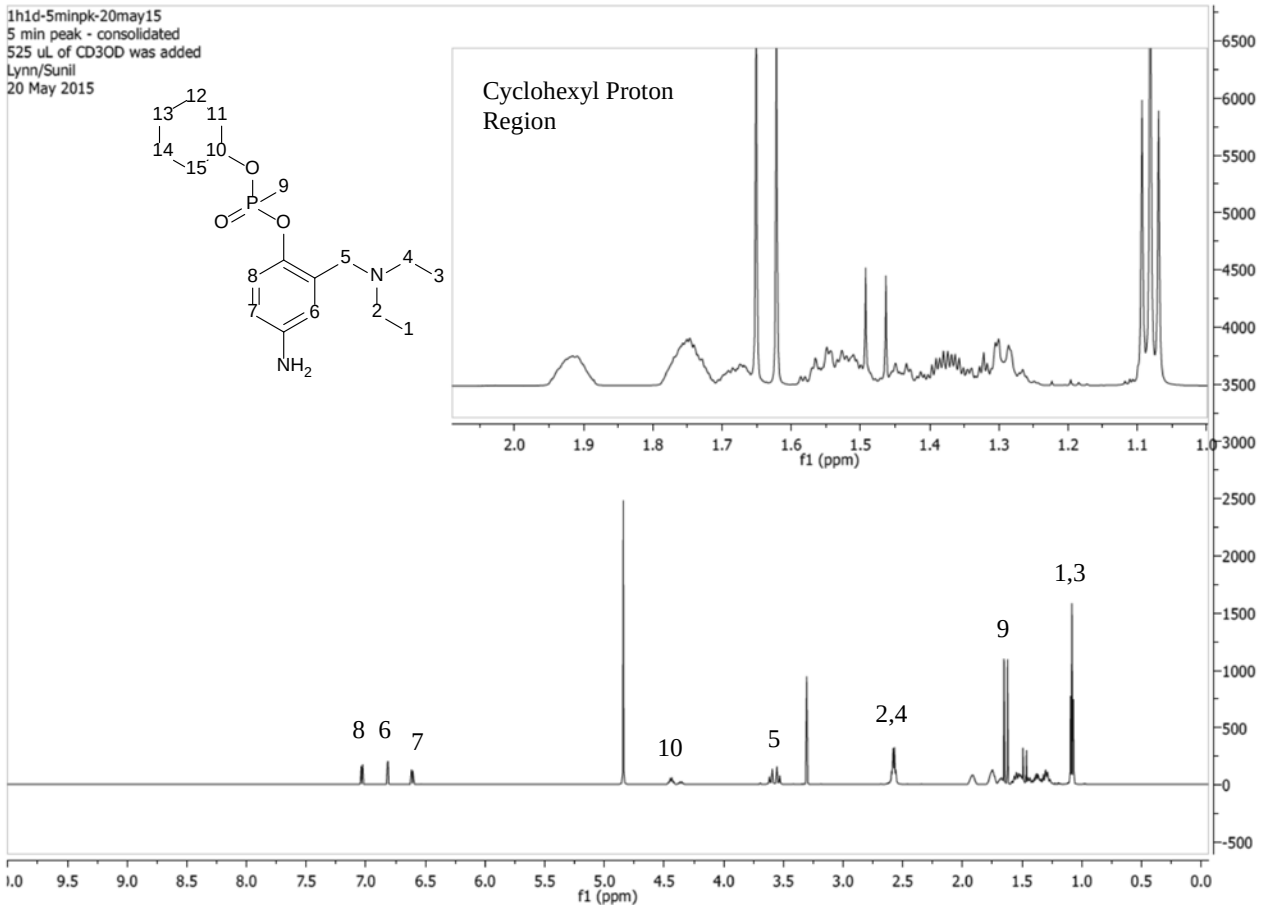

Figure 3-6. Proton (^{1}H) NMR spectrum of purified product of GF/ADOC solution reaction. For the purpose of assigning protons, GF is shown attached at the phenolic oxygen of ADOC.

3.2.2.3.2 Selective Interaction of Furfural

To determine whether the OP adduct was attached to the phenolic oxygen or the aniline nitrogen of ADOC, an experiment utilizing the selective addition properties of furfural was conducted. Furfural, the product of heating pentose in acidic solution, selectively interacts with primary aniline amines. The addition of furfural causes an aniline compound to form a colored adduct (typically reddish brown). This colorimetric readout has historically been used as a qualitative assay for carbohydrates [94-96]. In ADOC, furfural should interact with the aniline group only if it is intact as an amine not a phosphonamine. As a negative control, **12** (4-acetamido-2-[(diethylamino)methyl]phenol), used as an analog in Chapter 2, which has an acetyl group attached to the aniline nitrogen (making this group a secondary amide), should not be able to interact with furfural. Additionally, to increase the sensitivity of this assay, the reactions were monitored using mass spectrometry to detect product formation with ADOC (Figure A.11), negative control **12** (Figure A.12), and the purified product of the GF/ADOC solution reaction (Figure 3-7). The successful formation of the furfural adduct from the reaction with purified ADOC/GF product indicates that the aniline is intact as an amine, supporting the model that GF is attached to ADOC via the oxygen of the phenol.

While these data further support the conclusion of Chapter 2 that the phenol substituent of ADOC is important for reactivation and confirm the fact that ADOC can form a stable OP nerve agent-adducted product, none of the previous experiments, all of which have been conducted with a product formed in a solution reaction, conclusively determine the mechanism of reactivation at the active site of HuAChE. The active site serine of HuAChE is buried approximately 23 Å deep inside the enzyme at the bottom of a narrow hydrophobic gorge [69, 97]. The microenvironment

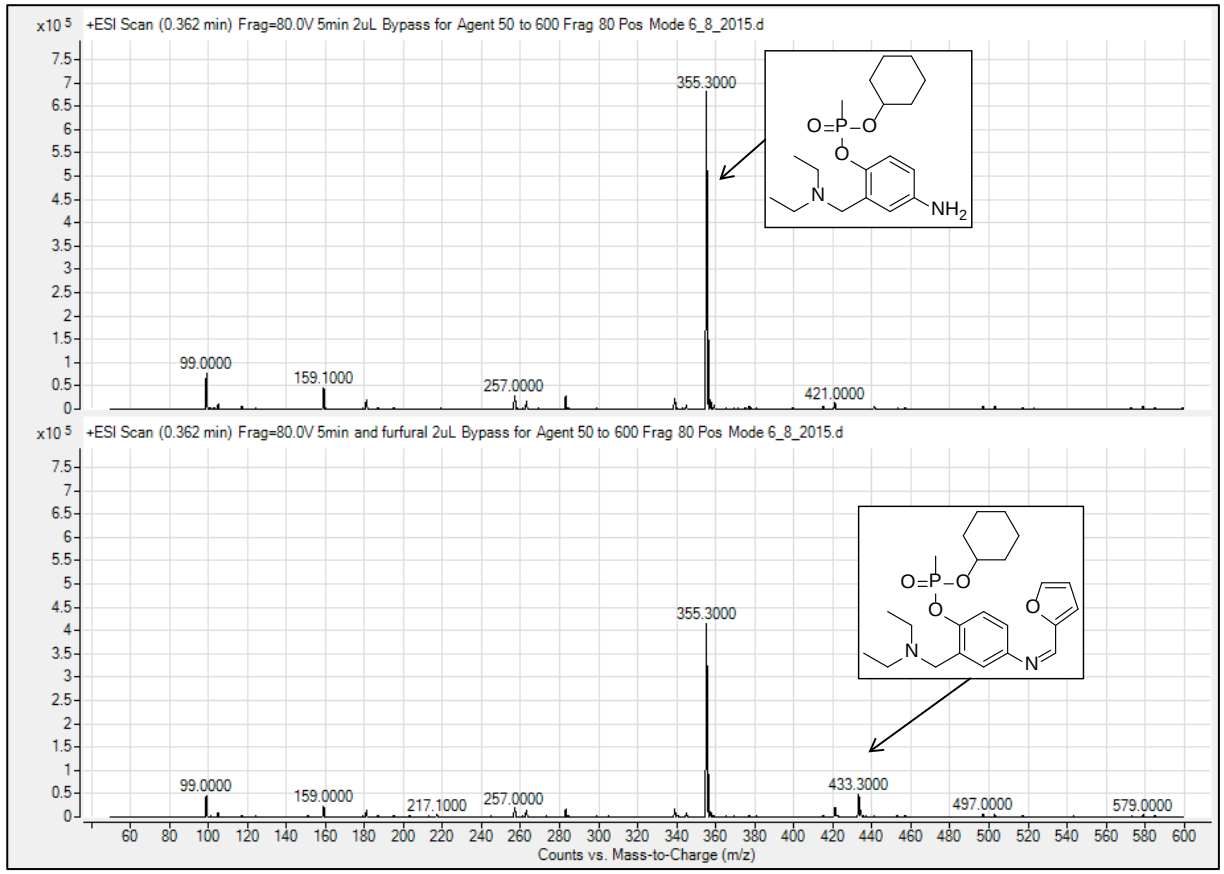

Figure 3-7. Product formation in reaction of furfural with the purified GF/ADOC product. In the top panel, the signal of purified GF/ADOC product is indicated. In the bottom panel, the appearance of signal with the mass/size ratio of the GF/ADOC product with the addition of furfural is indicated.

of the site of reactivation could be drastically different from that of a buffered solution. More importantly, the fluorine of intact GD or GF used in solution reactions above is a much better leaving group than the active site serine of HuAChE, and this could drastically alter the interaction of ADOC with the phosphorus moiety. In an effort to resolve this question of whether the same product is formed upon ADOC-mediated reactivation of GF-inhibited enzyme, an experiment was conducted to determine the structure of the product released from OP nerve agent-inhibited HuAChE upon reactivation by ADOC.

3.2.3 Product of ADOC-Mediated Reactivation of OP-Inhibited Enzyme

Detection of the product formed by reactivation has been accomplished for oxime-based reactivators, which reactivate via a direct nucleophilic attack of the phosphorus by the oxime [60]. If ADOC is interacting via a similar direct mechanism with the phosphonyl adducted to the active site of HuAChE to generate a product similar to that recovered from the solution reaction described earlier, detection of the product of non-oxime reactivation via ADOC should be possible. Additionally, the conditions under which the solution reaction of OP nerve agent and ADOC was performed are favorable for enzymatic reactivation and for allowing the use of LC/MS methods established earlier in this chapter for the detection of solution product formation. To this end, an experiment was designed using goat milk-derived recombinant human butyrylcholinesterase (HuBuChE) [38] in place of HuAChE. This substitution was made because 1) this enzyme was available in a highly purified and concentrated form (90.7 mg/mL of >95% pure enzyme), and 2) although faster than GF with HuAChE, the slow aging rate of GF with HuBuChE ($t_{1/2aging}$ = 2.2 hours [37]) alleviated concerns about a large portion of inhibited enzyme undergoing dealkylation

to the aged form during the time course of the experiment. As discussed in Chapter 1, BuChE and AChE are inhibited by OP nerve agent and reactivated in identical manners with differences between reactivation rates attributable to the altered binding characteristics of reactivators for each enzyme [84]. To eliminate the need for removal of excess nerve agent after enzyme inhibition, only the purified P(-) stereoisomer of GF [98] was used to inhibit the enzyme at 0.9 molar equivalents.

This sample, along with a positive control of apo enzyme, was split into two smaller samples, one of which was treated with ADOC and the other with a buffer control. Activity of the samples was monitored colorimetrically (Section 6.2.3 [68]) until GF-inhibited BuChE was reactivated >30% by ADOC as compared to apo BuChE samples. A portion of the sample was then analyzed using the LC/MS methods described earlier in this chapter to detect the formation of product. A standard curve, established earlier using purified product (Figure A.13), was used to calculate the amount of product detected, and this amount was compared to the theoretical total amount of product possible as calculated from the percent reactivation of a known amount of BuChE using colorimetric methods. A product was successfully detected that appeared to be equivalent to the molecule purified from the solution reaction of ADOC and GF. Unfortunately, the amount of product detected accounted for less than 0.5% of the amount of reactivated enzyme, suggesting that this material was generated by the direct interaction of ADOC with trace amounts of unbound GF in solution.

Conversely, under the same experimental conditions, cyclohexyl methylphosphonic acid (CMPA, the phosphonic acid of GF) was detected at a level that was calculated to be equivalent to 26% of the total moles of product generated by the reactivated sample. Once again a standard curve was determined with

commercially produced standards and used to calculate these values (Figure A.14). While this amount of CMPA only accounts for about one third of the predicted amount of material, it is substantially greater than the trace amount of phosphonylated ADOC detected (CMPA standard curve was linear with an R^2 value of 0.9999 and a lower limit of detection more than ten times lower than the measured signal). These results, combined with the trace amounts of phosphonylated ADOC detected, support the indirect reactivation mechanisms proposed earlier in this chapter. Briefly, in this mechanism, the phenolic oxygen acts as a base to remove a proton from a water molecule to form a hydroxide ion which could attack the OP adducted to the enzyme active site, thereby driving reactivation. Katz *et al.* [75] proposed this general base mechanism of reactivation as a possibility for ADOC-mediated reactivation as well.

3.2.4 Quinone Formation as a Mechanism of Reactivation

Despite the results discussed above, the possibility of an alternative mechanism of ADOC reactivation exists. Many studies of molecules with structural similarities to ADOC, including acetaminophen [99, 100] and the anti-malarial drug amodiaquine [101-103], have shown that these molecules form highly reactive quinone species. Similar forms of ADOC may be possible, including a quinone methide species [104] or a quinone imine species, likely through a semiquinone imine intermediate [102]. Any of these reactive species could participate in reactivation. That possibility is explored in the following discussions.

3.2.4.1 Quinone Methide Species

The formation of quinone methides (QM) is commonly known to occur with substituted phenolic compounds in both synthetic and biological systems [105]. While

the formation of *ortho*- and *para*-QMs is most common, *meta*-QM formation is known to happen as well (Figure 3-8). QMs in biological systems typically serve as electrophiles for Michael-type addition of nucleophiles [106]. Additionally, Weinert *et al*. [107] have shown that the rate of nucleophilic addition to an *ortho*-QM is dependent on the electron-donating or -withdrawing properties of the *para*-ring substituent with electron-withdrawing groups increasing the rate of product formation and electron-donating groups decreasing it. These rate changes appear to be mostly dependent upon the stability of the QM intermediate, so the presence of an electron-donating group at the *para*-position to the phenol may increase the likelihood of *ortho*-QM formation.

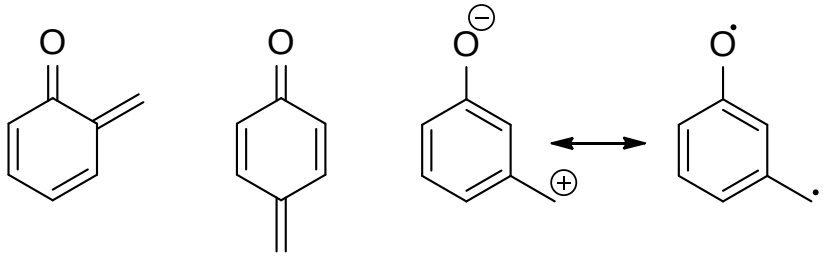

Figure 3-8. Common quinone methide (QM) structures.

ADOC would be a prime candidate for the formation of an *ortho*-QM via alkene formation by loss of the diethylbenzylic amine (Figure 3-9). However, the presence of the electron-donating *para*-aniline (σ_p = -0.66), while increasing the stability of the QM, would be likely to slow any subsequent nucleophilic addition. Also, if the phosphonyl adduct in the active site of HuAChE is not dealkylated, it

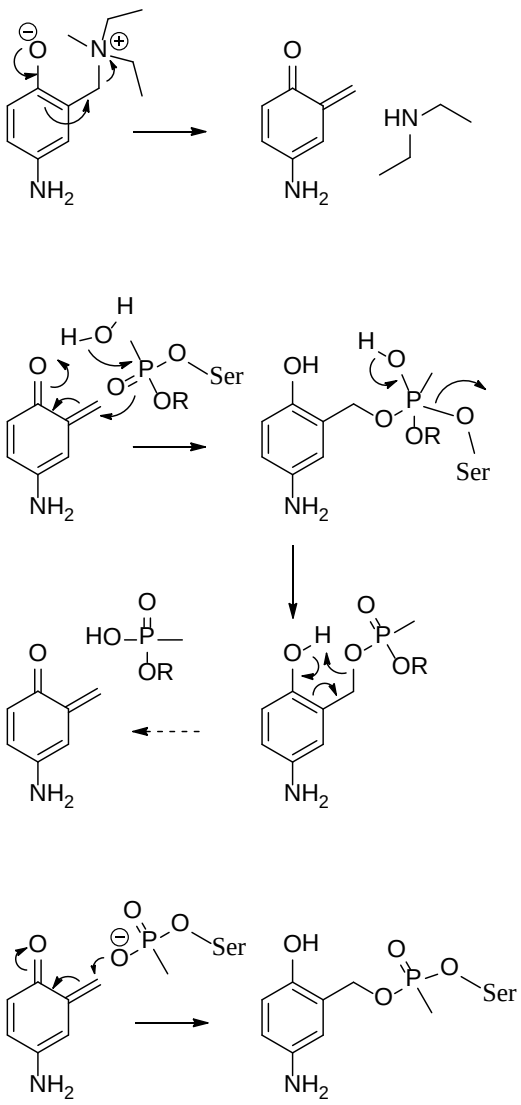

Figure 3-9. Quinone methide mechanisms of ADOC. a) ADOC QM formation. b) Postulated mechanism for reactivation of unaged phosphonylated AChE by ADOC QM. c) Postulated mechanism for addition of ADOC to aged phosphonylated AChE [104].

would be unlikely to act as a nucleophile. Molecules of this type have been postulated to have the capability to interact with the nucleophilic dealkylated “aged” phosphonyl adduct attached to the active site of HuAChE, regenerating a moiety that could then be

reactivated by conventional reactivators [104]. However, no evidence suggests that ADOC is able to accomplish this (note the lack of reactivation against GD, which ages extremely rapidly in HuAChE, in Chapter 2 Figure 2-5 and Table 2-1).

Finally, the inhibition and reactivation results of **9** and **10** (Table 3-1) offer further insight into the possibility of an ADOC QM mechanism of reactivation. If these molecules formed QMs, the benzyl amine substituent of each would be released to generate the same reactive intermediate as ADOC (Figure 3-9a). This would allow both molecules to reactivate OP nerve agent-inhibited HuAChE, likely at levels similar to ADOC. Conversely, if the QM does not form, it is likely that the steric congestion caused by the large groups attached to the amine (diisopropyl for **9** and dicyclohexyl for **10**) would reduce the binding affinity of these molecules for the active site of OP nerve agent-inhibited HuAChE. While neither of these compounds reactivates inhibited enzyme, **9** displays greater inhibition of apo HuAChE than ADOC, indicating that binding is enhanced by the diisopropyl amine substituent, possibly due to interactions of these groups at the peripheral binding site of HuAChE.

Several combined attributes of the QMs decrease the likelihood that ADOC QM formation is a preferable mechanism for reactivation of OP nerve agent-inhibited HuAChE. A QM typically acts as an electrophile in reactions, and the deactivation of an ADOC QM due to the presence of a *para*-amino group would likely make it a poor electrophile. The most convincing evidence that QM formation is not important for reactivation lies in the reactivation and inhibition characteristics of **9** and **10**. If QM formation occurred, either in solution or upon entering the active site of the enzyme, both of these molecules should be nearly as reactive as ADOC. Not only is that not the case, but **9** displays significant inhibition, indicating that it is likely interacting with

the enzyme intact. Therefore quinone methide formation is likely not a major mechanism of reactivation by ADOC of HuAChE inhibited by OP nerve agents.

Table 3-1. Compounds likely to form quinone methides as an intermediate of reactivation of OP nerve agent-inhibited HuAChE. Ratio (spontaneous/compound) of half-times ($t_{1/2}$) of reactivation for compounds (1mM) with HuAChE after inhibition by the indicated agent.

		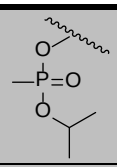 GB	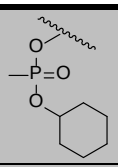 GF	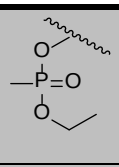 VX	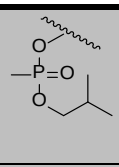 VR	Inhibition of HuAChE[Ŧ]
9	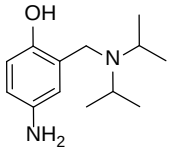	---	---	---	---	94% (±1)
10	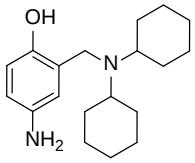	0.88 (0.65-1.20)	0.74 (0.60-0.90)	1.09 (0.60-1.98)	0.93 (0.76-1.14)	9% (±4)

---Reactivation could not be determined because of high level of inhibition by compound.
Grey boxes are not significantly greater than spontaneous reactivation.
Standard deviation of at least three independent experiments is indicated for spontaneous reactivation half-times in days. Ninety-five percent confidence intervals of ratios are indicated below each value.
[Ŧ]All half-times were determined using HuAChE in the presence of 1 mM compound as the positive control. The far right column indicates the level of inhibition of HuAChE caused directly by the compound at the concentration in the reaction well (~24.4 µM) when compared to a buffer only control of HuAChE. Standard deviation of this value determined using controls from all independent experiments is indicated.

3.2.4.2 Quinone Imine Formation as a Reactivation Mechanism

While quinone methide formation appears to be an unlikely mechanism of reactivation for ADOC, quinone imine (QI) or semiquinone imine (sQI) formation seems much more plausible. Amodiaquine is known to be associated with agranulocytosis and liver damage [108-111] caused in part by the formation of QIs

(Figure 3-10) [102]. Specifically, these reactive species are known to form on the portion of the molecule with structural properties identical to those of ADOC. Several other phenol compounds with *para*-amino groups, such as acetaminophen and 4-aminophenol, are known to undergo similar activation to QIs, usually via sQI formation [103, 112].

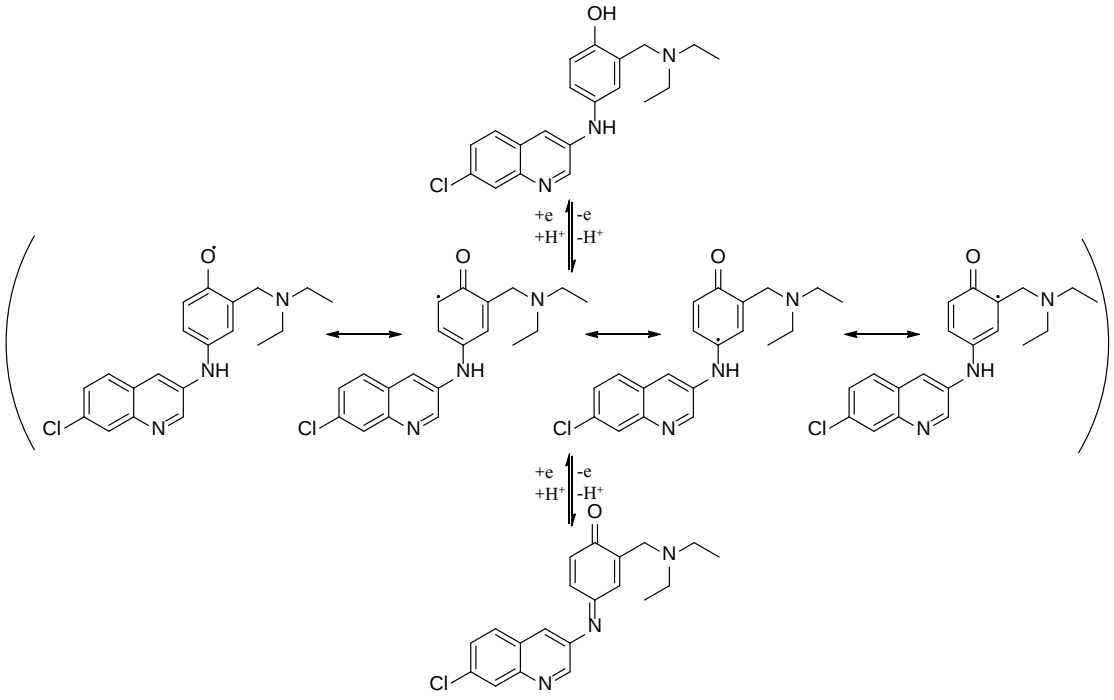

Figure 3-10. Structure of amodiaquine (top) and the formation of semiquinone imines (middle) and quinone imine of amodiaquine (bottom).

ADOC could undergo similar activation to a species capable of reactivation of OP nerve agent-inhibited HuAChE (Figure 3-11). Of note is the work of Huang *et al*. [112], in which the authors note that 4-aminophenol oxidation can occur at either the aniline or the phenol to generate the initial semiquinone intermediate. ADOC, with a

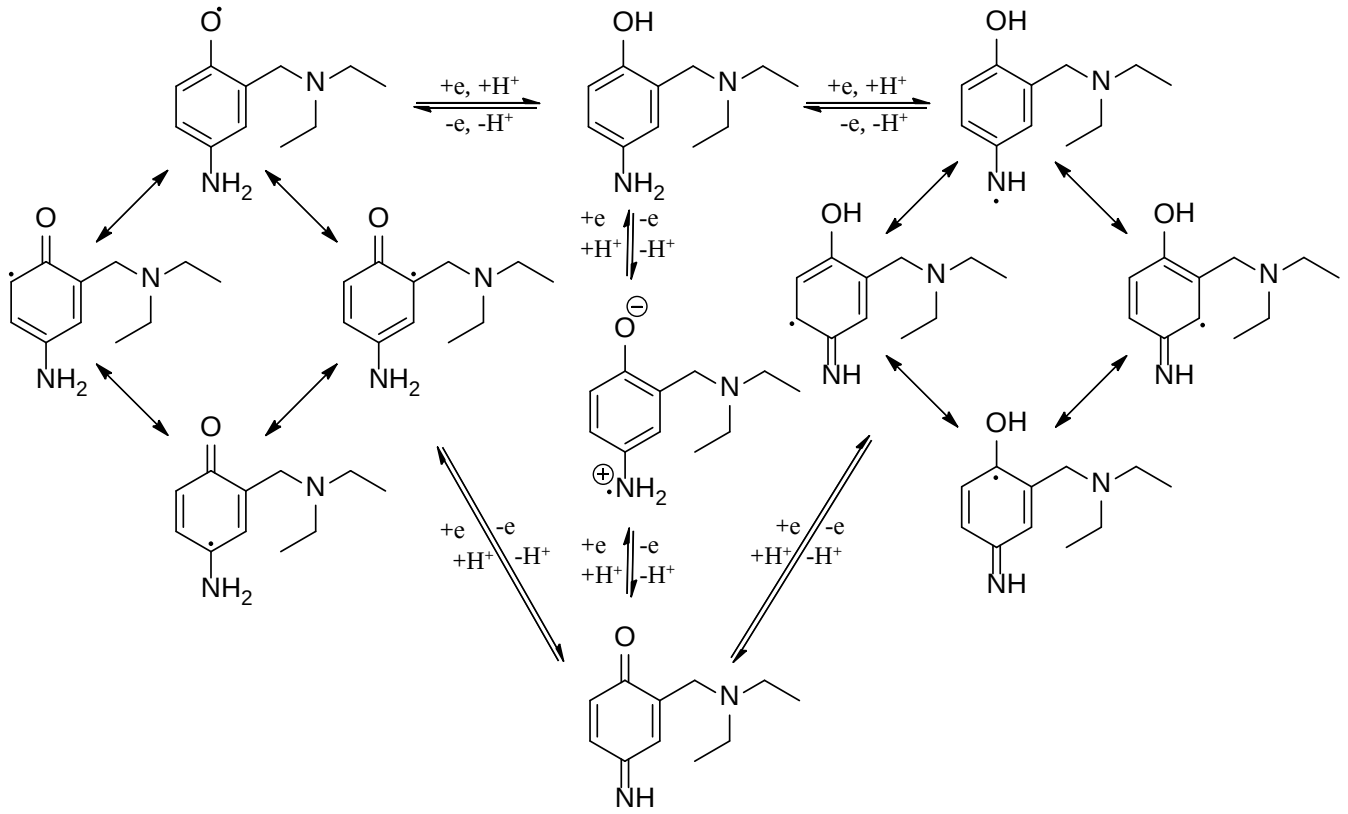

Figure 3-11. ADOC quinone imine formation via semiquinone. ADOC (top, center) could undergo the loss of one electron and one proton from the phenolic oxygen (top, left), the aniline nitrogen (top, right), or both to form a zwitterion semiquinone (center). All semiquinones undergo the loss of an additional electron and proton to form the ADOC quinone imine (bottom, center).

similar *para*- phenol/aniline relationship, could be similarly oxidized at the aniline nitrogen or the phenolic oxygen (Figure 3-11), and either of these species could proceed to form the same quinone imine. Additionally, under alkaline conditions a zwitterion radical has been shown to form in 4-aminophenol [113] which could form in ADOC as well, although this would be unlikely under the experimental conditions used here (pH = 7.0) in the presence of the protonated benzylic amine.

The QI of ADOC can interact electrophilically in an addition reaction, similar to the reaction known to occur between amodiaquine or acetaminophen and glutathione [99, 103]. This interaction would likely lead to a product in which the phosphonyl added directly to the ring, which NMR data presented earlier shows is not the case. However, one could imagine that the ADOC semiquinone intermediates pictured above could participate in reactivation. These species could interact directly with OP nerve agent adduct of inhibited HuAChE, most likely interacting at the phenolic oxygen (Figure 3-12), although this reaction is likely to be energetically unfavorable. More likely, these reactive species could act indirectly to achieve reactivation via the activation of a water molecule, leading to the production of the phosphonic acid product noted in the experiment described earlier in this chapter.

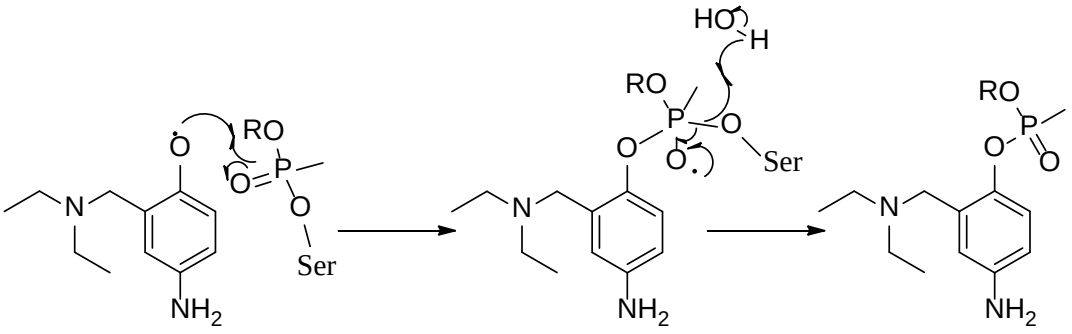

Figure 3-12. Possible semiquinone reactivation mechanism of ADOC.

3.2.5 The Role of Oxidation in Reactivation

The role of oxidation in ADOC-mediated reactivation of OP nerve agent-inhibited HuAChE was explored in an effort to shed light on any possible role of the quinone forms of ADOC in reactivation. Quinone imine formation is an oxidative process that can be promoted *in vitro* by the addition of horse radish peroxidase (HRP) and hydrogen peroxide, a technique established with both 4-aminophenol and amodiaquine [103, 112]. Assuming that ADOC can undergo activation in similar conditions and the mechanism of reactivation includes the formation of an oxidized species, these conditions should increase the rate of ADOC reactivation. Conversely, under conditions that limit oxidation of ADOC, achieved by utilizing Trolox (6-hydroxy-2,5,7,8-tetramethylchroman-2-carboxylic acid), the water-soluble Vitamin E analog, the reverse should be true [114-119]. To explore this hypothesis, reactivation half-time ($t_{1/2}$) of ADOC under both oxidizing (in the presence of HRP and hydrogen peroxide) and reducing (in the presence of Trolox using nitrogen-sparged media) conditions was measured (Section 6.2.4). Initially, this experiment was conducted with HuAChE inhibited by GA, GB, GD, GF, VX or VR and reactivated with either 2PAM or ADOC. 2PAM was used as a negative control because the nucleophilic potential of the oxime is driven by pH [62] and should not be affected by these conditions. Reactivation was only detected for GB-, GF-, VX-, or VR-inhibited enzyme, and the half-time of reactivation of replicate samples was determined for each reactivator with each of these agent-inhibited HuAChE samples (Figure 3-13).

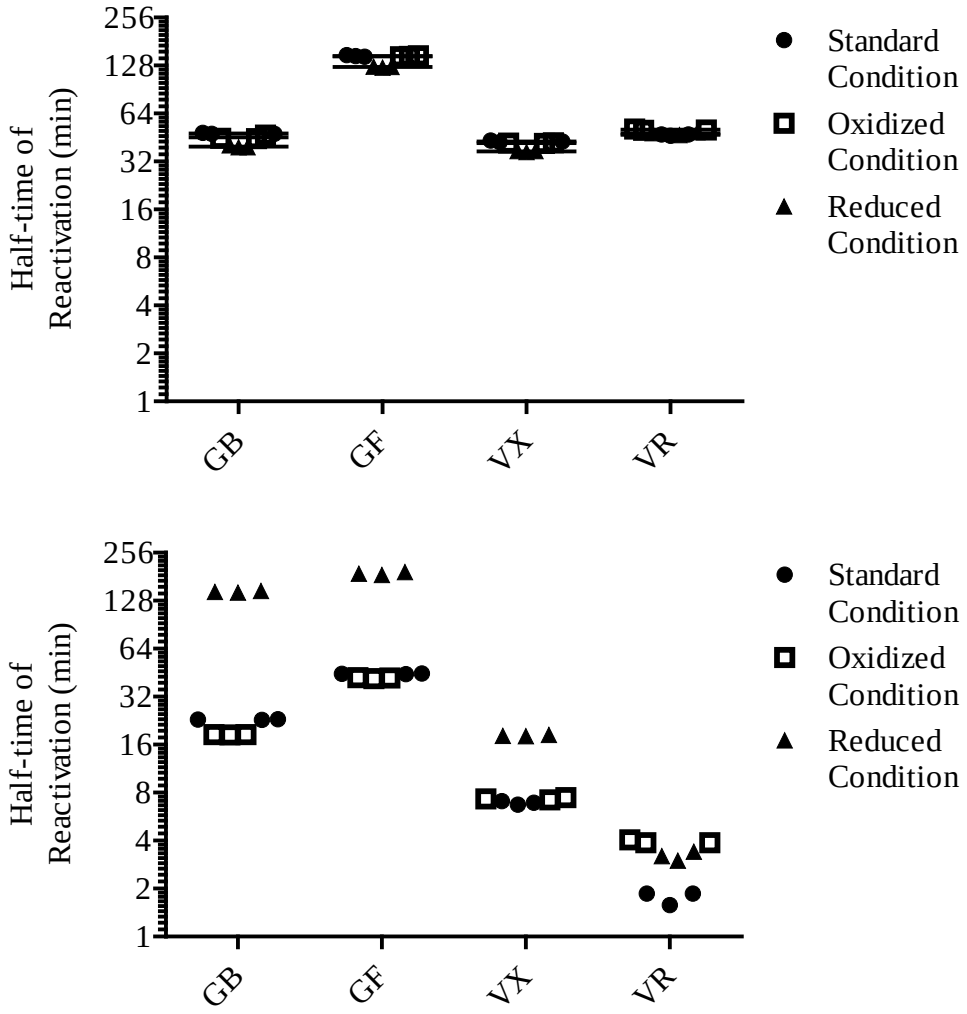

Figure 3-13. Reactivation of OP nerve agent-inhibited HuAChE by 2PAM (top) or ADOC (bottom) under standard (●), oxidizing (□), or reducing (▲) conditions. Each point represents the half-time of reactivation ($t_{1/2}$) in minutes calculated for a replicate sample in a single experiment.

In the case of 2PAM, no major differences in reactivation half-times were noted across the varied conditions for any of the agents tested. Meanwhile, ADOC reactivation half-times for GB-, GF-, and VX-inhibited HuAChE were increased 2- to 4-fold in reducing conditions as compared to either standard or oxidizing conditions. This trend was not noted for the reactivation of VR-inhibited HuAChE by ADOC, but this may be because this reactivation occurs so quickly that measurement is difficult using the discontinuous assay. Notably, no difference was seen between the reactivation half-times for ADOC in standard versus oxidizing conditions in this initial experiment. To determine if this observation was due to the extremely fast reactivation mediated by ADOC, reactivation of VX-inhibited HuAChE was conducted multiple times under all of the conditions using 2PAM or ADOC at a lower concentration to slow reactivation (Figure 3-14).

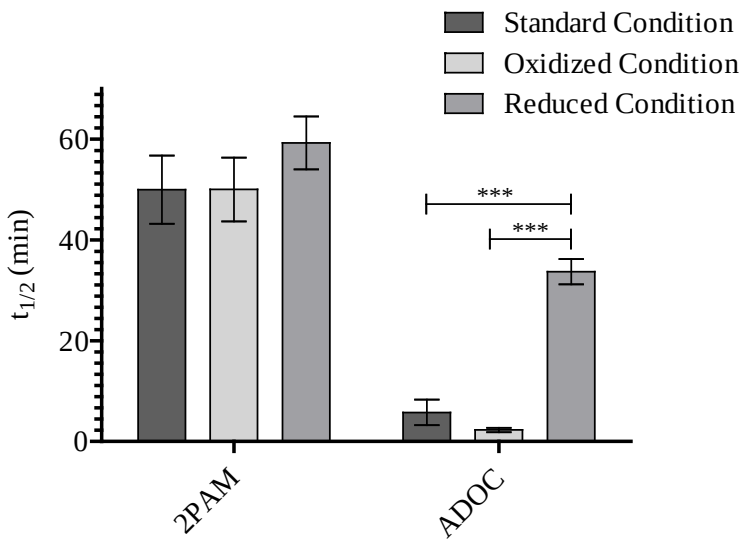

Figure 3-14. Reactivation half-times ($t_{1/2}$) of ADOC and 2PAM under standard, oxidizing and reducing conditions against VX-inhibited HuAChE. (***significant difference between these values, $p<0.001$)

Once again, no significant differences were noted in the half-times of reactivation for 2PAM under any sample conditions. Conversely, the half-time of reactivation was significantly increased for ADOC reactivation under reducing conditions as compared to both oxidizing and standard conditions. Half-time of reactivation was slightly, though not significantly, decreased under oxidizing conditions (2.5-fold less than standard conditions). Together these observations support the hypothesis that oxidation may play a role in the reactivation mechanism of ADOC. Interestingly, the reactivation half-time of ADOC under reducing conditions is similar to (i.e., not significantly different from) the reactivation of 2PAM, indirectly suggesting, once again, that the nucleophile-based, non-radical mechanism is important for reactivation.

Taken together with the finding presented earlier in this chapter, the evidence suggests that oxidation may play a role in reactivation, although the exact nature of this interaction has not been determined in this study. It may be difficult to determine the role of oxidation if it is secondary to the nucleophilic mechanism discussed earlier. The possibility remains that both mechanisms are viable with the predominant mechanism being dependent upon the environment prior to or upon entering the active site of the enzyme. All evidence supports the hypothesis that for either mechanism (oxidative activation or indirect nucleophilic attack), the phenol group is of primary importance. Armed with that knowledge and the narrowed possibilities for the mechanisms of reactivation, efforts were made to design a second generation reactivator with improved reactivation potential.

3.3 Designing a Better Reactivator

3.3.1 Activating the Phenol of ADOC

In an effort to better define the importance of phenol activation in the enzyme reactivation mechanism, compounds **11** and **12** of Chapter 2 (Table 2-4) were revisited. Briefly, **11** was an analog of ADOC in which the aniline had been substituted to a dimethyl amino group, slightly increasing the electron-donating potential across the benzyl ring per the decreased Hammett σ_p value as compared to ADOC (-0.83 and -0.66, respectively). Conversely, **12** was an analog with an acetyl amino group in place of the aniline, abolishing all electron-donating potential of that group ($\sigma_p = 0.00$). While the half-times of reactivation determined earlier for both of these compounds were much longer than for ADOC (reactivation was much slower than with ADOC), both compounds were capable of reactivating nerve agent-inhibited HuAChE at a rate significantly faster than spontaneous reactivation. In an effort to determine if these differences in reactivation were due to binding issues (high K_D, supported by the complete lack of inhibition of apo HuAChE by these analogs) or a decrease in the rate of the reactivation step (low k_r), reactivation kinetics for VR-inhibited HuAChE were measured (Table 3-2).

Both **11** and **12** display significantly decreased k_r compared to ADOC as well as significantly better binding to inhibited HuAChE (decreased K_D). This combination of results may arise from a situation in which the analogs bind to inhibited enzyme but the presence of sterically hindering groups attached to the aniline nitrogen causes the binding configuration to be non-productive in terms of reactivation.

Table 3-2. Reactivation kinetic parameters of ADOC and two analogs (**11** and **12**) for VR-inhibited HuAChE.

Reactivator	K_D (mM)	k_r (min^{-1})	k_{r2} (M^{-1} min^{-1})
ADOC	5.46 ±2.02	4.01 ±2.37	719 ±386
11	0.39* ±0.23	0.07* ±0.02	204 ±69.3
12	0.92* ±0.11	0.03* ±0.01	39.3* ±20.8

Standard deviation of two independent experiments with three replicates of each is indicated below value. Statistically significant decrease of value compared to ADOC is indicated by *(One-way ANOVA of log values followed by Tukey test, $p<0.05$). No significant difference between analogs was observed.

3.3.2 Designing a Better Reactivator Utilizing the Aniline of ADOC

In an effort to further explore the correlation between the size of any attachments at the aniline nitrogen of ADOC and increases in the binding affinity of a compound for OP-inhibited HuAChE, compounds **15** and **16** were designed and synthesized (Figure 3-15). Both of these compounds attempted to take advantage of the proposed distal binding site at the mouth of the HuAChE active site gorge [69, 120] by incorporating a diphenyl amine at the end of a seven-atom carbon chain attached to the aniline nitrogen. Compound **15** incorporated a non-branched alkyl chain, whereas compound **16** incorporated a branched amide structure into the chain attached at the aniline nitrogen.

Initial analysis of these compounds for reactivation potential revealed that they could reactivate OP-inhibited HuAChE but appeared to do so at a slower rate than

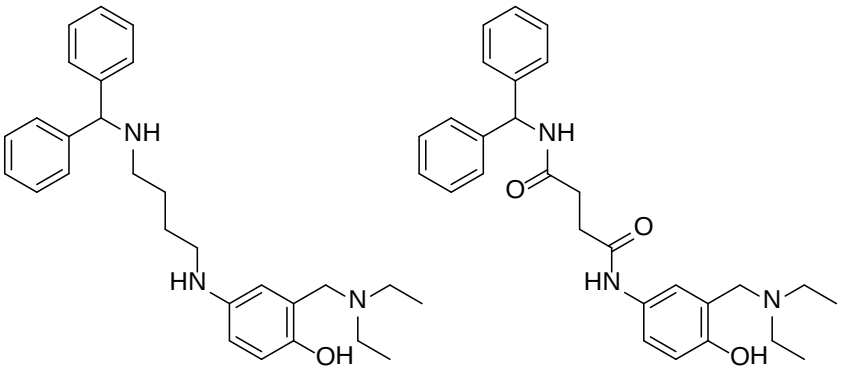

4-((4-(benzhydrylamino)butyl)amino)-2-((diethylamino)methyl)phenol; **15**

N^1-benzhydryl-N^4-(3-((diethylamino)methyl)-4-hydroxyphenyl)succinamide; **16**

Figure 3-15. Analogs incorporating either an alkyl chain, **15** (left), or a branched amide chain, **16** (right) from the aniline nitrogen of ADOC to a diphenyl amine group.

ADOC ($t_{1/2}$ was increased 4.5- and 10.5-fold for **15** and **16**, respectively, Figure A.15 and Table A.1). Additionally, inhibition of apo enzyme was reduced compared to the values with ADOC: **15** and **16** inhibited 22% of the apo activity when present at the concentration of ADOC that inhibits 40% of apo activity. Reactivation kinetics were determined for the compounds and compared to ADOC (Table 3-3). Although these values were determined using a single experiment, the reactivation rate (k_r) for both molecules is at least ten-fold slower, whereas binding (K_D) is comparable or much tighter than ADOC. Of particular interest are the kinetic values for the reactivation of VX-inhibited HuAChE, which indicate that both analogs have similar rates of reactivation, with **15** binding much better than **16**. Drawing from all of the previous data presented here, one wonders if reduction in the rate of reactivation is due, at least in part, to the altered positioning of these molecules within the active site, reducing the

number of opportunities for interaction between ADOC and any water molecules present in the active site.

Table 3-3. Reactivation kinetic parameters of analogs **15** and **16** for VX- or GB-inhibited HuAChE.

Reactivator		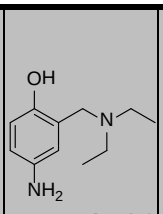 **ADOC**	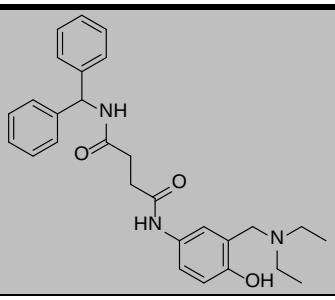	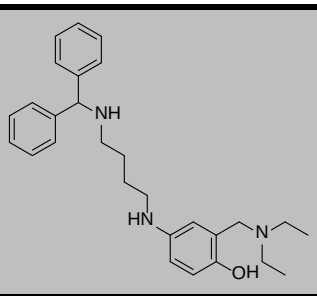
GB	K_D (mM)	7.61 ±4.08	2.75 ±0.64	2.12 ±0.39
	k_r (min^{-1})	0.34 ±0.14	0.007 ±0.001	0.039 ±0.004
	k_{r2} (M^{-1} min^{-1})	46.7 ±6.4	2.69 ±1.05	18.4 ±2.69
VX	K_D (mM)	2.08 ±0.94	3.64 ±0.54	0.65 ±0.11
	k_r (min^{-1})	0.50 ±0.2	0.033 ±0.003	0.047 ±0.004
	k_{r2} (M^{-1} min^{-1})	266 ±108	8.99 ±2.32	72.4 ±18.6
Standard deviation of triplicate readings of a single experiment is indicated below value with the exception of ADOC values, which are calculated using three individual experiments.				

To further explore the idea that altering the aniline group affects the binding and possibly the positioning of a compound in the active site of HuAChE, several factors were considered. First, large groups attached to the aniline amine seemed to greatly disrupt reactivation as evidenced by the compounds in Figure 3-15. Second, increasing the "bulk" of the aniline amine by either replacing both hydrogens with larger groups as in the dimethyl amino group of **11** or replacing one hydrogen with a

group that is immediately branched in nature as in the acetyl amino group of **12** and the branched amide chain of **16** seems to enhance binding to the OP-inhibited enzyme but simultaneously decreases the reactivation potential of these molecules. In an effort to enhance binding of a reactivator to OP-inhibited HuAChE without decreasing the reactivation potential of that molecule, novel compound **17** was synthesized and characterized (Figure 3-16).

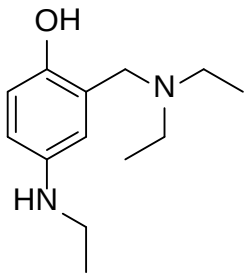

Figure 3-16. ADOC analog designed as a second generation reactivator of OP-inhibited HuAChE (**17**, EADOC)

While **17** incorporates a modest structural change compared to ADOC, the hope was that this molecule, which incorporated a short ethyl chain on the aniline nitrogen, would reduce the amount of inhibition in apo HuAChE and enhance binding to OP-inhibited HuAChE while retaining the reactivation potential of ADOC. Characterization of this molecule revealed that while inhibition of apo HuAChE was similar to that by ADOC, the K_D of **17** was significantly lower than that of ADOC for both GB- and VX-inhibited HuAChE, closely resembling the values of 2PAM (Figure 3-17 (A)). The rate of reactivation for this molecule was similar to ADOC's in the

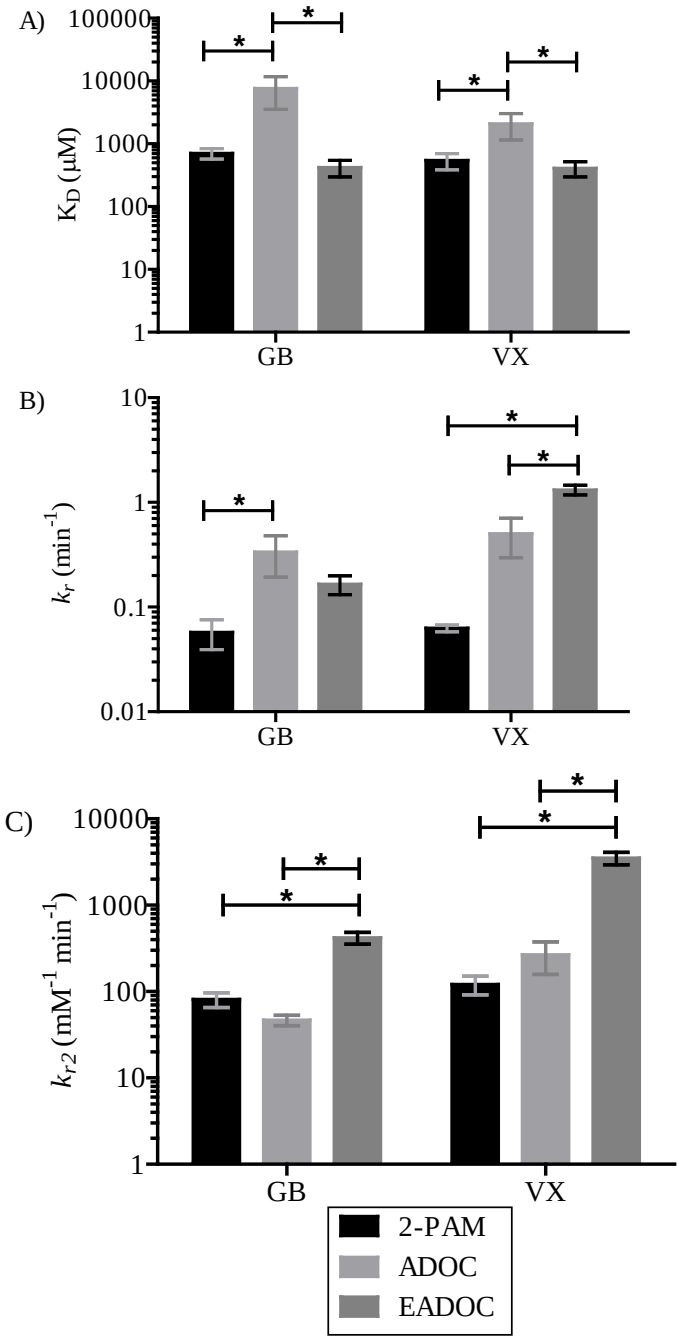

Figure 3-17. Reactivation kinetic parameters of **<u>17</u>** with GB- and VX-inhibited HuAChE. A) Dissociation constant (K_D), B) reactivation rate constant (k_r), and C) overall reactivation (k_{r2}) are reported. (*significant difference determined by one way ANOVA followed by Tukey test, $p<0.05$)

case of GB and increased in the case of VX (Figure 3-17(B)). Finally, **17** displayed significantly increased reactivation efficiency of both GB- and VX-inhibited HuAChE as compared to both 2PAM and ADOC (Figure 3-17 (C)).

3.4 Summary

In summary, several proposed mechanisms of reactivation were evaluated using a variety of techniques. While the formation of a phosphonylated ADOC product occurred in a solution reaction, confirming that direct interaction of ADOC and OP nerve agent can lead to a product, no similar product was detected in significant amounts during an enzyme reactivation event. The phosphonic acid of the agent was detected in significant amounts during the same reactivation experiment, supporting the hypothesis that reactivation occurs via the activation of a water molecule which attacks the phosphorus. Precedent for this type of reactivation event can be found in the postulated mechanism of G117H BuChE in which the additional histidine in the active site can act as a general base to form a reactive hydroxide which attacks the phosphorus to catalyze hydrolysis. While G117H BuChE is not suitable for development as a bioscavenger or treatment for other reasons, the evidence presented here suggests that ADOC acts in a similar general base manner to activate water in an indirect nucleophilic attack mechanism.

This is additionally supported by the observation that, when the oxygen levels of the environment are reduced, ADOC-mediated reactivation of VX-inhibited HuAChE slows to the same rate as 2PAM-mediated reactivation, which is known to occur via a nucleophilic attack mechanism, albeit a direct one. The effects of oxygenation in ADOC-mediated reactivation of inhibited HuAChE suggest that a secondary mechanism involving the formation of a semiquinone or quinone imine may

contribute to reactivation under standard conditions. Two possible mechanisms of reactivation may help to explain the speed of reactivation comparable to or improved over 2PAM achieved by ADOC as a non-oxime reactivator with no permanent charge.

Finally, the observed reactivation trends of ADOC analogs with groups attached at the aniline nitrogen (increased bulk lessened or abolished inhibition of apo enzyme while increasing affinity to inhibited enzyme) were used to design **17**, a second generation reactivator compound. Unfortunately, **17** retained apo enzyme inhibition characteristics similar to ADOC. However, this reactivator displayed binding affinity to inhibited enzyme similar to that of 2PAM while simultaneously retaining or increasing the rate of reactivation displayed by ADOC, effectively improving reactivation efficiency significantly over both ADOC (8.5- and 13-fold for GB and VX, respectively) and 2PAM (5- and 29-fold for GB and VX, respectively). This new compound represents the first known instance of a reactivator lacking both an oxime and a permanent charge as a pyridinium that can mediate reactivation of OP nerve agent-inhibited HuAChE with greater efficiency than 2PAM, the currently fielded treatment of the United States Army.

Chapter 4

ISOTHERMAL TITRATION CALORIMETRY: A POSSIBLE TOOL TO MEASURE REACTIVATION

Isothermal titration calorimetry (ITC) is a technique typically used to characterize binding events, especially those that cannot be easily tracked using other methods. ITC takes advantage of changes in enthalpy, the fact that heat is generated or absorbed in every chemical process, to measure interactions. This technique has been used to successfully study the kinetic properties of several enzyme-substrate interactions [121-127]. The following chapter discusses the feasibility of utilizing this method to determine the kinetic parameters of small molecule-mediated reactivation of OP nerve agent-inhibited cholinesterases.

4.1 General Calorimetry Concepts

The modern calorimeter instrument utilized in ITC techniques is known as a differential instrument and consists of two identical cells (sample and reference) made of chemically inert, thermally conducting material such as an alloy or gold. The reference cell is filled with water or a buffer and is then sealed; the reference cell does not interact directly in the experiment. The sample cell is filled with a molecule of interest (generally a protein or other macromolecule) in a suitably compatible buffer. In a typical binding experiment, the second molecule of interest (typically a ligand for the protein of interest) is loaded into a specialized syringe system capable of both injecting the ligand solution and mixing the sample in the sample cell.

An ITC experiment is conducted by initially establishing the sample and reference cells at the same temperature, generally selected by the user. Once this baseline is established, repeated small volume injections of the ligand solution are made into the sample cell while mixing. Each injection of ligand will cause the temperature of the sample cell to change at a magnitude directly proportional to the strength of the interaction between the two experimental components. That temperature change is monitored by sensors and constantly compared to the reference cell temperature. Via a thermocouple, the two cells are constantly maintained at the same temperature. The electrical energy required to maintain the temperature of the sample cell is measured and converted into the heat either absorbed or generated by the reaction [128].

Experiments are generally designed so that over the course of all the injections, the concentration of ligand increases to be two- to three-fold higher than that of the protein in the sample cell. Under these conditions, the heat of the first injection of ligand into a solution of completely unbound protein will be the maximal heat of interaction, with subsequent injections generating less heat as fewer binding events occur. This continues until all binding sites are occupied, at which point any new injections will only generate a small heat of mixing. The changes in heat are plotted for the time course of the experiment, and the areas of the peaks generated by injections can be used to determine several parameters of the interaction (Figure 4-1).

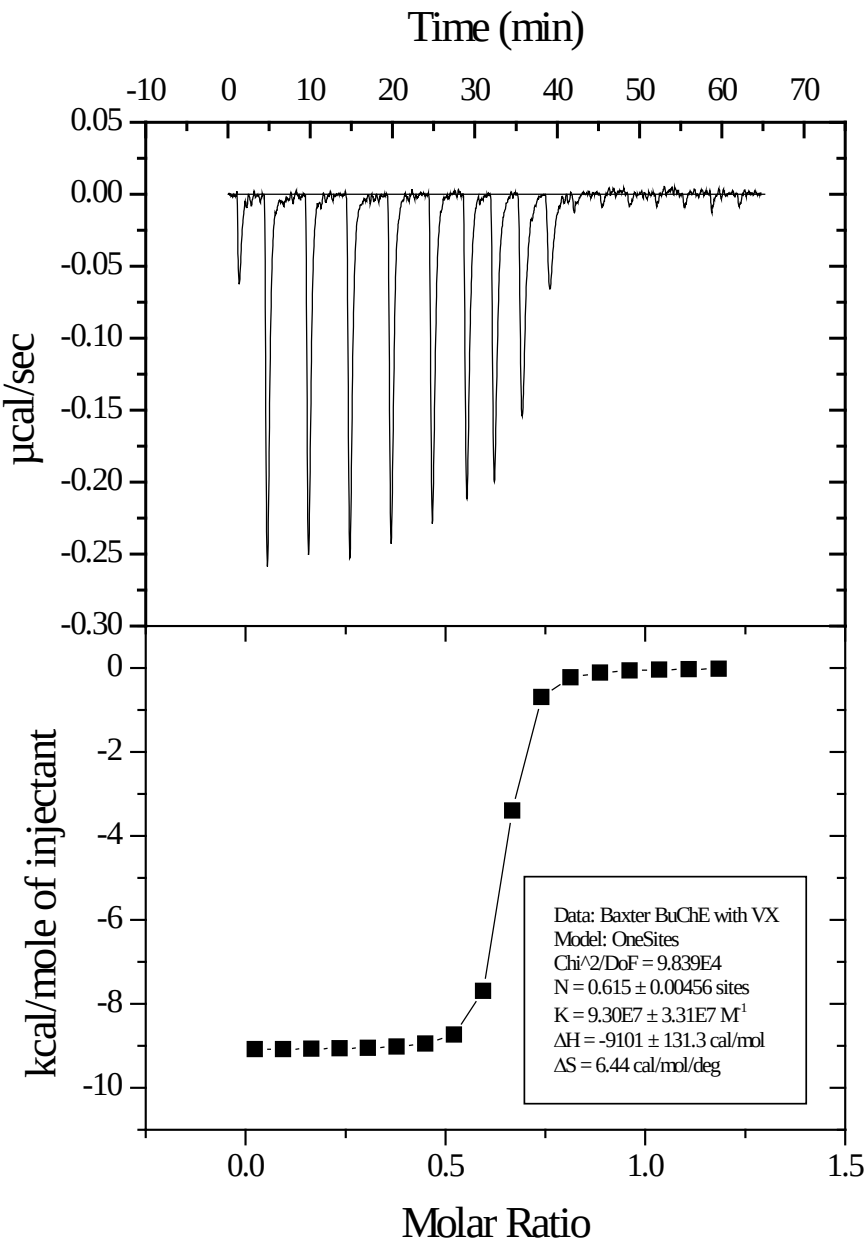

Figure 4-1. Example of data generated during binding experiment using ITC. Binding of racemic VX to human butyrylcholinesterase was measured. The top panel shows the raw power measurements collected during the experiment while the bottom panel displays the fit to a single-site model for the data in the top panel.

Measuring enzymatic hydrolysis of substrates can be accomplished using similar experiments. Todd *et al*. [121] proved this using several different enzymatic reactions and was further able to provide the mathematical relationship between heat (Q), product formed (n), and the measured molar enthalpy (ΔH_{app}) by incorporating the volume of the ITC sample cell (V_0) (Equation 2).

$$Q = n \cdot \Delta H_{app} = [P]_{Total} \cdot V_0 \cdot H_{app} \tag{2}$$

Given that the calorimeter measures the power needed to maintain temperature over time (Equation 3), these power measurements can be directly related to the change in the concentration of product over time, otherwise known as the rate of the reaction (Equation 4).

$$Power = \frac{dQ}{dt} \tag{3}$$

$$Rate = \frac{d[P]_{Total}}{dt} = \frac{1}{V_0 \cdot \Delta H_{app}} \cdot \frac{dQ}{dt} \tag{4}$$

These relationships have been used to describe classical Michaelis-Menten kinetic interactions many times [121, 122, 124, 125], including experiments conducted by the author (similar to those conducted by Tsai *et al.* [129]); shown in Figure 4-2 is an example of a multiple injection method enzymatic activity measurement using a calorimeter.

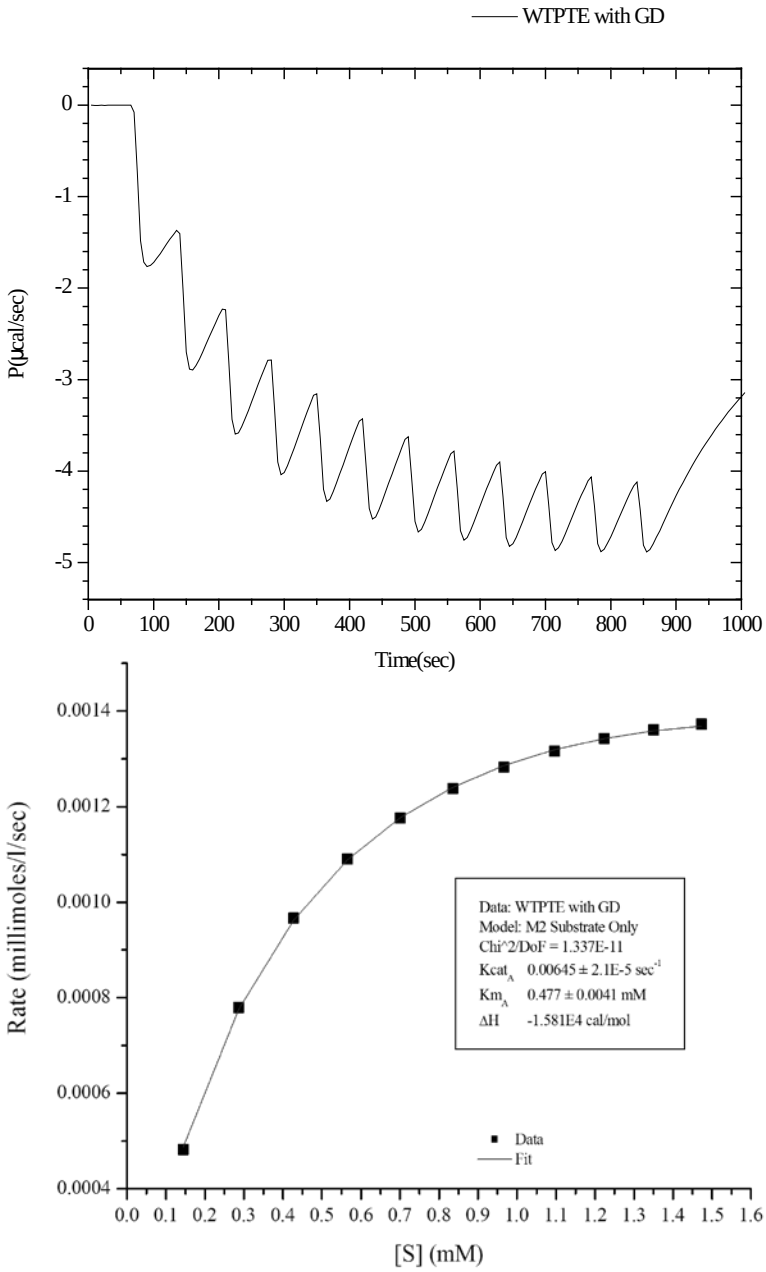

Figure 4-2. Example of hydrolysis activity as measured by ITC. Activity of phosphotriesterase enzyme against GD as measured using a multiple injection ITC method. Top panel graphs the raw power data measured during the experimental time course. Bottom panel illustrates data processed using Equation 4.

The precedent for using ITC to determine Michaelis-Menten kinetic parameters combined with the currently used pseudo-Michaelis-Menten model which describes the reactivation of OP nerve agent-inhibited enzyme by reactivators (Section 1.4.2) suggested that this technique could potentially be used to measure reactivation rates of OP-inhibited cholinesterases. This possibility was appealing for several reasons. First, ITC would allow for a direct measurement of the reactivation event, in contrast to the indirect measurement of the "return of enzyme activity" currently used. Additionally, reactivation in a calorimeter would remove a substantial amount of the error introduced by the large amount of liquid handling required by current methods. Finally, the measurement of heat would remove the need to use the enzyme activity reporter system and alleviate any concerns about direct reactivator interaction with that system which can convolute reactivation measurements.

4.2 ITC to Measure Reactivation

With this in mind, an experiment looking at the reactivation of VX-inhibited human plasma-derived butyrylcholinesterase (HuBuChE; Baxter Healthcare, Corp.) by 2PAM was conducted. These conditions were chosen because the reactivation rate of VX-inhibited HuBuChE by 2PAM is documented [130] to be slower than acetylcholinesterase reactivation rates, which should make it relatively easy to track using a calorimeter. Initially, the results of these experiments looked quite promising, as seen in Figure 4-3. The values for reactivation kinetic constants calculated using the ITC measurements (k_r = 0.00605±0.00013 sec^{-1}; K_D = 0.197±0.019 mM) were in reasonable agreement with the previously reported values (k_r = 0.00467 sec^{-1}; K_D = 0.759 mM [130]) determined using standard reactivation measurement techniques.

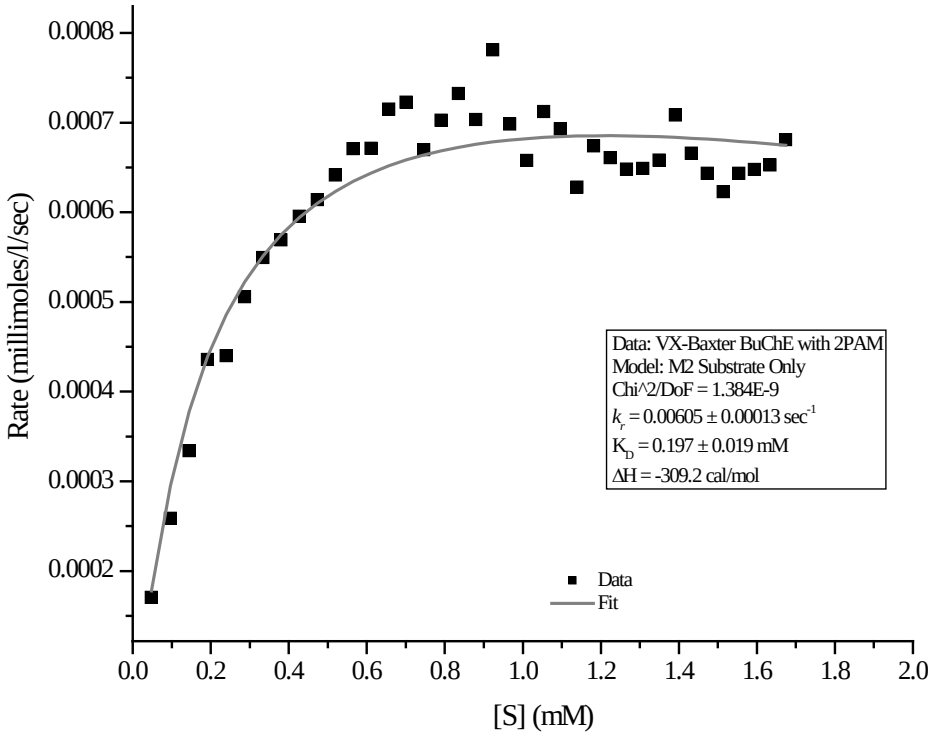

Figure 4-3. Initial reactivation assay measured via ITC. 2PAM was injected into a solution of VX-inhibited HuBuChE, and the resulting heat of reaction was measured.

However, a closer look at the data revealed several incongruities with this analysis. First, colorimetric measurement of the activity of the sample recovered from the reactivation cell showed that less than 1% of the enzyme had been reactivated (Figure A.16). Second, the raw data do not have the typical appearance of an ITC experiment measuring catalysis of substrate to product (refer to the top panel of Figure 4-2), appearing more like that of a binding experiment (Figure 4-4).

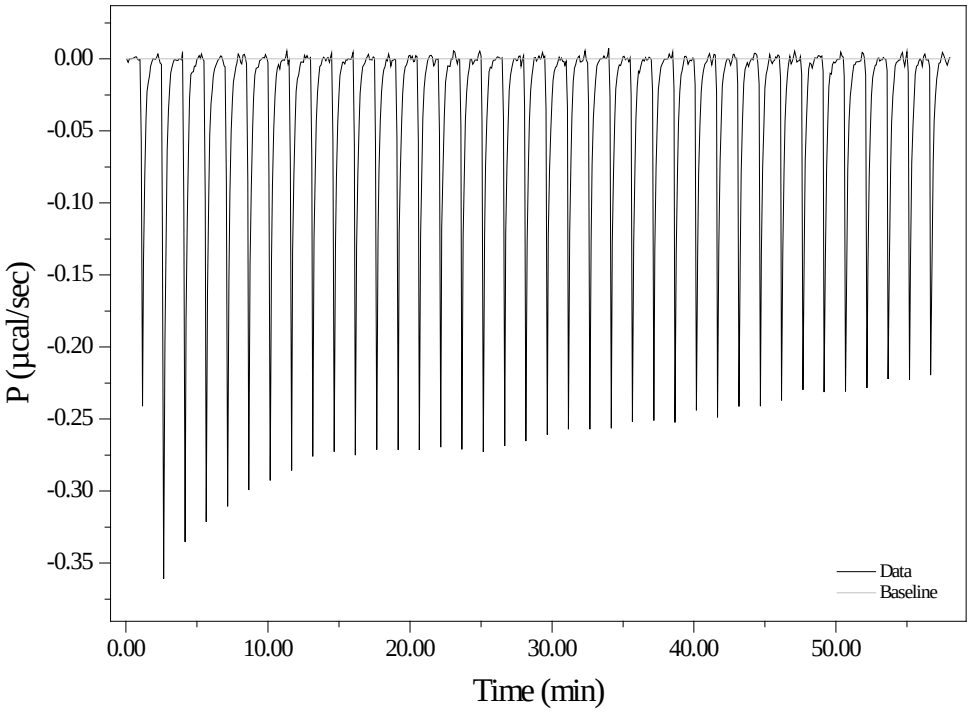

Figure 4-4. Graph of raw power measurements during injections of 2PAM into VX-inhibited HuBuChE.

Initially, this oddity was thought to be due to the experimental conditions for the reaction not being optimized. However, after several iterations of the experiment altering substrate concentration, enzyme concentration, injection volumes, etc., with similar raw data characteristics and greatly varied calculated kinetic parameters, revisiting the fundamental experimental assumptions seemed to be advisable.

In general terms, the ITC kinetics model assumes that the enzyme is acting as a catalyst that interacts with substrate to create product until the source of substrate is exhausted [127]. Like all catalysts, the enzyme itself is not changed by this process. These assumptions allow the heat generated in this process to be related directly to the

amount of product formed by the reaction (much the same way that product formation or substrate depletion can be directly related to a colorimetric or absorbance-based readout in other systems).

Unfortunately, these assumptions do not hold true for a reactivation interaction. In reactivation, the enzyme is not a catalyst. In fact, the inhibited enzyme would be better described as a "substrate" that undergoes a process to form the "product" of uninhibited enzyme. Following through with the comparison, the reactivator would be the candidate for "enzyme" in the reactivation interaction. However, oxime reactivators (such as 2PAM) would become phosphonylated and so would not meet the catalyst criteria of an "enzyme" because they would remain altered at the completion of the reactivation event. Upon further evaluation the reactivation event could be better classified as a transfer event in which the phosphonyl adduct is transferred from the enzyme to the small molecule reactivator.

This may be further complicated in the case of a reactivator with an alternative mechanism, such as ADOC. Given that ADOC appears to reactivate via an indirect mechanism, at least in part, it is possible that this reactivator could act as a "catalyst" in an ITC experiment. All of the other complications discussed earlier would still apply to the experiment, making analysis of such a system additionally convoluted, assuming that this difference in mechanism could even be detected using a measurement of enthalpy.

For the purposes of using enthalpy as a measurement to track the progression of a reaction, the fact that the reactivation interaction does not follow a traditional enzymatic process sheds light on the observation earlier that the ITC data of 2PAM and VX-inhibited HuBuChE more closely resembles a binding experiment than a

kinetic experiment. In reactivation, the majority of the enthalpy change of the interaction would likely be during the initial binding event of the small molecule to the much larger inhibited enzyme. The nucleophilic attack of the oxime reactivator which would follow binding would result in the counteracting exothermic bond formation and endothermic bond breaking in the active site of the enzyme. The resulting phosphonylated reactivator would then dissociate from the enzyme, but discerning any enthalpic contributions of this event as separate from the initial binding event would be experimentally difficult.

Additionally, review of the techniques for current assays to measure reactivation brings to light conditions that promote detection of product in the form of uninhibited enzyme. Namely, a dilution step before enzyme substrate is added for detection lowers the reactivator concentration such that substrate will out-compete reactivator at the active site of the enzyme. While this procedure is useful for colorimetric detection of uninhibited enzyme, a similar interaction would not occur in the experiments described earlier using ITC to measure reactivation. Effectively, the reactivator would reach a binding equilibrium in the sample cell of the calorimeter with both the inhibited and uninhibited enzyme without the presence of a substrate to compete for the active site. While an experiment including the enzyme substrate in the ITC method might be designed, careful evaluation of the data would be required to determine the viability of any such experiment as the enthalpic contributions of a progressive reactivation event coupled with the enzymatic hydrolysis of the substrate would be difficult to parse out in a single experiment.

As another possible complication, while 2PAM is not a prime example of an inhibitor of apo enzyme, other reactivators, including ADOC in this study, have been

found to have substantial inhibitory capacity towards apo enzyme. While ITC can be used to determine inhibition parameters for an inhibitor, a separate experiment with different conditions would be needed to measure this interaction. Any inhibition could not be detected in the reactivation ITC experiment described earlier in this chapter but would be easily detected in the discontinuous assay currently used to measure reactivation.

4.3 Additional Thoughts about ITC as a Tool for Reactivation

Recently, an alternative analysis method for ITC data has been proposed in which the initial binding and a subsequent event (in this case, RNA folding) in a kinetic interaction have been dissected in a single experiment [131, 132]. Each injection of a multiple injection method experiment is analyzed separately, and then these results are combined and described using a bimolecular association model with or without a subsequent kinetic step. While this method was useful for calculating quantitative parameters for the RNA binding/folding system tested and is postulated to be useful for other systems that incorporate a structural element into kinetic interactions [132], reactivation almost certainly does not include a large structural rearrangement. It is possible that comparing the measured heats after injection of a reactivator into a sample of inhibited enzyme across many different reactivators could offer a qualitative comparison system, but the value of those data is questionable.

4.4 Summary

While ITC appeared to offer a possible alternative to current methods used to measure reactivation, experiments appeared to measure the initial binding of reactivator with little or no enthalpy measured for the actual reactivation event. While

this measurement may be utilized for qualitative comparison purposes, determining the exact experimental parameters for this comparison is beyond the scope of this study. ITC likely cannot be used to measure reactivation kinetic parameters quantitatively because of the nature of the reactivation reaction as compared to traditional enzymatic hydrolysis reactions as outlined in this chapter.

Chapter 5

DISCUSSIONS AND FUTURE DIRECTIONS

5.1 ADOC as a Reactivator

ADOC shows promise as a first-generation compound of a novel class of reactivators, one of the first reactivators to incorporate neither an oxime motif nor a permanent charge since 2PAM was discovered in the mid-twentieth century. Of particular interest is the opportunity ADOC may afford the scientific community to leverage the knowledge that has been gained in the last century about drug design. Most pharmaceutical drug design efforts are focused on modulating the binding affinity of a small molecule. Historically, reactivators have posed a unique problem in that these molecules not only must bind their target but then must perform a function and dissociate from that target to be successful candidates.

Most reactivators today, including 2PAM, bind inhibited enzyme fairly well but proceed through the "work" of reactivation at a relatively slow rate. ADOC poses the unique problem of displaying poor binding affinity towards the inhibited enzyme active site, only coming to the attention of the reactivation community because of an extremely high rate of reactivation which was able to overcome poor binding. This initial study to elucidate the mechanistically important portions of ADOC versus those significant for binding will provide insight useful for the design of improved future reactivators, as has been demonstrated here with **17**.

Finally, this study uncovered the two mechanistic pathways by which ADOC may be achieving reactivation. While a nucleophilic attack mechanism involving the

activation of a water molecule appears to be the primary mechanism of reactivations, the results indicating that oxidation plays a role in ADOC reactivation are extremely interesting. Hopefully, future studies will be able to determine the exact nature of the mechanism of ADOC reactivation that is oxygen dependent and utilize this mechanistic insight in the design of improved reactivators.

5.2 ITC as a Tool for Measuring Reactivation

While ITC has been utilized to measure enzymatic hydrolysis in other systems successfully, the use of this method to measure reactivation reactions seems to be quite limited. The pseudo-Michaelis –Menten kinetic model currently used to describe reactivation reactions utilizes the formation of an active enzyme as the "product" which is formed, differing substantially from the catalytic process assumed for other Michaelis-Menten processes. Combined with the possibility that any ITC method optimized for reactivation by oxime-mediated nucleophilic attack of the phosphonylated active site may not be viable for a reactivator that operates via another mechanism, the non-classical nature of the reactivation reaction currently diminishes the potential of ITC as a robust measurement tool. Future work may find that the recently developed analysis methods could be utilized to better model the enthalpy measurements made during a reactivation ITC experiment, but currently the utility of ITC in reactivation may be limited only to characterization of reactivator binding to enzyme.

Chapter 6

MATERIALS AND METHODS

6.1 General Materials

6.1.1 Buffers

23. 0.1 M potassium phosphate buffer: 1 M K_2HPO_4 and 1M KH_2PO_4 were mixed to a measured pH of 7.0 and diluted to 0.1 M with ddH_2O. Buffer was filtered using a 0.22 µm pore cellulose acetate vacuum filter system (Corning, Inc.).

24. 0.1 M MOPS buffer: 3-(N-Morpholino)propanesulfonic acid sodium salt was made to 0.1 M in ddH_2O and the pH of the solution was adjusted using 0.1 M MOPS acid solution. Buffer was used at pH 7.0 or 7.4 depending on the experiment. Buffer was supplemented with 50 µM $CoCl_2$, if indicated. Buffer was filtered using a 0.22 µm pore cellulose acetate vacuum filter system (Corning, Inc.).

6.1.2 Common Reagents

1. Recombinant human acetylcholinesterase (HuAChE; AA780, Chesapeake PERL, Inc., Savage, MD)

2. Acetylthiocholine iodide (AtCh; Sigma-Aldrich Co. LLC., Catalog# A5751)

3. 5,5′-dithiobis-2-nitrobenzoic acid (DTNB; Sigma-Aldrich Co. LLC., Catalog# D8130)

4. Bovine serum albumin (BSA; Sigma-Aldrich Co. LLC., Catalog# A7906)

5. Organophosphorus nerve agents (tabun [GA], sarin [GB], soman [GD], cyclosarin [GF], VX and VR; US Army Edgewood Chemical Biological Center, Aberdeen Proving Ground, MD)

6. Trolox ((±)-6-Hydroxy-2,5,7,8-tetramethylchromane-2-carboxylic acid, Sigma-Aldrich Co. LLC Catalog # 238813)

7. Protexia recombinant butyrylcholinetserase (PharmAthene, Inc., Annapolis, MD)

8. Cyclohexyl methylphosphonic acid (Sigma-Aldrich Co. LLC Catalog # ERC-034)

9. Human plasma-derived butyrylcholinesterase (Baxter Healthcare, Corp., New Providence, NJ)

6.1.3 Study Specific Compounds

10. 4-amino-α-diethylamino-O-cresol (ADOC; Sigma-Aldrich Co. LLC Catalog # S561274)

11. 2-[(diethylamino)methyl]phenol (Princeton BioMolecular Research Catalog# OSSK_515806)

12. 4-aminophenol (Sigma-Aldrich Co. LLC Catalog # 60034)

13. (3-aminobenzyl)diethylamine (Sigma-Aldrich Co. LLC Catalog # CBR00121)

14. 3-[(diethylamino)methyl]-4-ethoxyaniline (Enamine Catalog# EN300-80977)

15. 4-amino-3-((diethylamino)methyl)phenol [74]

16. 4-amino-2-((dimethylamino)methyl)phenol [74]

17. 4-amino-3-((dimethylamino)methyl)phenol [74]

18. 4-amino-3-((diisopropylamino)methyl)phenol [74]

19. 4-amino-2-((dicyclohexylamino)methyl)phenol [74]

20. 2-((diethylamino)methyl)-4-(dimethylamino)phenol [74]

21. 4-acetamido-2-[(diethylamino)methyl]phenol (Sigma-Aldrich Co. LLC Catalog # S414026)

22. 2-amino-6-((diethylamino)methyl)phenol [74]

23. 2-amino-6-((dimethylamino)methyl)phenol [74]

24. 4-((4-(benzhydrylamino)butyl)amino)- 2-((diethylamino)methyl)phenol (synthesized for this study by Yuchen Zhang)

25. N^1-benzhydryl-N^4-(3-((diethylamino) methyl)-4-hydroxyphenyl)succinamide (synthesized for this study by Yuchen Zhang)

26. 2-((diethylamino)methyl)-4-(ethylamino)phenol (synthesized for this study by Benjamin Rupert)

6.1.4 Equipment

27. SpectraMax Plus 384 Microplate Spectrometer (Molecular Devices, Sunnyvale, CA)

28. Liquid Chromatography/Triple Quadrapole Mass Spectrometry System (LC/QQQ): 1260/1290 mixed module Infinity Quaternary Liquid Chromatography System with 6460 Triple Quadrapole Mass Spectrometer with Electrospray (ESI) source (Agilent Technologies, Santa Clara, CA)

29. Liquid Chromatography/Mass Spectrometry System (LC/MS): 1100 series mixed module Quaternary Liquid Chromatography System with 6130 Single Quadrapole Mass Spectrometer with Electrospray (ESI) source (Agilent Technologies, Santa Clara, CA)

30. Triple TOF 5600+ System (AB Sciex Pte. Ltd., Framingham, MA)

31. Varian Unity Inova 600 MHz Nuclear Magnetic Resonance System with 5mm PFG Penta probe controlled via VNMRJ 3.2 (Agilent Technologies, Inc., Santa Clara, CA)

32. MicroCal iTC200 Isothermal Titration Calorimeter (Malvern Instruments, Ltd., Worcestershire, UK)

6.1.5 Software

33. Prism, GraphPad Software, Inc. (La Jolla, CA)

34. Origin 7, OriginLab Corporation (Northampton, MA)

6.2 Methods

All inhibition and reactivation assays were conducted using recombinant human acetylcholinesterase (HuAChE, AA780, Chesapeake PERL, Inc., Savage, MD). Hydrolysis of acetylthiocholine iodide (AtCh, A5751, Sigma-Aldrich Co. LLC., St. Louis, MO) was measured using 5,5′-dithiobis-2-nitrobenzoic acid (DTNB, D8130, Sigma-Aldrich Co. LLC., St. Louis, MO). Measurements were made using a SpectraMax Plus 384 microplate reader (Molecular Devices, Sunnyvale, CA) utilizing 96-well clear bottom plates (655101, Greiner Bio-One GmbH, Frickenhausen, Germany). Unless otherwise indicated, all assays were performed in 0.1 M potassium phosphate buffer at pH 7.0 with 1 mg/mL bovine serum albumin (BSA, A7906, Sigma-Aldrich Co. LLC., St. Louis, MO) included to help stabilize HuAChE.

6.2.1 Measurement of IC_{50}

In 96-well plates, HuAChE activity against AtCh was measured in the presence of the indicated compound at concentrations ranging from 60 nM to125 mM. Maximum activity (100%) was determined using a negative control containing enzyme alone, and all activities were compared relative to this control. The resulting activities were plotted against the log value of the compound concentration and fit using a variable slope dose-response curve (Prism, GraphPad Software, Inc., La Jolla, CA).

6.2.2 Inhibition Assay

To determine the type of inhibition displayed by ADOC, the activity of HuAChE was measured in the presence of several concentrations of that compound at varying concentrations of AtCh. Inverse velocities were plotted according to the

inverse AtCh concentration and fit using a linear regression analysis (Prism, GraphPad Software, Inc., La Jolla, CA) to determine the nature of the inhibition [75].

6.2.3 Discontinuous Reactivation Assay

HuAChE was inhibited with a molar excess of nerve agent for a minimum of 10 min at room temperature. Excess free nerve agent was removed using Centri-Sep spin columns (Life Technologies, Grand Island, NY), and the inhibited sample was diluted to an appropriate concentration for use in further assays. An uninhibited positive control was similarly treated using buffer in place of nerve agent. Enzyme samples were mixed with reactivator compound to initiate reactivation, and aliquots were removed at various time points, diluted twenty-fold and measured for activity against AtCh. Percent reactivation was calculated by comparing each sample to a row-matched positive control of uninhibited HuAChE in the presence of reactivator. Residual activity at time zero was subtracted from each following time point to account for incomplete inhibition, and then triplicates were averaged. Nonlinear regression assuming maximal reactivation of 100% was used to determine k_{obs} [133, 134] at each reactivator concentration. These k_{obs} values were plotted against reactivator concentration and fit using a modified Michaelis-Menten equation [80] to calculate all parameters and associated standard deviations. Alternatively, the half-time of reactivation ($t_{1/2}$) was calculated for compounds tested at a single concentration (1 mM) using a one-phase association fit of the percent reactivation over time (Prism, GraphPad Software, Inc., La Jolla, CA), and these times were then compared to the spontaneous reactivation half-time of sample-matched inhibited enzyme using a ratio t-test.

6.2.4 Oxidation Dependence Experimental Conditions

An initial reactivation experiment to determine the reactivation half-times of 2PAM or ADOC against enzyme inhibited by GA, GB, GD, GF, VX, or VR was conducted using the conditions described below. Reactivators were present at 0.5 mM during reactivation incubation. No statistical analysis was conducted on these results, which were only used qualitatively to inform further experiments.

Additional experiments measured reactivation of VX-inhibited HuAChE to determine half-times of reactivation for 2PAM or ADOC at 0.2 mM using the discontinuous method described in the previous section. These data were analyzed using repeated measures one-way analysis of variances (ANOVA) followed by Tukey's multiple comparison tests. Measurements were repeated three times for each condition with each set of conditions (standard, oxidizing and reducing) in a replicate being performed on a single batch of inhibited enzyme.

6.2.4.1 Oxidizing Conditions

Potassium phosphate buffer as described earlier was used with the addition of 0.25 µg/mL horse radish peroxidase conjugated antibody (Innovative Research, Novi, MI) and 10 mM hydrogen peroxide. Incubation of the reactivation sample was conducted in a 96-well 1mL plate with a sealing cap (Nunc Thermo Fisher Scientific, Waltham, MA) at room temperature (approximately 25ºC).

6.2.4.2 Reducing Conditions

Potassium phosphate buffer as described earlier was sparged with nitrogen for at least one hour before adding Trolox (Sigma-Aldrich, St. Louis, MO) to a concentration of 320 µM. All media manipulations were conducted under a nitrogen

cone, and incubation of the reactivation sample was conducted in a 96-well 1 mL plate with a sealing cap at room temperature (approximately 25ºC).

6.2.5 ADOC/GF Solution Reactions

6.2.5.1 Absorbance Spectra Measurement

Using quartz cuvettes, the absorbance of ADOC was determined in 0.1 M MOPS buffer (pH 7.4, 50 µM $CoCl_2$) at wavelengths from 200 nm to 400 nm at concentrations ranging from 15 µM to 6.67 mM using a SpectraMax Plus384 microplate spectrometer. The linear range of detection was determined to be between 15 and 878 µM ($R^2 = 0.9975$) at 303 nm.

For the measurement of ADOC/agent interaction, 75 µL ADOC at 2 mM in 0.1 M MOPS (pH 7.4, 50 µM $CoCl_2$) was added to 1.425 mL 10.5 mM GF, GD, or 0.1 M MOPS (pH 7.4, 50 µM $CoCl_2$) (agents were provided in this buffer) to begin time course. Absorbance spectra at wavelengths from 255 nm to 355 nm or 500 nm were measured in 1 nm increments at time points ranging from <1 min after addition of ADOC to 208 min after addition. Samples were kept in quartz cuvettes sealed with Parafilm at room temperature (~25ºC) away from light except during measurement for the entire time course of the experiment.

6.2.5.2 Liquid Chromatography/Mass Spectrometry

6.2.5.2.1 Initial Characterization of ADOC/Agent Reaction Product

ADOC and GF, GD, or buffer were mixed as described in Section 6.2.5.1, and ions were measured using the LC/QQQ system described in Section 6.1.4 (1 µL direct injection, mobile phase: 50:50 H_2O:MeOH, 0.1% formic acid, fragmentation: 80,

mode: positive, Detection: scan 50 to 600 m/z). Peak area was determined after extracting detection of ions at 355 m/z (ADOC-GF^{+1}), 357 m/z (ADOC-GD^{+1}), and 195 m/z (ADOC^{+1}) and plotted versus time to determine rates of formation and decay, respectively.

6.2.5.2.2 ADOC/Agent Reaction Product Isolation

An ADOC/GF mixture similar to that described in 6.2.5.1, with the exception of having equimolar amounts of ADOC and GF, was used to generate the phosphonylated-ADOC product (ADOC-GF) described earlier. To purify the product from the reaction mixture, the solution was passed over a Zorbax Eclipse C-18 Plus liquid chromatography column (2.1 x 50 mm, 5 µm, Agilent Biotechnologies, Inc. Catalog # 959746-902) using a water:methanol gradient program eight minutes long in total (0 to 3 min = 23% MeOH/77% H_2O, 3 to 4 min = gradient ramp to 85% MeOH/15% H_2O, 4 to 6 min = 85% MeOH/15% H_2O, 6 to 7 min = gradient ramp to 23% MeOH/77% H_2O, 7 to 8 min = 23% MeOH/77% H_2O). Separation was followed using both absorption at 303 nm and mass spectrometry with ADOC appearing between 0 and 2 minutes, the protonated form of the product appearing between 2.1 and 2.6 minutes, GF appearing between 4 and 4.5 min, and the deprotonated form of the product appearing between 5.1 and 5.3 minutes (Figure A.4 and A.5). The products eluted at 2.5 and 5.2 minutes from several injections (typically 10 to 12 injections performed in a single day) were collected separately and exchanged into 100% MeOH by binding it to an Oasis HLB 3 cc cartridge (Waters Corp., Milford, MA), washing, and eluting as described in the product's recommended protocol. The purified products in MeOH were then lyophilized, weighed, and subsequently stored in MeOH at -80ºC for use in later experiments.

Later experiments determined that the products eluted at 2.5 and 5.2 minutes respectively were actually the same compound at different protonation states (Appendix) and all later experiments were conducted using the 5.2-minute ADOC-GF product only.

The purified ADOC-GF was analyzed in a time of flight (TOF) mass spectrometer (see section 6.1.4) to determine the mass/charge ratio of the molecule at a high resolution. In short, 5 µL of the purified sample in MeOH was directly injected into a Sciex 5600+ system. The detected mass was then used to predict the elemental composition of the compound, which after elimination of three candidates that were not possible, corresponded to the predicted structure of the product.

6.2.6 NMR

All NMR measurements were conducted on sample dissolved in deuterated methanol (CD_3OH). Proton and carbon NMR was conducted using a standard 2-pulse sequence (S2PUL). 1D and 2D gradient-selected heteronuclear multiple quantum coherence (g-HMQC) NMR was conducted using standard pulse sequences.

6.2.7 Specific Reaction of Furfural

In a solution of 1 N hydrochloric acid, approximately equimolar amounts of furfural was mixed with ADOC, **12**, or phosphonylated ADOC and allowed to incubate at room temperature. Each sample was measured via direct injection of 2 µL in 100% MeOH mobile phase using LC/QQQ (no column; Mode: Positive, Scan: 50 to 600 m/z; Fragmentation: 80). Control samples of each compound in 1 N HCl were also analyzed.

6.2.8 Enzyme Product Detection

6.2.8.1 Standard Curve Measurements

Initially, standard curves to determine the limits of detection for the ions corresponding to phosphonylated ADOC (ADOC-GF^{+1} m/z = 355) and cyclohexylmethyl phosphonic acid (CMP^{-1} = 177) were determined using purified ADOC-GF (isolation described earlier) and a commercially available standard, respectively. ADOC-GF was detected after injection over the column system described in section 6.2.5.2.2 with the addition of a Zorbax Eclipse Plus-C18 narrow bore guard column (2.1 x 12.5 mm, 5 µm, Agilent Technologies, Inc. Catalog # 821125-936). CMP was detected using only the guard column and detection was achieved using negative mode ionization (Mobile phase: 100% MeOH, fragmentation: 80, mode: negative, Detection: scan 50 to 350 m/z). The area of each of the detected ions was determined using several compound concentrations. The resulting plots were analyzed to determine the relationship between the number of moles injected and the signal detected (Appendix).

6.2.8.2 ADOC-mediated Enzyme Reactivation Product Detection

Protexia BuChE, 267.5 nmols in 250 µL, was mixed with 0.9 molar equivalents of the P(-) isomer of GF and incubated at room temperature for one hour. Residual activity of the sample was measured by AtCh hydrolysis and compared to a buffer control to determine the level of inhibition (~85% inhibited). To a portion of the inhibited sample, along with a matched uninhibited control, containing 51.4 nmols of enzyme (43.6 nmols of which should be phosphonylated) was added ADOC to a final concentration of 40 mM (~100-fold molar excess of phosphonylated enzyme) to begin

reactivation. Reactivation was monitored using the assay described in 6.2.3 until greater than 50% of the sample had regained activity (~1 hour).

ADOC-GF and CMP production in the samples, including controls, was measured as described in the previous sections, and the detection levels were compared to the standard curve to calculate the moles of each.

6.2.9 Isothermal Titration Calorimetry

Human plasma-derived butyrylcholinesterase was inhibited with a ten-fold molar excess of racemic VX incubated at room temperature for 15 minutes. Excess VX was removed using a Centri-Sep spin column as described in Section 6.2.3. This sample was diluted to a final concentration of 150 μM in 0.1 M KPO_4 buffer at pH 7.0 and added to the sample cell of a MicroCal iTC200 calorimeter. The sample was not degassed, although care was taken to avoid introduction of excess air to the cell. 2PAM at 20 mM or 10 mM in identical buffer as enzyme sample was loaded into the syringe of the calorimeter using the semi-automatic program included in the MicroCal iTC200 software for this purpose. Assay was conducted at 30°C with no less than 20 injections at volumes of 1 to 1.5 μL each. An initial baseline of 60 seconds was used for all experiments. All experimental data were visualized and analyzed using Origin 7 software with the MicroCal specific add on provided by the instrument manufacturer.

REFERENCES

If you want to number your bibliographic entries, change the style of the items to *Bib Entry - numbered*.

1. Romano, J. A., Salem, H. & Lukey, B. J. (2007) Chemical Warfare Agents: Chemistry, Pharmacology, Toxicology, and Therapeutics, Second Edition, CRC Press.

2. Sartori, M. & Marisson, L. W. (1943) The War Gases, Chemistry and Analysis, Churchill.

3. Prentiss, A. M. & Fisher, G. J. B. (1937) Chemicals in war: a treatise on chemical warfare, McGraw-Hill, New York.

4. Tucker, J. (2007) War of Nerves: Chemical Warfare from World War I to Al-Qaeda, Knopf Doubleday Publishing Group.

5. LeRoy, W. S. & Yanka, D. E. (1947) The History of Captured Enemy Toxic Munitions in the American Zone, European Theater, May 1945 to June 1947, Office of the Chief of Chemical Corps, Headquarters, European Command.

6. Koelle, G. B. (2013) Cholinesterases and Anticholinesterase Agents, Springer Berlin Heidelberg.

7. Ghosh, R. & Newman, J. E. (1955) A new group of organophosphorus pesticides., Chemistry and Industry. **118**.

8. Rossman, Y., Eisenkraft, A., Milk, N., Shiyovich, A., Ophir, N., Shrot, S., Kreiss, Y. & Kassirer, M. (2014) Lessons Learned from the Syrian Sarin Attack: Evaluation of the Clinical Syndrome through Social Media, Annals of Internal Medicine. **160**, 644-649.

9. Gilman, A. G., Rall, T. W., Nies, A. S. & Taylor, P. (1990) Goodman and Gilman's The Pharmacological Basis of Therapeutics 8th edn, Mcgraw-Hill New York.

10. Benschop, H. P., Konings, C. A., van Genderen, J. & de Jong, L. P. (1984) Isolation, in vitro activity, and acute toxicity in mice of the four stereoisomers of soman, Fundamental and applied toxicology : official journal of the Society of Toxicology. **4**, S84-95.

11. Benschop, H. P., Konings, C. A., Van Genderen, J. & De Jong, L. P. (1984) Isolation, anticholinesterase properties, and acute toxicity in mice of the four stereoisomers of the nerve agent soman, Toxicol Appl Pharmacol. **72**, 61-74.

12. Jong, L. P. A. d. & Benschop, H. P. (1988) Biochemical and Toxicological Implications of Chirality in Anticholinesterase Organophosphates in Stereoselectivity of Pesticide; Biological and Chemical Problems (E.J. Ariens, J. J. S. v. R., W. Welling, ed) pp. 109-130, Elsevier Science Publishers, Amsterdam.

13. Benschop, H. P., Trap, H. C., Spruit, H. E., Van Der Wiel, H. J., Langenberg, J. P. & De Jong, L. P. (1998) Low level nose-only exposure to the nerve agent soman: toxicokinetics of soman stereoisomers and cholinesterase inhibition in atropinized guinea pigs, Toxicol Appl Pharmacol. **153**, 179-85.

14. Shafferman, A., Ordentlich, A., Barak, D., Stein, D., Ariel, N. & Velan, B. (1996) Aging of phosphylated human acetylcholinesterase: catalytic processes mediated by aromatic and polar residues of the active centre, Biochemical Journal. **318**, 833-840.

15. Masson, P., Nachon, F. & Lockridge, O. (2010) Structural approach to the aging of phosphylated cholinesterases, Chem Biol Interact. **187**, 157-62.

16. Sanson, B., Nachon, F., Colletier, J. P., Froment, M. T., Toker, L., Greenblatt, H. M., Sussman, J. L., Ashani, Y., Masson, P., Silman, I. & Weik, M. (2009) Crystallographic snapshots of nonaged and aged conjugates of soman with acetylcholinesterase, and of a ternary complex of the aged conjugate with pralidoxime, J Med Chem. **52**, 7593-603.

17. Kwong, T. C. (2002) Organophosphate pesticides: biochemistry and clinical toxicology, Ther Drug Monit. **24**, 144-9.

18. Worek, F., Thiermann, H., Szinicz, L. & Eyer, P. (2004) Kinetic analysis of interactions between human acetylcholinesterase, structurally different organophosphorus compounds and oximes, Biochem Pharmacol. **68**, 2237-48.

19. Aas, P. (2003) Future considerations for the medical management of nerve-agent intoxication, Prehospital and disaster medicine. **18**, 208-16.

20. Cone, D. C. & Koenig, K. L. (2005) Mass casualty triage in the chemical, biological, radiological, or nuclear environment, European journal of emergency medicine : official journal of the European Society for Emergency Medicine. **12**, 287-302.

21. Khoshnevis, M. A., Panahi, Y., Ghanei, M., Borna, H., Sahebkar, A. & Aslani, J. (2015) A Triage Model for Chemical Warfare Casualties, Trauma monthly. **20**, e16211.

22. Eckert, S., Eyer, P., Muckter, H. & Worek, F. (2006) Kinetic analysis of the protection afforded by reversible inhibitors against irreversible inhibition of acetylcholinesterase by highly toxic organophosphorus compounds, Biochem Pharmacol. **72**, 344-57.

23. Layish, I., Krivoy, A., Rotman, E., Finkelstein, A., Tashma, Z. & Yehezkelli, Y. (2005) Pharmacologic prophylaxis against nerve agent poisoning, The Israel Medical Association journal : IMAJ. **7**, 182-7.

24. Lorke, D. E., Hasan, M. Y., Nurulain, S. M., Shafiullah, M., Kuca, K. & Petroianu, G. A. (2011) Pretreatment for acute exposure to diisopropylfluorophosphate: in vivo efficacy of various acetylcholinesterase inhibitors, J Appl Toxicol. **31**, 515-23.

25. Patocka, J., Jakl, A., Bajgar, J. & Fusek, J. (1991) Efficacy of various pretreatment and therapy regimens against soman lethality in mice, Sbornik vedeckych praci Lekarske fakulty Karlovy university v Hradci Kralove. **34**, 243-7.

26. Stitcher, D. L., Harris, L. W., Heyl, W. C. & Alter, S. C. (1978) Effects of pyridostigmine and cholinolytics on cholinesterase and acetylcholine in Soman poisoned rats, Drug and chemical toxicology. **1**, 355-62.

27. Temple, R. (2003) Pyridostigmine Bromide Approval Letter in (Administration, U. S. F. a. D., ed)

28. Satu, M. S., Romano, J. A., Romano, J. A., Salem, H. & Lukey, B. J. (2000) Chemical Warfare Agents: Toxicity at Low Levels, CRC Press.

29. Allderdice, P. W., Gardner, H. A., Galutira, D., Lockridge, O., LaDu, B. N. & McAlpine, P. J. (1991) The cloned butyrylcholinesterase (BCHE) gene maps to a single chromosome site, 3q26, Genomics. **11**, 452-4.

30. Massoulie, J. & Bon, S. (1982) The molecular forms of cholinesterase and acetylcholinesterase in vertebrates, Annu Rev Neurosci. **5**, 57-106.

31. Chatonnet, A. & Lockridge, O. (1989) Comparison of butyrylcholinesterase and acetylcholinesterase, Biochem J. **260**, 625-34.

32. Chatonnet, A. & Lockridge, O. (1989) Comparison of butyrylcholinesterase and acetylcholinesterase, Biochemical Journal. **260**, 625-634.

33. Massoulie, J., Bon, S., Perrier, N. & Falasca, C. (2005) The C-terminal peptides of acetylcholinesterase: cellular trafficking, oligomerization and functional anchoring, Chem Biol Interact. **157-158**, 3-14.

34. Radic, Z., Pickering, N. A., Vellom, D. C., Camp, S. & Taylor, P. (1993) Three distinct domains in the cholinesterase molecule confer selectivity for acetyl- and butyrylcholinesterase inhibitors, Biochemistry. **32**, 12074-12084.

35. Nicolet, Y., Lockridge, O., Masson, P., Fontecilla-Camps, J. C. & Nachon, F. (2003) Crystal structure of human butyrylcholinesterase and of its complexes with substrate and products, J Biol Chem. **278**, 41141-7.

36. Vellom, D. C., Radic, Z., Li, Y., Pickering, N. A., Camp, S. & Taylor, P. (1993) Amino acid residues controlling acetylcholinesterase and butyrylcholinesterase specificity, Biochemistry. **32**, 12-17.

37. Nachon, F., Asojo, O. A., Borgstahl, G. E., Masson, P. & Lockridge, O. (2005) Role of water in aging of human butyrylcholinesterase inhibited by echothiophate: the crystal structure suggests two alternative mechanisms of aging, Biochemistry. **44**, 1154-62.

38. Cerasoli, D. M., Griffiths, E. M., Doctor, B. P., Saxena, A., Fedorko, J. M., Greig, N. H., Yu, Q. S., Huang, Y., Wilgus, H., Karatzas, C. N., Koplovitz, I. & Lenz, D. E. (2005) In vitro and in vivo characterization of recombinant human butyrylcholinesterase (Protexia) as a potential nerve agent bioscavenger, Chem Biol Interact. **157-158**, 363-5.

39. Lenz, D. E., Maxwell, D. M., Koplovitz, I., Clark, C. R., Capacio, B. R., Cerasoli, D. M., Federko, J. M., Luo, C., Saxena, A., Doctor, B. P. & Olson, C. (2005) Protection against soman or VX poisoning by human butyrylcholinesterase in guinea pigs and cynomolgus monkeys, Chem Biol Interact. **157-158**, 205-10.

40. Huang, Y. J., Huang, Y., Baldassarre, H., Wang, B., Lazaris, A., Leduc, M., Bilodeau, A. S., Bellemare, A., Cote, M., Herskovits, P., Touati, M., Turcotte, C., Valeanu, L., Lemee, N., Wilgus, H., Begin, I., Bhatia, B., Rao, K., Neveu, N., Brochu, E., Pierson, J., Hockley, D. K., Cerasoli, D. M., Lenz, D. E., Karatzas, C. N. & Langermann, S. (2007) Recombinant human butyrylcholinesterase from milk of transgenic animals to protect against organophosphate poisoning, Proc Natl Acad Sci U S A. **104**, 13603-8.

41. Lenz, D. E., Clarkson, E. D., Schulz, S. M. & Cerasoli, D. M. (2010) Butyrylcholinesterase as a therapeutic drug for protection against percutaneous VX, Chem Biol Interact. **187**, 249-52.

42. Mumford, H., Price, M. E., Cerasoli, D. M., Teschner, W., Ehrlich, H., Schwarz, H. P. & Lenz, D. E. (2010) Efficacy and physiological effects of human butyrylcholinesterase as a post-exposure therapy against percutaneous poisoning by VX in the guinea-pig, Chem Biol Interact. **187**, 304-8.

43. Mumford, H., M, E. P., Lenz, D. E. & Cerasoli, D. M. (2011) Post-exposure therapy with human butyrylcholinesterase following percutaneous VX challenge in guinea pigs, Clinical toxicology (Philadelphia, Pa). **49**, 287-97.

44. Millard, C. B., Lockridge, O. & Broomfield, C. A. (1995) Design and Expression of Organophosphorous Acid Anhydride Hydrolase Activity in Human Butyrylcholinesterase, Biochemistry. **34**, 15925-15933.

45. Geyer, B. C., Kannan, L., Garnaud, P. E., Broomfield, C. A., Cadieux, C. L., Cherni, I., Hodgins, S. M., Kasten, S. A., Kelley, K., Kilbourne, J., Oliver, Z. P., Otto, T. C., Puffenberger, I., Reeves, T. E., Robbins, N., 2nd, Woods, R. R., Soreq, H., Lenz, D. E., Cerasoli, D. M. & Mor, T. S. (2010) Plant-derived human butyrylcholinesterase, but not an organophosphorous-compound hydrolyzing variant thereof, protects rodents against nerve agents, Proc Natl Acad Sci U S A. **107**, 20251-6.

46. Valiyaveettil, M., Alamneh, Y., Biggemann, L., Soojhawon, I., Farag, H. A., Agrawal, P., Doctor, B. P. & Nambiar, M. P. (2011) In vitro efficacy of paraoxonase 1 from multiple sources against various organophosphates, Toxicol In Vitro. **25**, 905-13.

47. Valiyaveettil, M., Alamneh, Y., Rezk, P., Biggemann, L., Perkins, M. W., Sciuto, A. M., Doctor, B. P. & Nambiar, M. P. (2011) Protective efficacy of catalytic bioscavenger, paraoxonase 1 against sarin and soman exposure in guinea pigs, Biochem Pharmacol. **81**, 800-9.

48. Sarkar, M., Harsch, C. K., Matic, G. T., Hoffman, K., Norris, J. R., 3rd, Otto, T. C., Lenz, D. E., Cerasoli, D. M. & Magliery, T. J. (2012) Solubilization and humanization of paraoxonase-1, Journal of lipids. **2012**, 610937.

49. Kirby, S. D., Norris, J. R., Richard Smith, J., Bahnson, B. J. & Cerasoli, D. M. (2013) Human paraoxonase double mutants hydrolyze V and G class organophosphorus nerve agents, Chem Biol Interact. **203**, 181-5.

50. Mata, D. G., Rezk, P. E., Sabnekar, P., Cerasoli, D. M. & Chilukuri, N. (2014) Investigation of evolved paraoxonase-1 variants for prevention of organophosphorous pesticide compound intoxication, J Pharmacol Exp Ther. **349**, 549-58.

51. Worek, F., Seeger, T., Goldsmith, M., Ashani, Y., Leader, H., Sussman, J. S., Tawfik, D., Thiermann, H. & Wille, T. (2014) Efficacy of the rePON1 mutant IIG1 to prevent cyclosarin toxicity in vivo and to detoxify structurally different nerve agents in vitro, Arch Toxicol. **88**, 1257-66.

52. Trovaslet-Leroy, M., Musilova, L., Renault, F., Brazzolotto, X., Misik, J., Novotny, L., Froment, M. T., Gillon, E., Loiodice, M., Verdier, L., Masson, P., Rochu, D., Jun, D. & Nachon, F. (2011) Organophosphate hydrolases as catalytic bioscavengers of organophosphorus nerve agents, Toxicol Lett. **206**, 14-23.

53. Wales, M. E. & Reeves, T. E. (2012) Organophosphorus hydrolase as an in vivo catalytic nerve agent bioscavenger, Drug Test Anal. **4**, 271-81.

54. Worek, F., Seeger, T., Reiter, G., Goldsmith, M., Ashani, Y., Leader, H., Sussman, J. L., Aggarwal, N., Thiermann, H. & Tawfik, D. S. (2014) Post-exposure treatment of VX poisoned guinea pigs with the engineered phosphotriesterase mutant C23: a proof-of-concept study, Toxicol Lett. **231**, 45-54.

55. Goldsmith, M., Eckstein, S., Ashani, Y., Greisen, P., Jr., Leader, H., Sussman, J. L., Aggarwal, N., Ovchinnikov, S., Tawfik, D. S., Baker, D., Thiermann, H. & Worek, F. (2015) Catalytic efficiencies of directly evolved phosphotriesterase variants with structurally different organophosphorus compounds in vitro, Arch Toxicol.

56. Masson, P. & Lushchekina, S. V. (2016) Emergence of catalytic bioscavengers against organophosphorus agents, Chem Biol Interact.

57. Worek, F., Thiermann, H. & Wille, T. (2016) Catalytic bioscavengers in nerve agent poisoning: A promising approach?, Toxicol Lett. **244**, 143-8.

58. Gupta, R. C. (2009) Handbook of Toxicology of Chemical Warfare Agents, Elsevier Science.

59. Becker, C., Worek, F. & John, H. (2010) Chromatographic analysis of toxic phosphylated oximes (POX): a brief overview, Drug Test Anal. **2**, 460-8.

60. Luo, C., Saxena, A., Smith, M., Garcia, G., Radic, Z., Taylor, P. & Doctor, B. P. (1999) Phosphoryl Oxime Inhibition of Acetylcholinesterase during Oxime Reactivation Is Prevented by Edrophonium, Biochemistry. **38**, 9937-9947.

61. Becker, G., Kawan, A., Gutzeit, D., Worek, F. & Szinicz, L. (2007) Direct reaction of oximes with crotylsarin, cyclosarin, or VX in vitro, Arch Toxicol. **81**, 415-20.

62. Davies, D. R. & Green, A. L. (1956) The kinetics of reactivation, by oximes, of cholinesterase inhibited by organophosphorus compounds., Biochem J. **63**, 529-35.

63. Wong, L., Radić, Z., Brüggemann, R. J. M., Hosea, N., Berman, H. A. & Taylor, P. (2000) Mechanism of Oxime Reactivation of Acetylcholinesterase Analyzed by Chirality and Mutagenesis†, Biochemistry. **39**, 5750-5757.

64. Demar, J. C., Clarkson, E. D., Ratcliffe, R. H., Campbell, A. J., Thangavelu, S. G., Herdman, C. A., Leader, H., Schulz, S. M., Marek, E., Medynets, M. A., Ku, T. C., Evans, S. A., Khan, F. A., Owens, R. R., Nambiar, M. P. & Gordon, R. K. (2010) Pro-2-PAM therapy for central and peripheral cholinesterases, Chem Biol Interact. **187**, 191-8.

65. Shih, T. M., Skovira, J. W., O'Donnell, J. C. & McDonough, J. H. (2010) Treatment with tertiary oximes prevents seizures and improves survival following sarin intoxication, J Mol Neurosci. **40**, 63-9.

66. Skovira, J. W., O'Donnell, J. C., Koplovitz, I., Kan, R. K., McDonough, J. H. & Shih, T. M. (2010) Reactivation of brain acetylcholinesterase by monoisonitrosoacetone increases the therapeutic efficacy against nerve agents in guinea pigs, Chem Biol Interact. **187**, 318-24.

67. Michaelis, L., Menten, M. L., Johnson, K. A. & Goody, R. S. (2011) The original Michaelis constant: translation of the 1913 Michaelis-Menten paper, Biochemistry. **50**, 8264-9.

68. Ellman, G., Courtney, K., V Andres, J. & Featherstone, R. (1961) A New and Rapid Colorimetric Determination of Acetylcholinesterase Activity, Biochemical Pharmacology. **7**, 88-95.

69. Colletier, J. P., Fournier, D., Greenblatt, H. M., Stojan, J., Sussman, J. L., Zaccai, G., Silman, I. & Weik, M. (2006) Structural insights into substrate traffic and inhibition in acetylcholinesterase, EMBO J. **25**, 2746-56.

70. Worek, F., Eyer, P., Aurbek, N., Szinicz, L. & Thiermann, H. (2007) Recent advances in evaluation of oxime efficacy in nerve agent poisoning by in vitro analysis, Toxicol Appl Pharmacol. **219**, 226-34.

71. Worek, F., Reiter, G., Eyer, P. & Szinicz, L. (2002) Reactivation kinetics of acetylcholinesterase from different species inhibited by highly toxic organophosphates, Arch Toxicol. **76**, 523-9.

72. Worek, F. & Thiermann, H. (2011) Reactivation of organophosphate-inhibited human acetylcholinesterase by isonitrosoacetone (MINA): a kinetic analysis, Chem Biol Interact. **194**, 91-6.

73. Kovarik, Z., Radic, Z., Berman, H. A., Simeon-Rudolf, V., Reiner, E. & Taylor, P. (2004) Mutant Cholinesterases Possessing Enhanced Capacity for Reactivation of Their Phosphonylated Conjugates, Biochemistry. **43**, 3222-29.

74. Cadieux, C. L., Wang, H., Zhang, Y., Koenig, J. A., Shih, T., McDonough, J., Koh, J. & Cerasoli, D. M. (2016) Probing the Activity of a Non-Oxime Reactivator for Acetylcholinesterase Inhibited by Organophosphorus Nerve Agents in Chem Biol Interact.

75. Katz, F. S., Pecic, S., Tran, T. H., Trakht, I., Schneider, L., Zhu, Z., Ton-That, L., Luzac, M., Zlatanic, V., Damera, S., Macdonald, J., Landry, D. W., Tong, L. & Stojanovic, M. N. (2015) Discovery of New Classes of Compounds that Reactivate Acetylcholinesterase Inhibited by Organophosphates, Chembiochem.

76. Shih, T. M., Skovira, J. W., O'Donnell, J. C. & McDonough, J. H. (2009) Evaluation of nine oximes on in vivo reactivation of blood, brain, and tissue cholinesterase activity inhibited by organophosphorus nerve agents at lethal dose, Toxicol Mech Methods. **19**, 386-400.

77. Abbara, C., Rousseau, J., Lelièvre, B., Turcant, A., Lallement, G., Ferec, S., Bardot, I. & Diquet, B. (2010) Pharmacokinetic analysis of pralidoxime after its intramuscular injection alone or in combination with atropine-avizafone in healthy volunteers, British Journal of Pharmacology. **161**, 1857-1867.

78. Krupka, R. M. (1963) The Mechanism of Action of Acetylcholinesterase: Substrate Inhibition and the Binding of Inhibitors, Biochemistry. **2**, 76-82.

79. Worek, F., Szinicz, L. & Thiermann, H. (2005) Estimation of oxime efficacy in nerve agent poisoning: a kinetic approach, Chem Biol Interact. **157-158**, 349-52.

80. Aurbek, N., Thiermann, H., Szinicz, L., Eyer, P. & Worek, F. (2006) Analysis of inhibition, reactivation and aging kinetics of highly toxic organophosphorus compounds with human and pig acetylcholinesterase, Toxicology. **224**, 91-9.

81. Hawley, S. R., Bray, P. G., O'Neill, P. M., Park, B. K. & Ward, S. A. (1996) The role of drug accumulation in 4-aminoquinoline antimalarial potency: The influence of structural substitution and physicochemical properties, Biochemical Pharmacology. **52**, 723-733.

82. Warhurst, D. C., Steele, J. C. P., Adagu, I. S., Craig, J. C. & Cullander, C. (2003) Hydroxychloroquine is much less active than chloroquine against chloroquine-resistant Plasmodium falciparum, in agreement with its physicochemical properties, Journal of Antimicrobial Chemotherapy. **52**, 188-193.

83. Hansch, C., Leo, A. & Taft, R. W. (1991) A survey of Hammett substituent constants and resonance and field parameters, Chem Rev. **91**, 165-195.

84. Bierwisch, A., Wille, T., Thiermann, H. & Worek, F. (2016) Kinetic analysis of interactions of amodiaquine with human cholinesterases and organophosphorus compounds, Toxicol Lett. **246**, 49-56.

85. Bruice, P. Y. (2004) Organic Chemistry, 4th edn, Pearson/Prentice Hall, Upper Saddle River, NJ.

86. Hall, H. K. (1957) Correlation of the Base Strengths of Amines1, Journal of the American Chemical Society. **79**, 5441-5444.

87. Gross, K. C. & Seybold, P. G. (2001) Substituent effects on the physical properties and pKa of phenol, International Journal of Quantum Chemistry. **85**, 569-579.

88. Gross, K. C. & Seybold, P. G. (2000) Substituent effects on the physical properties and pKa of aniline, International Journal of Quantum Chemistry. **80**, 1107-1115.

89. Lockridge, O., Blong, R. M., Masson, P., Froment, M. T., Millard, C. B. & Broomfield, C. A. (1997) A single amino acid substitution, Gly117His, confers phosphotriesterase (organophosphorus acid anhydride hydrolase) activity on human butyrylcholinesterase., Biochemistry. **36**, 786-795.

90. Masson, P., Nachon, F., Broomfield, C. A., Lenz, D. E., Verdier, L., Schopfer, L. M. & Lockridge, O. (2008) A collaborative endeavor to design cholinesterase-based catalytic scavengers against toxic organophosphorus esters, Chem Biol Interact. **175**, 273-80.

91. Amitay, M. & Shurki, A. (2011) Hydrolysis of organophosphate compounds by mutant butyrylcholinesterase: a story of two histidines, Proteins. **79**, 352-64.

92. Vyas, S., Beck, J. M., Xia, S., Zhang, J. & Hadad, C. M. (2010) Butyrylcholinesterase and G116H, G116S, G117H, G117N, E197Q and G117H/E197Q mutants: a molecular dynamics study, Chem Biol Interact. **187**, 241-5.

93. EPSTEIN, J., Michel, H. O., Rosenblatt, D. H., Plapinger, R. E., Stephani, R. A. & Cook, E. (1964) Reactions of Isopropyl Methylphosphonofluoridate with Substituted Phenols. II, Journal of the American Chemical Society. **86**, 4959-63.

94. Friedemann, T. E., Keegan, P. K. & Witt, N. F. (1964) Determination of Furan Aldehydes. Reaction with Aniline in Acetic and Hydrochloric Acid Solutions, Anal Biochem. **8**, 300-11.

95. Goodwin, J. F. (1972) Reaction of aniline and its alkyl derivatives with hexoses and pentoses, Anal Biochem. **48**, 120-8.

96. Mulliken, S. P. (1904) A Method for the Identification of Pure Organic Compounds by a Systematic Analytical Procedure Based on Physical Properties and Chemical Reactions, J. Wiley & sons, Incorporated.

97. Sussman, J. L., Harel, M., Frolow, F., Oefner, C., Goldman, A., Toker, L. & Silman, I. (1991) Atomic structure of acetylcholinesterase from Torpedo californica: a prototypic acetylcholine-binding protein, Science. **253**, 872-9.

98. Kasten, S. A., Zulli, S., Jones, J. L., Dephillipo, T. & Cerasoli, D. M. (2014) Chiral separation of G-type chemical warfare nerve agents via analytical supercritical fluid chromatography, Chirality. **26**, 817-24.

99. Potter, D. W. & Hinson, J. A. (1987) Mechanisms of acetaminophen oxidation to N-acetyl-P-benzoquinone imine by horseradish peroxidase and cytochrome P-450, J Biol Chem. **262**, 966-73.

100. Potter, D. W. & Hinson, J. A. (1987) The 1- and 2-electron oxidation of acetaminophen catalyzed by prostaglandin H synthase, J Biol Chem. **262**, 974-80.

101. Harrison, A. C., Kitteringham, N. R., Clarke, J. B. & Park, B. K. (1992) The mechanism of bioactivation and antigen formation of amodiaquine in the rat, Biochem Pharmacol. **43**, 1421-30.

102. Maggs, J. L., Tingle, M. D., Kitteringham, N. R. & Park, B. K. (1988) Drug-protein conjugates--XIV. Mechanisms of formation of protein-arylating intermediates from amodiaquine, a myelotoxin and hepatotoxin in man, Biochem Pharmacol. **37**, 303-11.

103. Naisbitt, D. J., Williams, D. P., O'Neill, P. M., Maggs, J. L., Willock, D. J., Pirmohamed, M. & Park, B. K. (1998) Metabolism-dependent neutrophil cytotoxicity of amodiaquine: A comparison with pyronaridine and related antimalarial drugs, Chem Res Toxicol. **11**, 1586-95.

104. Ercegovic, S. M. (2011) Synthesis and Characterization of Quinone Methide Precursors as Acetylcholinesterase Reactivators, Ohio State University.

105. (2009) Quinone Methides, John Wiley & Sons, Inc., New Jersey.

106. Bolton, J. L. & Thompson, J. A. (2009) Formation and Reactions of Xenobiotic Quinone Methides in Biology in Quinone Methides pp. 329-356, John Wiley & Sons, Inc.

107. Weinert, E. E., Dondi, R., Colloredo-Melz, S., Frankenfield, K. N., Mitchell, C. H., Freccero, M. & Rokita, S. E. (2006) Substituents on quinone methides strongly modulate formation and stability of their nucleophilic adducts, J Am Chem Soc. **128**, 11940-7.

108. Hatton, C. S., Peto, T. E., Bunch, C., Pasvol, G., Russell, S. J., Singer, C. R., Edwards, G. & Winstanley, P. (1986) Frequency of severe neutropenia associated with amodiaquine prophylaxis against malaria, Lancet. **1**, 411-4.

109. Larrey, D., Castot, A., Pessayre, D., Merigot, P., Machayekhy, J. P., Feldmann, G., Lenoir, A., Rueff, B. & Benhamou, J. P. (1986) Amodiaquine-induced hepatitis. A report of seven cases, Ann Intern Med. **104**, 801-3.

110. Neftel, K. A., Woodtly, W., Schmid, M., Frick, P. G. & Fehr, J. (1986) Amodiaquine induced agranulocytosis and liver damage, Br Med J (Clin Res Ed). **292**, 721-3.

111. Rhodes, E. G., Ball, J. & Franklin, I. M. (1986) Amodiaquine induced agranulocytosis: inhibition of colony growth in bone marrow by antimalarial agents, Br Med J (Clin Res Ed). **292**, 717-8.

112. Huang, J. & Dunford, H. B. (1990) Oxidation of substituted anilines by horseradish peroxidase compound II, Can J Chem. **68**, 2159-2163.

113. Josephy, P. D., Eling, T. E. & Mason, R. P. (1983) Oxidation of p-aminophenol catalyzed by horseradish peroxidase and prostaglandin synthase, Molecular Pharmacology. **23**, 461-466.

114. Giulivi, C., Romero, F. J. & Cadenas, E. (1992) The interaction of Trolox C, a water-soluble vitamin E analog, with ferrylmyoglobin: reduction of the oxoferryl moiety, Arch Biochem Biophys. **299**, 302-12.

115. Nakamura, M. & Hayashi, T. (1992) Oxidation mechanism of vitamin E analogue (Trolox C, 6-hydroxy-2,2,5,7,8-pentamethylchroman) and vitamin E by horseradish peroxidase and myoglobin, Arch Biochem Biophys. **299**, 313-9.

116. Re, R., Pellegrini, N., Proteggente, A., Pannala, A., Yang, M. & Rice-Evans, C. (1999) Antioxidant activity applying an improved ABTS radical cation decolorization assay, Free Radic Biol Med. **26**, 1231-7.

117. Castro, I. A., Rogero, M. M., Junqueira, R. M. & Carrapeiro, M. M. (2006) Free radical scavenger and antioxidant capacity correlation of alpha-tocopherol and Trolox measured by three in vitro methodologies, Int J Food Sci Nutr. **57**, 75-82.

118. Franzoni, F., Colognato, R., Galetta, F., Laurenza, I., Barsotti, M., Di Stefano, R., Bocchetti, R., Regoli, F., Carpi, A., Balbarini, A., Migliore, L. & Santoro, G. (2006) An in vitro study on the free radical scavenging capacity of ergothioneine: comparison with reduced glutathione, uric acid and trolox, Biomed Pharmacother. **60**, 453-7.

119. Poljsak, B. & Raspor, P. (2008) The antioxidant and pro-oxidant activity of vitamin C and trolox in vitro: a comparative study, J Appl Toxicol. **28**, 183-8.

120. Colletier, J. P., Sanson, B., Nachon, F., Gabellieri, E., Fattorusso, C., Campiani, G. & Weik, M. (2006) Conformational flexibility in the peripheral site of Torpedo californica acetylcholinesterase revealed by the complex structure with a bifunctional inhibitor, J Am Chem Soc. **128**, 4526-7.

121. Todd, M. J. & Gomez, J. (2001) Enzyme kinetics determined using calorimetry: a general assay for enzyme activity?, Anal Biochem. **296**, 179-87.

122. Bianconi, M. L. (2003) Calorimetric determination of thermodynamic parameters of reaction reveals different enthalpic compensations of the yeast hexokinase isozymes, J Biol Chem. **278**, 18709-13.

123. Lonhienne, T. G. & Winzor, D. J. (2004) A potential role for isothermal calorimetry in studies of the effects of thermodynamic non-ideality in enzyme-catalyzed reactions, J Mol Recognit. **17**, 351-61.

124. Bianconi, M. L. (2007) Calorimetry of enzyme-catalyzed reactions, Biophys Chem. **126**, 59-64.

125. Miller, J. R., Ohren, J., Sarver, R. W., Mueller, W. T., de Dreu, P., Case, H. & Thanabal, V. (2007) Phosphopantetheine adenylyltransferase from Escherichia coli: investigation of the kinetic mechanism and role in regulation of coenzyme A biosynthesis, J Bacteriol. **189**, 8196-205.

126. Freyer, M. W. & Lewis, E. A. (2008) Isothermal Titration Calorimetry: Experimental Design, Data Analysis, and Probing Macromolecule/Ligand Binding and Kinetic Interactions. **84**, 79-113.

127. Haq, I. (2011) Calorimetry in the fast lane: The use of ITC for obtaining enzyme kinetic constants. in, GE Healthcare,

128. O'Brien, R., Ladbury, J. E. & Chowdhry, B. Z. (2001) Isothermal titration calorimetry of biomolecules in Protein-ligand Interactions: Hydrodynamics and Calorimetry : a Practical Approach (Harding, S. E. & Chowdhry, B. Z., eds) pp. 263-286, Oxford University Press.

129. Tsai, P. C., Bigley, A., Li, Y., Ghanem, E., Cadieux, C. L., Kasten, S. A., Reeves, T. E., Cerasoli, D. M. & Raushel, F. M. (2010) Stereoselective hydrolysis of organophosphate nerve agents by the bacterial phosphotriesterase, Biochemistry. **49**, 7978-87.

130. Aurbek, N., Thiermann, H., Eyer, F., Eyer, P. & Worek, F. (2009) Suitability of human butyrylcholinesterase as therapeutic marker and pseudo catalytic scavenger in organophosphate poisoning: a kinetic analysis, Toxicology. **259**, 133-9.

131. Burnouf, D., Ennifar, E., Guedich, S., Puffer, B., Hoffmann, G., Bec, G., Disdier, F., Baltzinger, M. & Dumas, P. (2012) kinITC: a new method for obtaining joint thermodynamic and kinetic data by isothermal titration calorimetry, J Am Chem Soc. **134**, 559-65.

132. Dumas, P., Ennifar, E., Da Veiga, C., Bec, G., Palau, W., Di Primo, C., Pineiro, A., Sabin, J., Munoz, E. & Rial, J. (2016) Extending ITC to Kinetics with kinITC, Methods Enzymol. **567**, 157-80.

133. Worek, F., Wille, T., Aurbek, N., Eyer, P. & Thiermann, H. (2010) Reactivation of organophosphate-inhibited human, Cynomolgus monkey, swine and guinea pig acetylcholinesterase by MMB-4: a modified kinetic approach, Toxicol Appl Pharmacol. **249**, 231-7.

134. Sit, R. K., Radic, Z., Gerardi, V., Zhang, L., Garcia, E., Katalinic, M., Amitai, G., Kovarik, Z., Fokin, V. V., Sharpless, K. B. & Taylor, P. (2011) New structural scaffolds for centrally acting oxime reactivators of phosphylated cholinesterases, J Biol Chem. **286**, 19422-30.

Appendix

ADDITIONAL FIGURES AND TABLES

A.1 Mass spectrometry analyses of ADOC/agent solution reaction

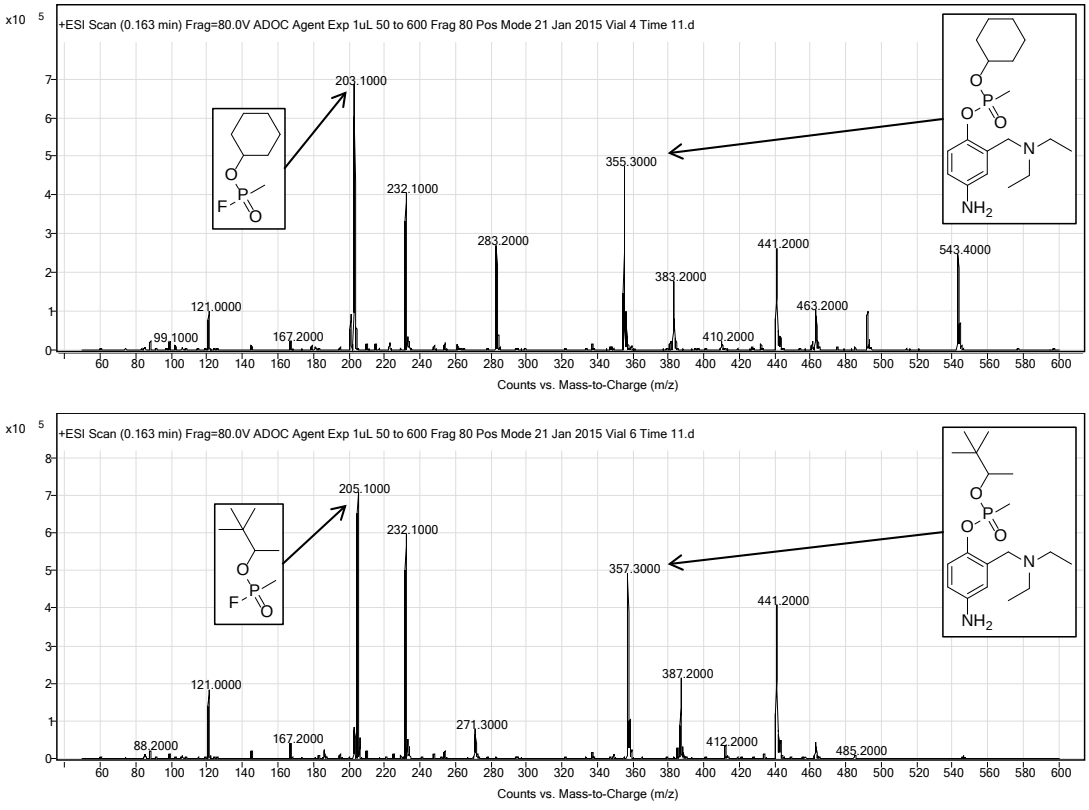

Figure A.1. Mass spectrometry ion spectra of ADOC/agent reactions highlighting the ions of the agent (GF or GD) and the corresponding phosphonylated ADOC product.

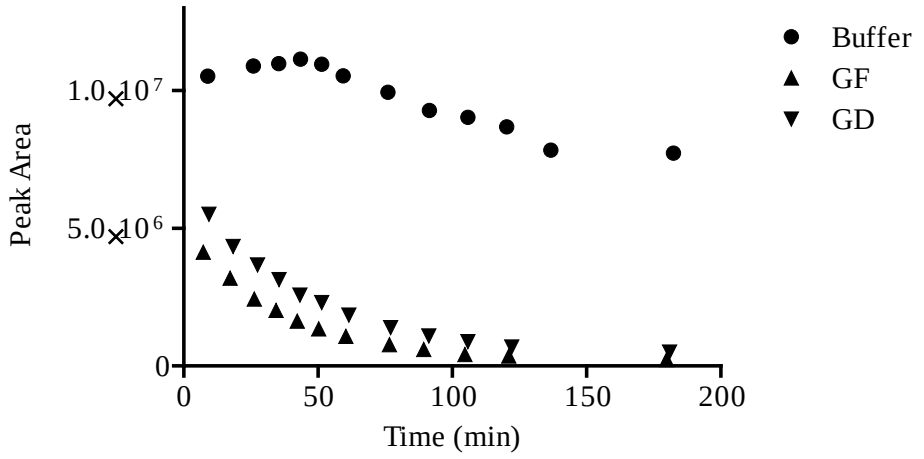

Figure A.2. Peak area of ADOC ion (m/z = 195) in buffer only (●), buffer with GF (▲), or buffer with GD (▼) over the time course of ADOC/agent solution reaction.

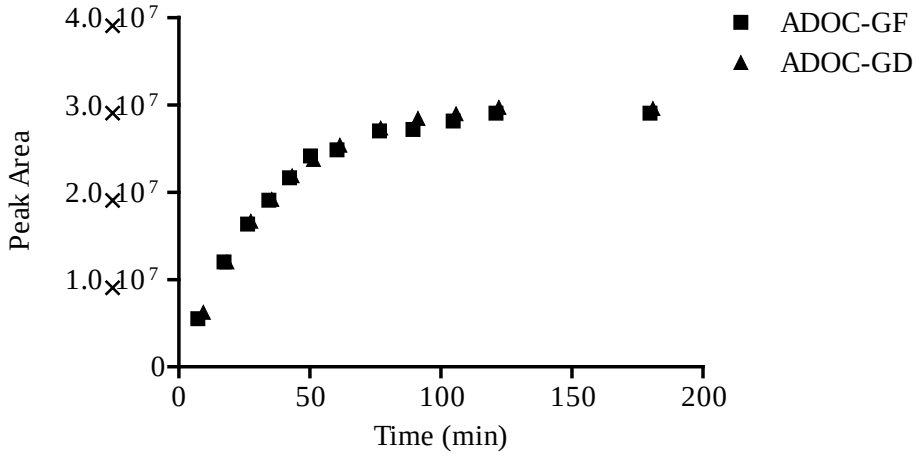

Figure A.3. Peak area of phosphonylated ADOC ion (GF m/z = 355; GD m/z = 357) over the time course of ADOC/agent solution reaction.

A.2 Separation of phosphonylated ADOC product using LC/MS

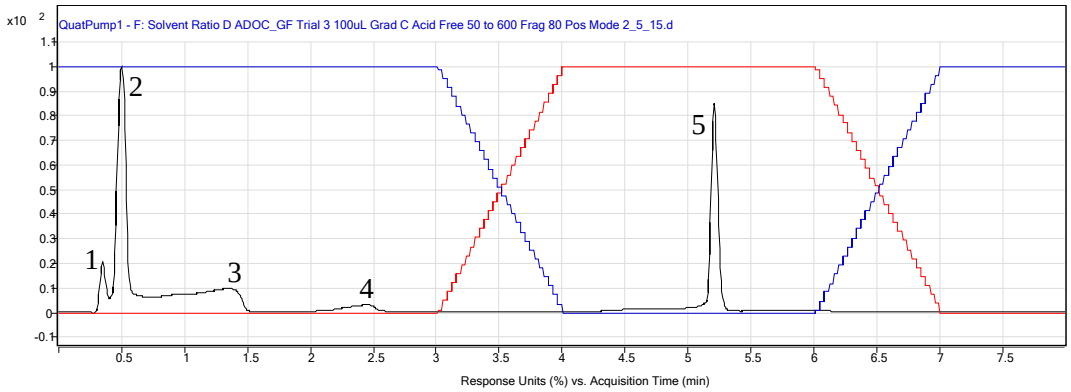

Figure A.4. Gradient used to separate phosphonylated ADOC product (Section 6.2.5.2.2). The blue line represents the percent water in the mobile phase; the red line represents the percent methanol in the mobile phase. The black line represents the absorbance measured at 303 nm over the course of the experiment with peaks numbered 1 through 5.

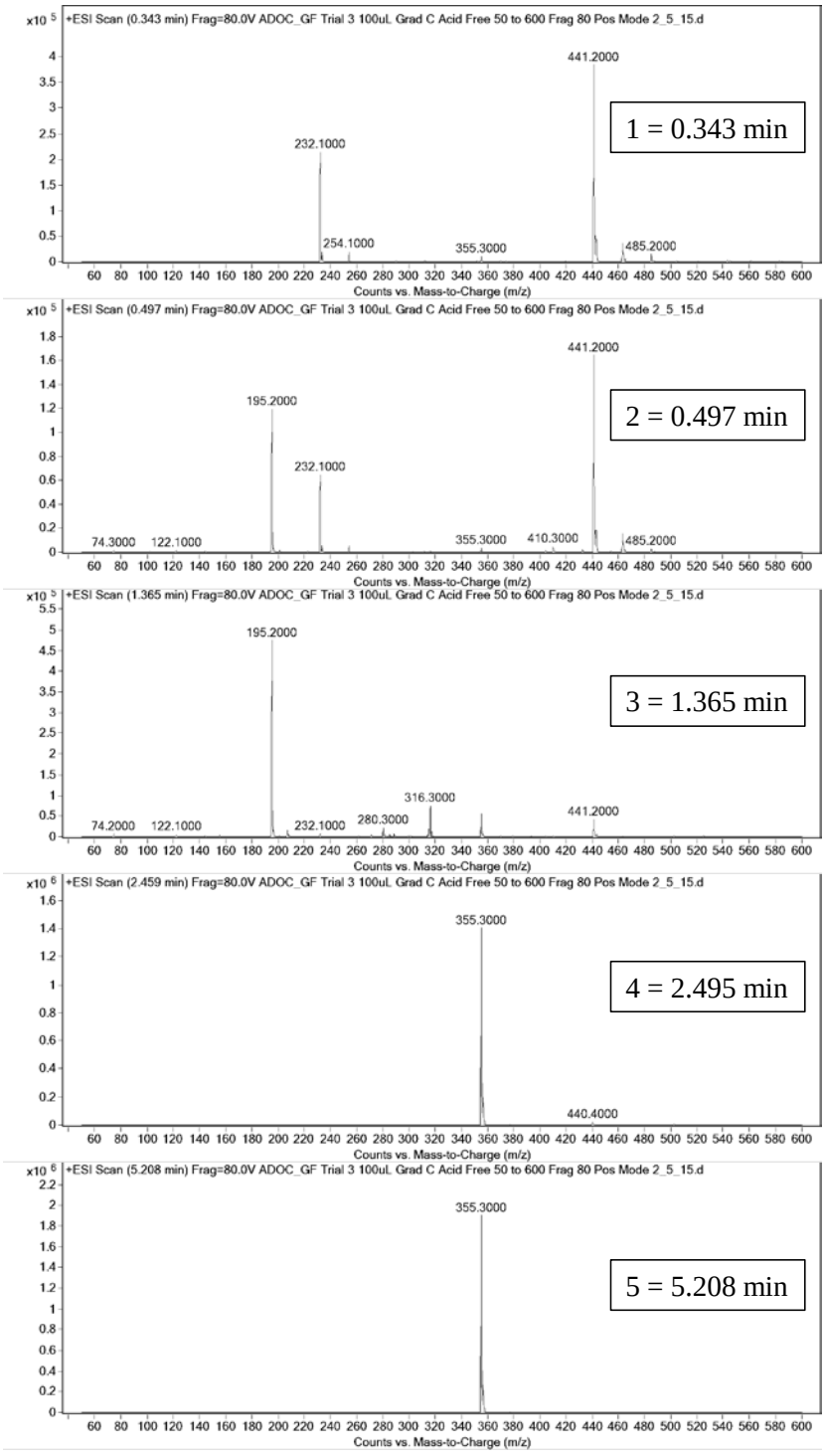

Figure A.5. Mass spectrometry spectra for each of the peaks labeled in Figure A.4. Peak 1 appears to be buffer only, Peaks 2 and 3 are comprised of mainly ADOC, and Peaks 4 and 5 are the phosphonylated ADOC product.

A.3 Deconvolution of phosphonylated ADOC product forms

To determine nature of the two products (2.5- and 5.2-minute elution) collected using the method described in Section 6.2.5.2.2 (Figure A.4), the purified samples were analyzed by injecting them into the LC/QQQ system described earlier using the column and gradient conditions for purification with small modifications:

1. The time course of the gradient method was extended from eight minutes to thirteen minutes (0 to 3 min = 23% MeOH/77% H_2O, 3 to 4 min = gradient ramp to 85% MeOH/15% H_2O, 4 to 10 min = 85% MeOH/15% H_2O, 10 to 11 min = gradient ramp to 23% MeOH/77% H_2O, 11 to 13 min = 23% MeOH/77% H_2O)

2. The gradient program described in 1 was performed with either water/methanol only or water/methanol with 0.1% formic acid to lower the pH of the mobile phase.

The ion corresponding to phosphonylated ADOC (m/z = 355) was measured over the time course of the experiment via mass spectrometry, and the level of detection was graphed versus time in the figure below (Figure A.6).

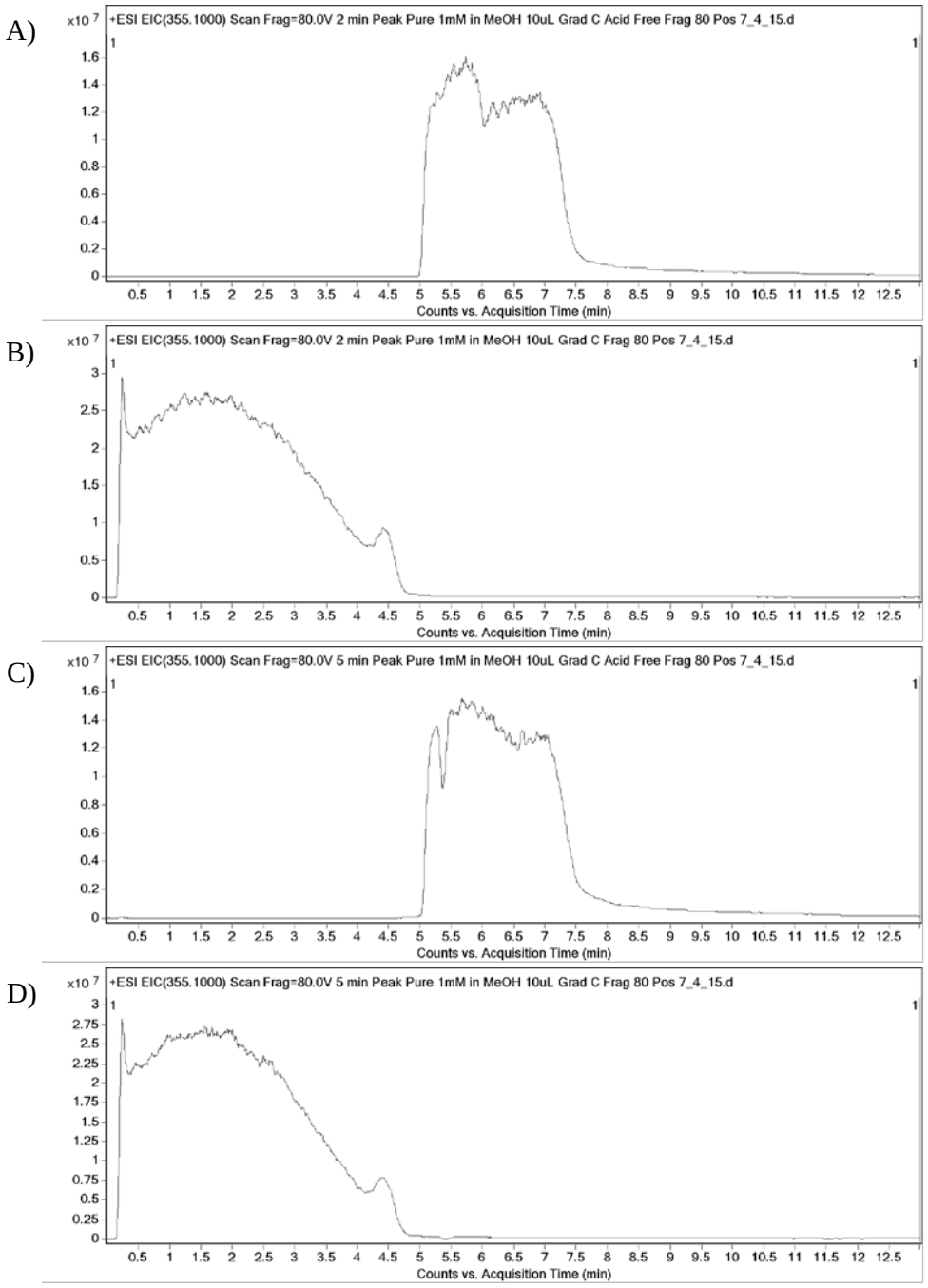

Figure A.6. Chromatogram of phosphonylated ADOC ion (m/z = 355). A) and C) are purified products collected at 2.5 and 5.2 minutes respectively injected in a water/methanol mobile phase. B) and D) are the same samples injected in a water/methanol + 0.1% formic acid mobile phase.

A.4 High resolution mass spectrometry of phosphonylated ADOC purified product

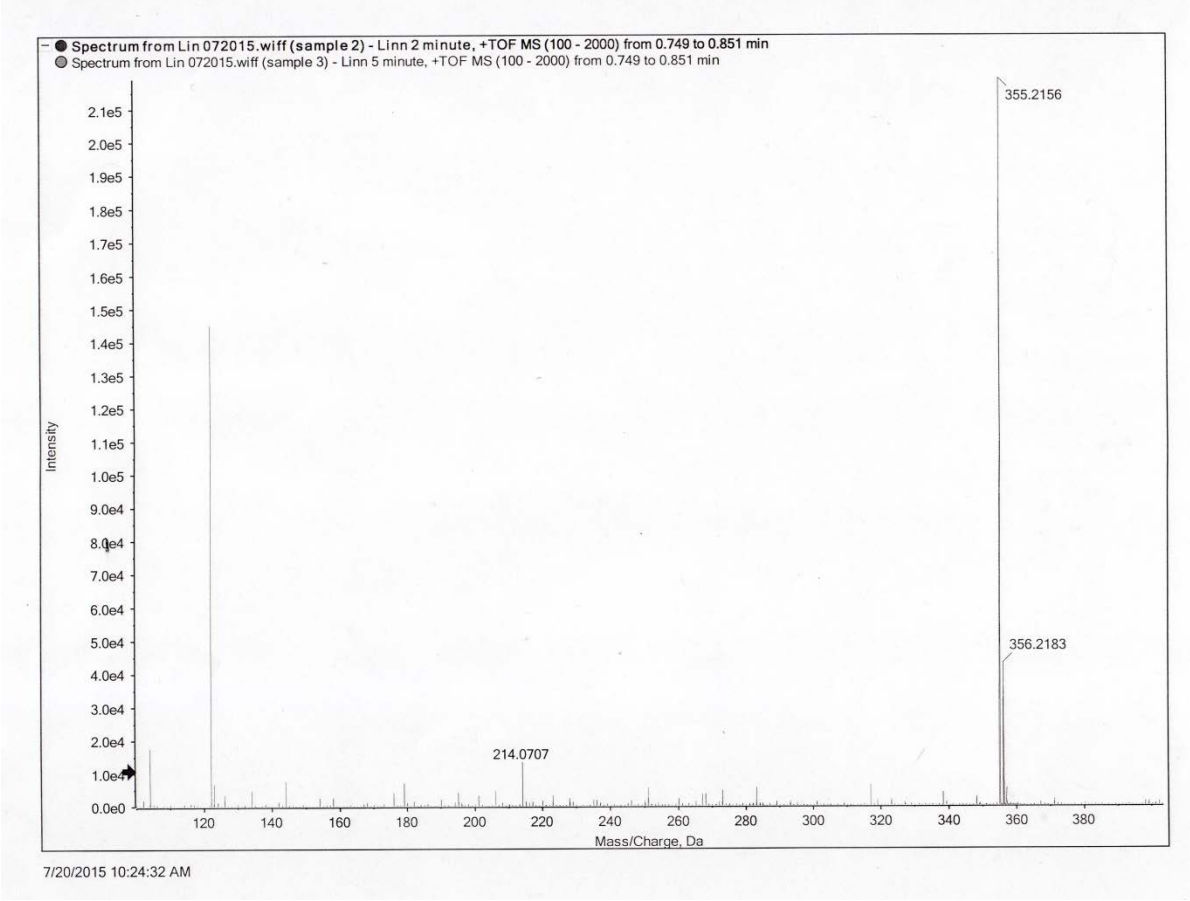

Figure A.7. High resolution mass spectrometry of purified product with ion corresponding to product as major detected peak.

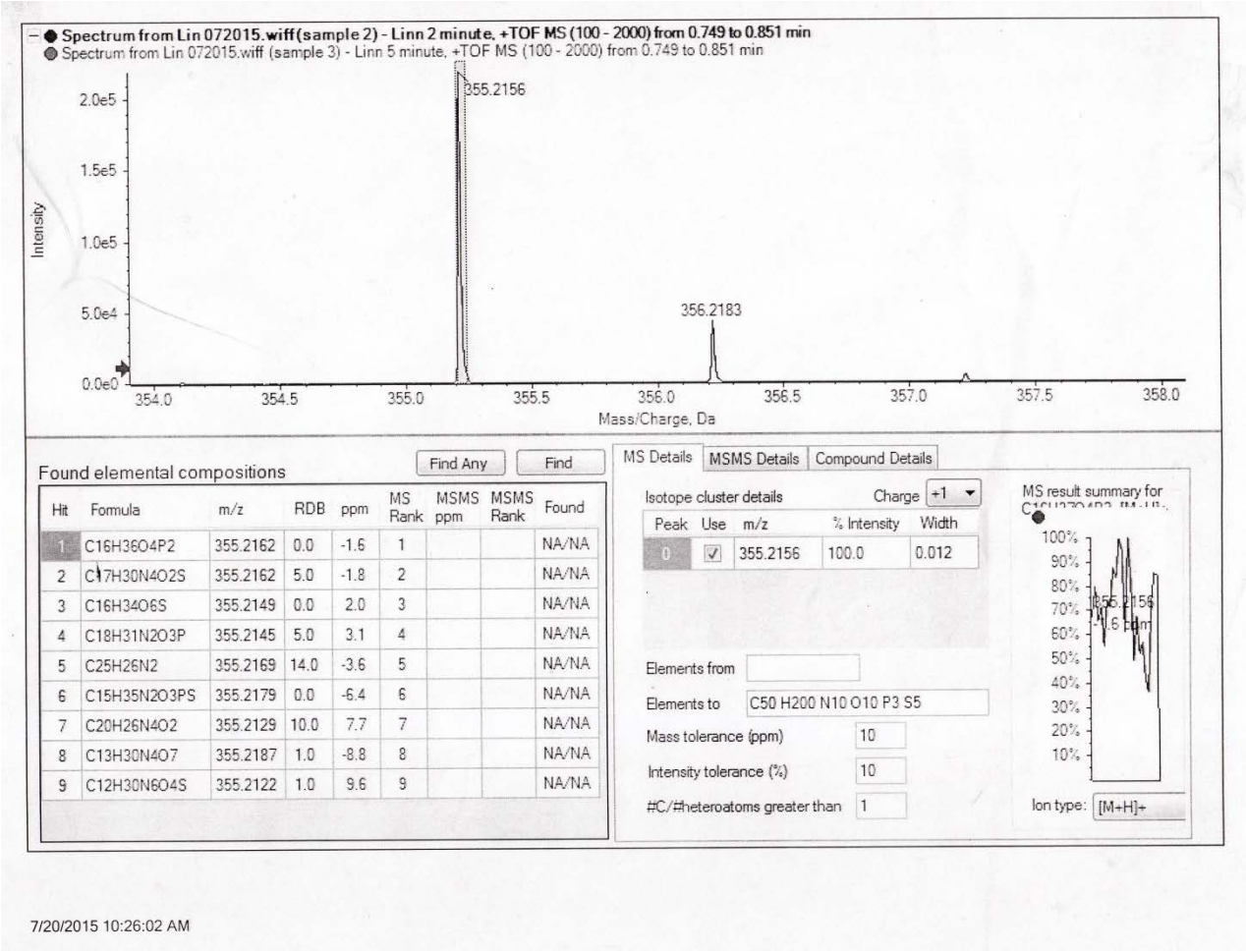

Hit	Formula	m/z	RDB	ppm	MS Rank	MSMS ppm	MSMS Rank	Found
1	C16H36O4P2	355.2162	0.0	-1.6	1			NA/NA
2	C17H30N4O2S	355.2162	5.0	-1.8	2			NA/NA
3	C16H34O6S	355.2149	0.0	2.0	3			NA/NA
4	C18H31N2O3P	355.2145	5.0	3.1	4			NA/NA
5	C25H26N2	355.2169	14.0	-3.6	5			NA/NA
6	C15H35N2O3PS	355.2179	0.0	-6.4	6			NA/NA
7	C20H26N4O2	355.2129	10.0	7.7	7			NA/NA
8	C13H30N4O7	355.2187	1.0	-8.8	8			NA/NA
9	C12H30N6O4S	355.2122	1.0	9.6	9			NA/NA

Figure A.8. Elemental composition determination of the major ion detected using high resolution mass spectrometry (Figure A.7). Note that the fourth candidate is the elemental composition predicted for the product of the ADOC-GF reaction.

A.5 NMR spectrum of phosphonylated ADOC purified product

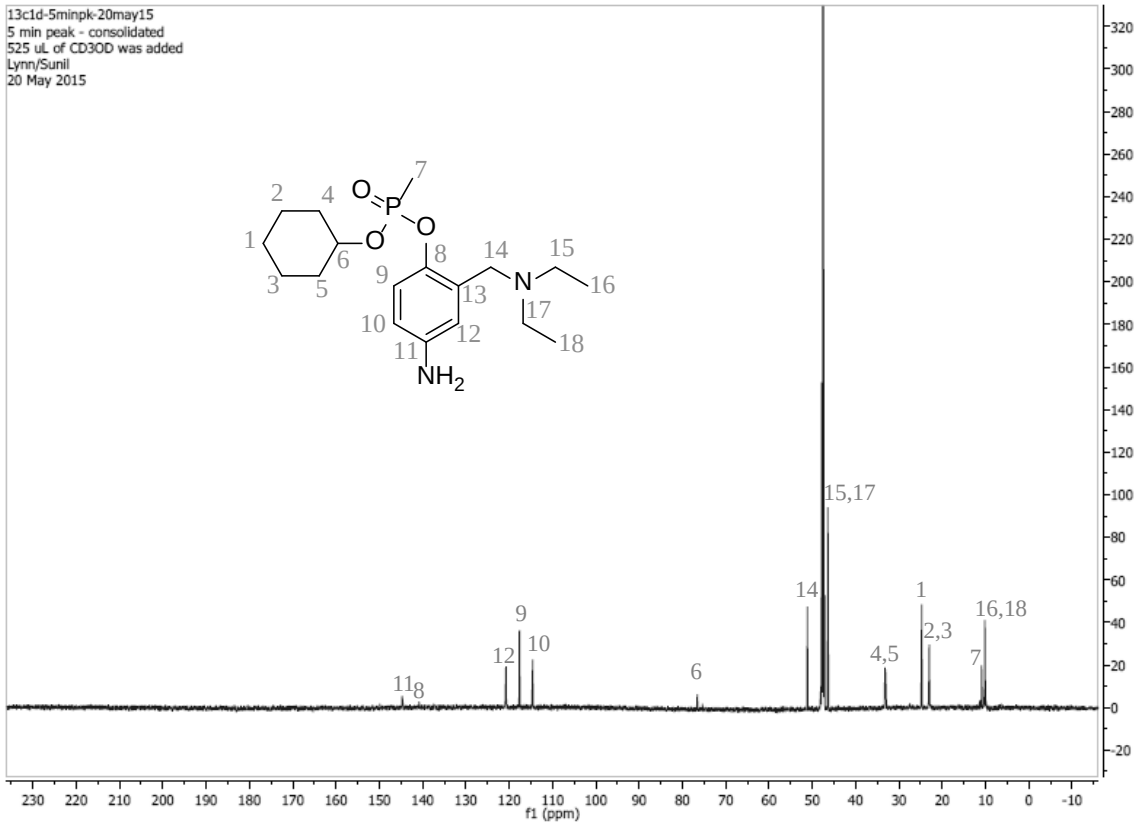

Figure A.9. Carbon[13] NMR spectrum of phosphonylated ADOC.

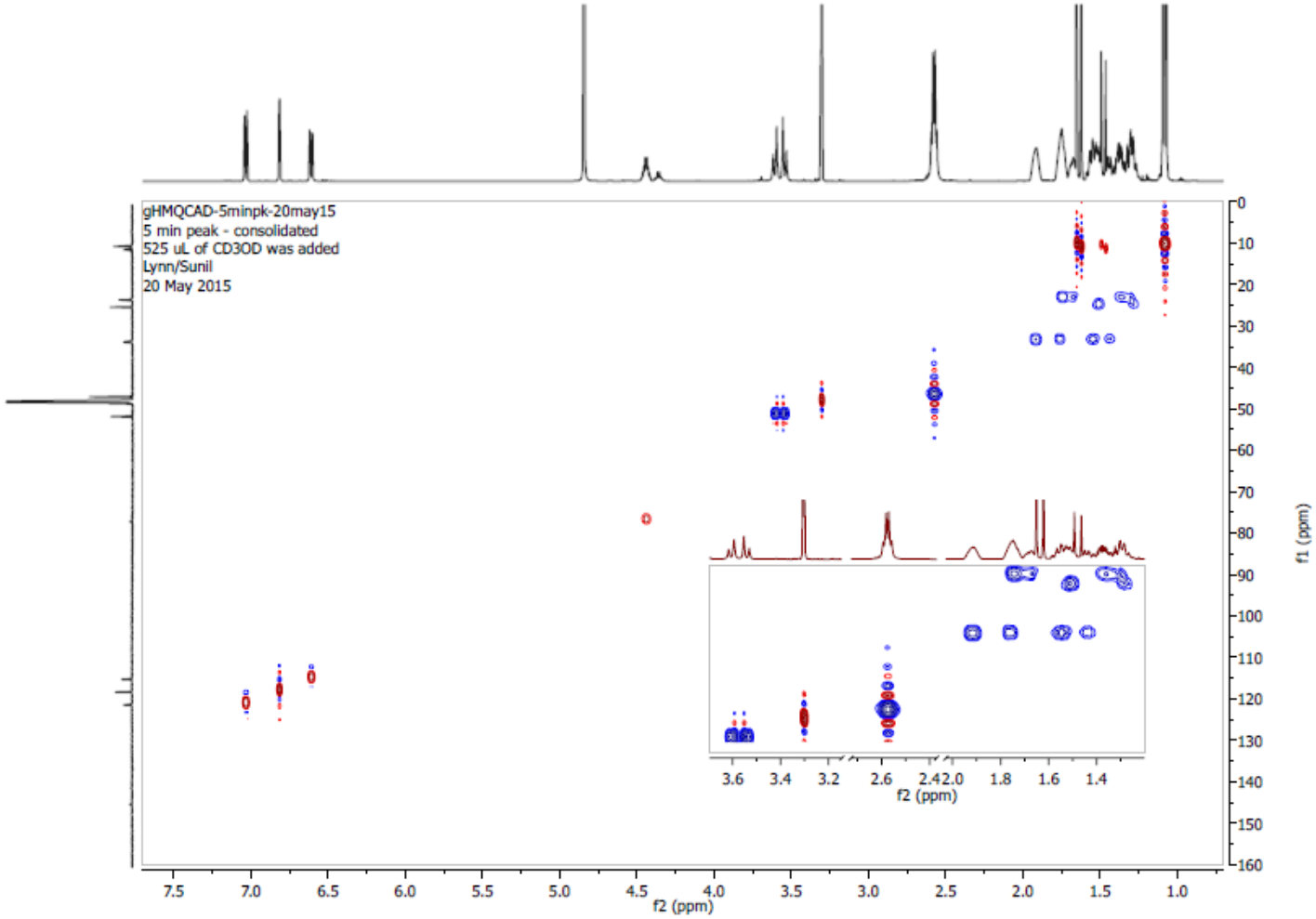

Figure A.10. HMQC NMR spectrum. Red indicates an odd number of protons attached to the corresponding carbon, whereas blue indicates an even number of protons.

A.6 Mass spectrometry results of selective furfural addition

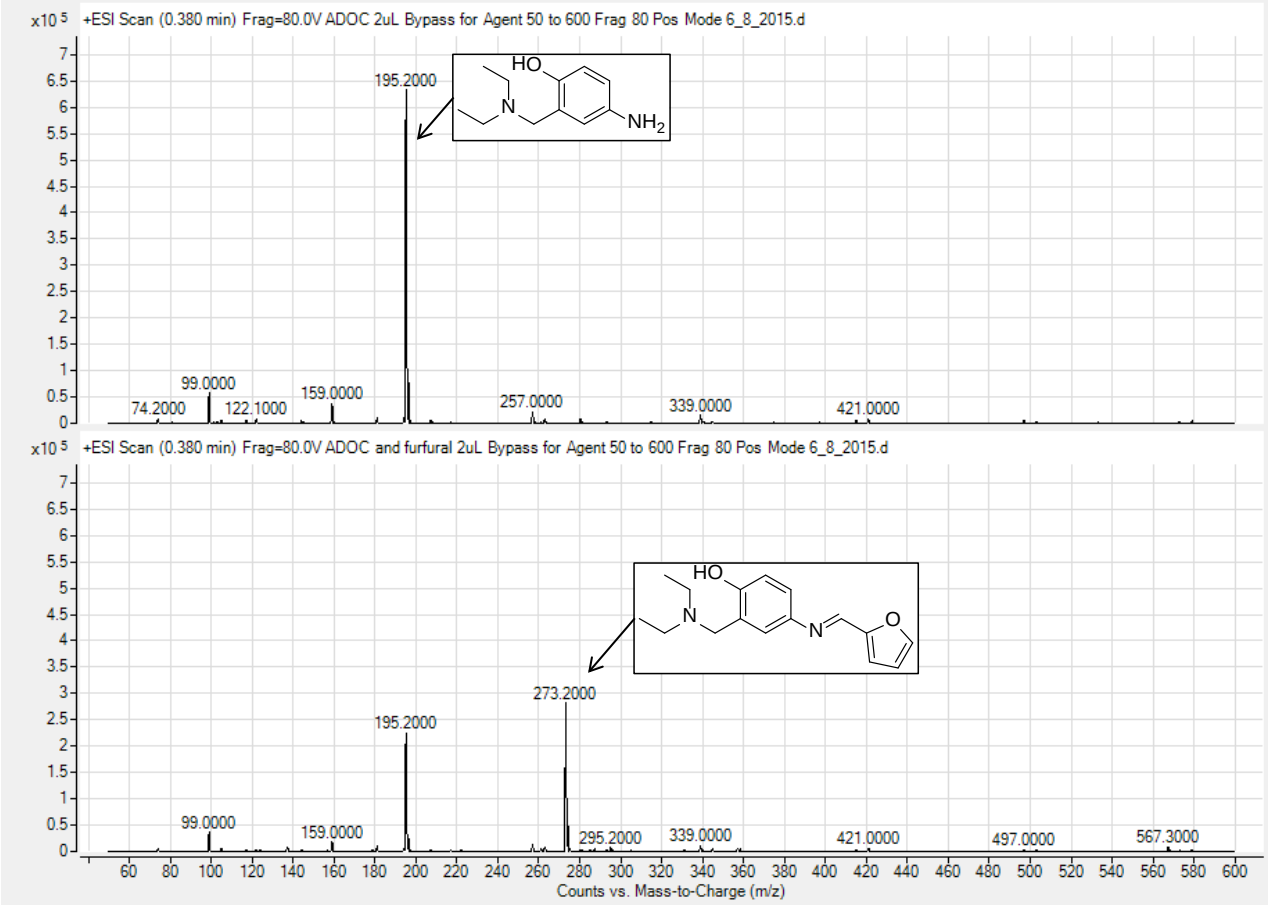

Figure A.11. Mass spectrometry chromatogram of ADOC and furfural-ADOC product after reaction described in Section 6.2.7.

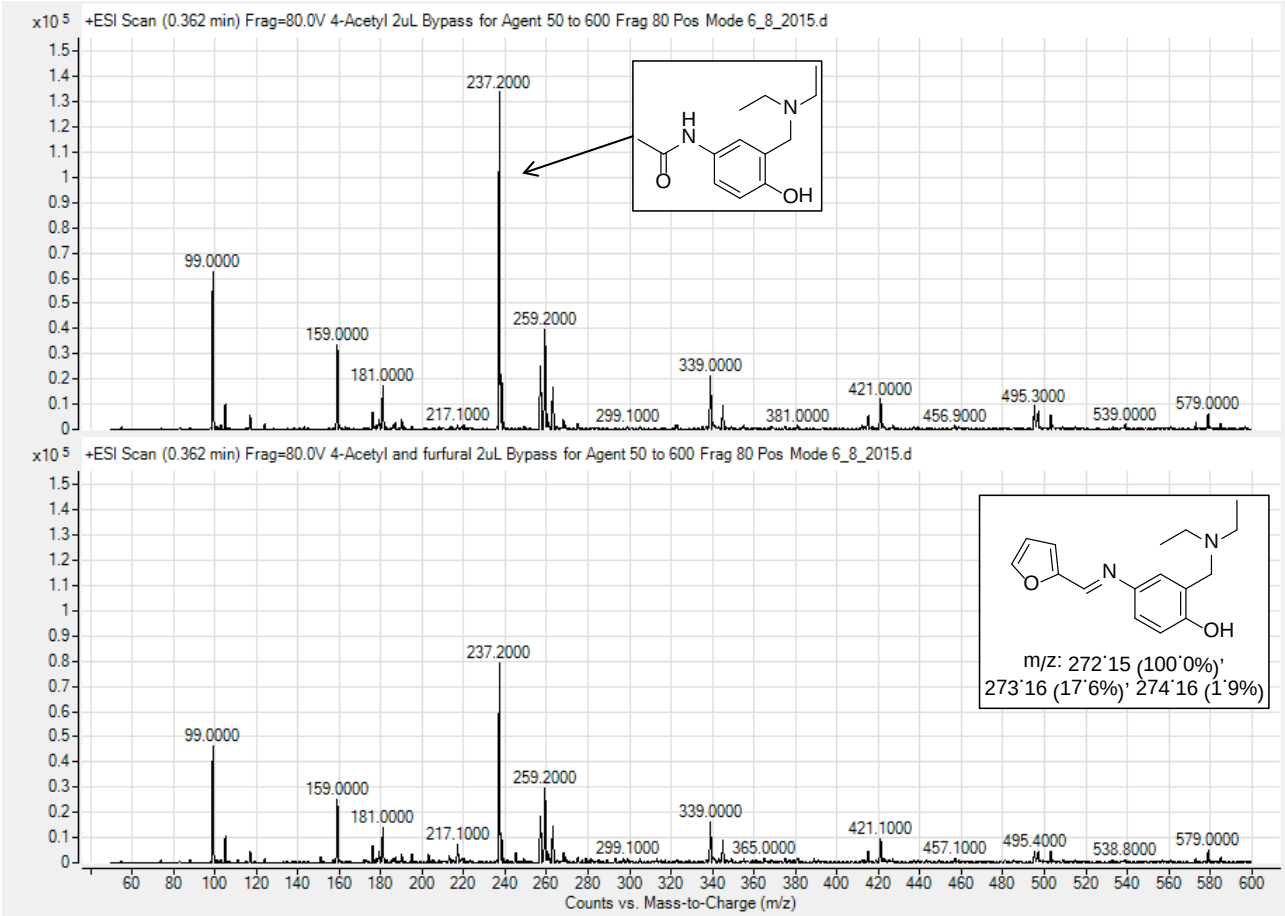

Figure A.12. Mass spectrometry chromatogram of **12** and reaction mixture of furfural and **12** with no detectable product formation.

A.7 Standard curves for the detection of ADOC and CMP using mass spectrometry

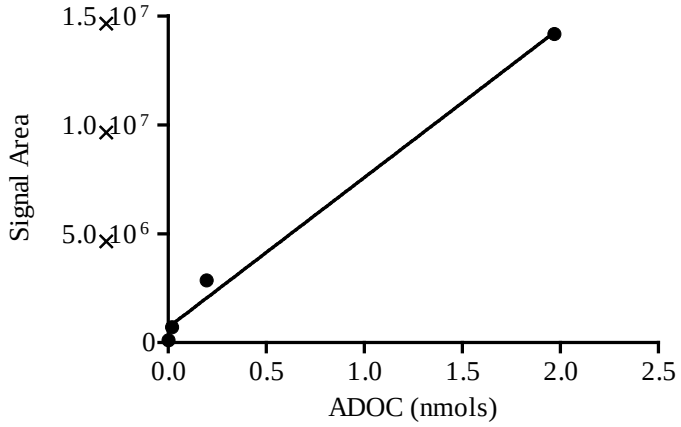

Figure A.13. Standard curve (linear) generated using purified phosphonylated ADOC. (Linear fit Y=mX+b; m = $6.878 \times 10^6 \pm 0.433 \times 10^6$; b = $6.961 \times 10^5 \pm 4.292 \times 10^5$; $R^2 = 0.9921$)

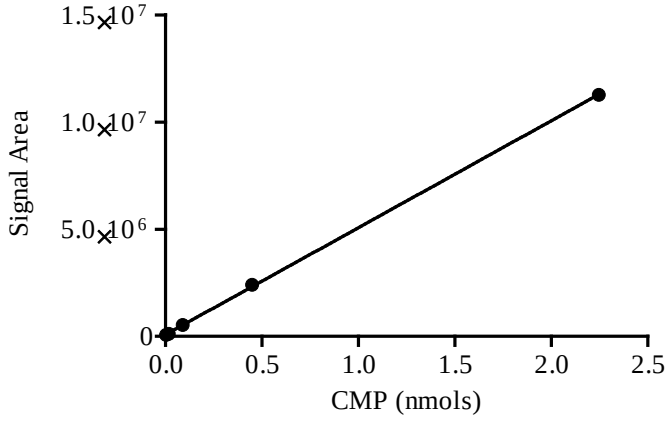

Figure A.14. Standard curve (linear) generated using purified CMP. (Linear fit Y=mX+b; m = $4.991 \times 10^6 \pm 0.031 \times 10^6$; b = $7.485 \times 10^4 \pm 3.141 \times 10^4$; $R^2 = 0.9999$)

A.8 Half-time of reactivation of **15** and **16**

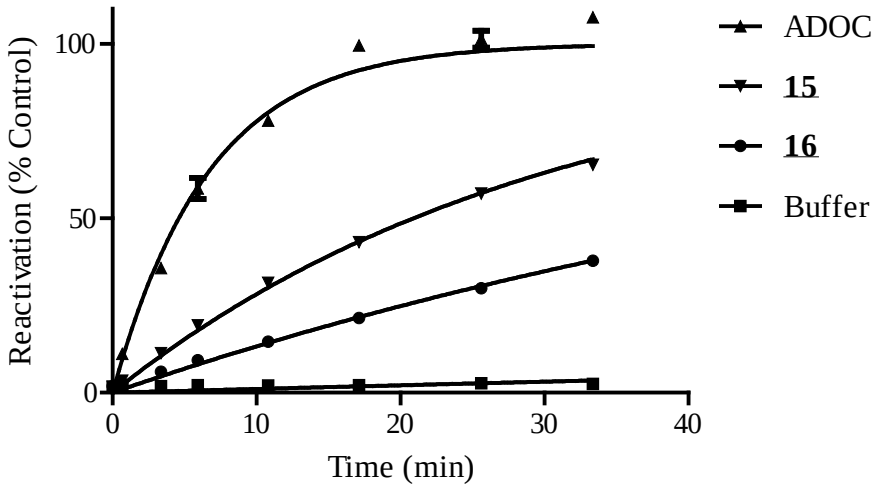

Figure A.15. Reactivation of VX-inhibited HuAChE by ADOC (▲), **15** (▼), **16** (●), and buffer control (■). Black lines indicate the non-linear regression analysis used to determine half-times of reactivation.

Table A.1. Half-times of reactivation of VX-inhibited HuAChE by ADOC, **15**, and **16**

Compound	**Half-time of Reactivation ($t_{1/2}$, min)**
Buffer Only Control	649.3 (491.1 to 958.0)
ADOC	4.616 (4.202 to 5.121)
15	20.91 (20.34 to 21.52)
16	48.65 (47.04 to 50.37)

A.9 Colorimetric reactivation assay of sample measured via ITC

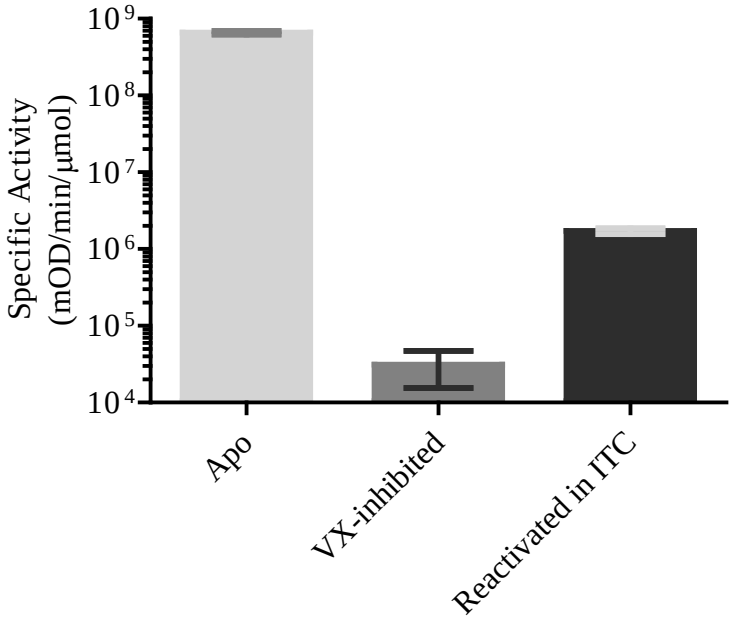

Figure A.16. Specific activity of enzyme samples used in ITC kinetic assay. “Apo” is the apo enzyme sample in the presence of 2PAM, “VX-inhibited” is the inhibited enzyme sample which has not been exposed to 2PAM, and “Reactivated in ITC” is the VX-inhibited enzyme sample recovered from the ITC sample cell after 2PAM injections. VX-inhibited sample = 0.005±0.002% activity of Apo while reactivated in ITC = 0.26±0.02% activity of Apo. Activities were measured after completion of ITC assay which was conducted over the course of 58.3 minutes.